(2)

Annual Report

Experimental, Modeling, and Sensitivity Analysis Studies of Gas-Phase Reaction Mechanisms Important to the Combustion of High Energy Density Materials

Prepared by:
R.A. Yetter and F.L. Dryer
Department of Mechanical and Aerospace Engineering
Princeton University
Princeton, NJ 08544

Frederick L. Dryer
Co-Principal Investigator
Professor
(Correspondent)

Richard A. Yetter
Co-Principal Investigator
Research Scientist and Lecturer

Prepared for:
R.S. Miller
Office of Naval Research
Department of the Navy
Arlington, VA

September 1990

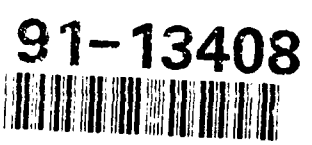

First Annual Project Summary

Title: Experimental, Modeling, and Sensitivity Analysis Studies of Gas-Phase Reaction Mechanisms Important to the Combustion of High Energy Density Materials

Principal Investigators: Prof. F.L. Dryer (Correspondent)
Dr. R.A. Yetter
Department of Mechanical and Aerospace Engineering
Princeton University
Princeton, NJ 08544

Research Personnel: M.A. Yolanda Stein, Technical Staff
Mr. Paul Michniewicz, Technical Specialist
Mr. Mark Allen, 1st Year Graduate Student
Mr. Nenad Ilincic, 1st Year Graduate Student

Inclusive Dates: 1 May 1990 - 1 April 1991

Contract Number: N00014-90-J-4062

Research Objective: The objective of this research program is to develop a fundamental understanding of the gas-phase reaction mechanisms associated with the combustion process of energetic polycyclic nitramines and energetic polymers.

Summary of Major Accomplishments:

1. Kinetic experiments on N_2O and NO_2 decomposition and on the reactions between N_2O and NO_2 with H_2, all with dilute mixtures in N_2, have been performed in a flow reactor over the temperature range of 803-1100 K and pressure range of 1-6 atm. Species concentration profiles measured include H_2, H_2O, NO, NO_2, N_2O, and O_2.
2. A detailed chemical kinetic model has been constructed from literature rate constants and model predictions have been compared with experimental data. Agreement between model predictions and experiment for the H_2/N_2O system were generally good, while for the H_2/NO_2 system, the model predicts a reaction rate approximately a factor of 2.5 times too fast.
3. Sensitivity and reaction flux analyses have been performed and crucial reactions requiring further theoretical and experimental study have been identified.
4. For the H_2/N_2O system, the reaction $OH + N_2O \rightarrow HO_2 + N_2$ was found to be an important reaction leading to inhibition. This reaction produces HO_2 radicals which makes their kinetics also important to the system. The channel $H + N_2O \rightarrow NH + NO$ was also observed to inhibit the reaction, but to have a much smaller effect. Nitric oxide formation was not observed in the experimental data and hence this latter step may not be important for the present conditions.

5. For the H_2/NO_2 system, HONO formation and consumption were found to be important. The rates of the initiation reaction $H_2 + NO_2 \rightarrow HONO + H$ and the reaction $HONO + OH \rightarrow H_2O + NO_2$ are likely responsible for the observed discrepancies between model and experiment.

Abstract

The objective of this research program is to develop a fundamental understanding of the gas-phase reaction mechanisms associated with the combustion process of energetic polycyclic nitramines and energetic polymers. Kinetic experiments are performed in a variable temperature (600 $K < T < 1200$ K), variable pressure (1 $atm. < P < 18$ $atm.$) flow reactor with residence times ranging from 10 ms to 10 s. Reaction mechanisms, based on the principle of hierarchical model construction, are developed and validated by detailed kinetic modeling of the experiments along with reaction flux and sensitivity analyses. During the past year, a Nicolet Model 730 FTIR was installed and calibrated for the measurement of oxides of nitrogen, simple hydrocarbons, CO, CO_2, and H_2O. Under other support, the development of a continuous analytical technique for hydrogen was also developed. Experiments and modeling calculations were conducted on the kinetics of N_2O and NO_2 decomposition (1000 K -1100 K, 3 $atm.$ - 6 $atm.$), and on the reactions of H_2 with N_2O (925 K - 1073 K, 1 $atm.$ - 3 $atm.$) and H_2 with NO_2 (803 K - 873 K, 3 $atm.$). These experiments and models represent the basis for current and future gas-phase kinetic studies on the chemical systems consisting of the fuels CO, CH_2O, CH_4, C_2H_4, HCN, and NH_3 and the oxidizers NO_2 and N_2O.

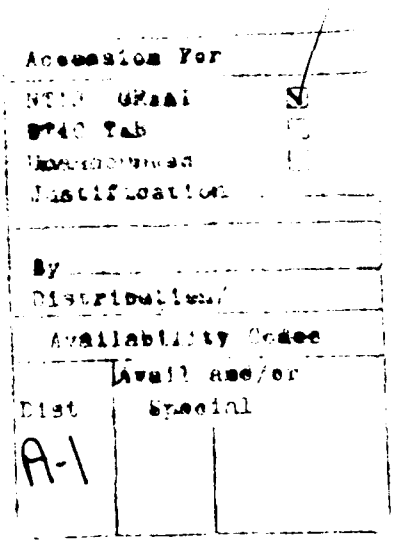

TABLE OF CONTENTS

LIST OF TABLES

LIST OF FIGURES

1.0 INTRODUCTION

1.1 Statement of the Problem and Research Objectives

Newly developed energetic polycyclic nitramines and energetic polymers have the potential to offer significant energy density and plume signature advantages over current state-of-the-art propellants in strategic, tactical rocket and gun propulsion. Current state-of-the-art propellants, such as HMX and RDX, were developed empirically over a lengthy period of time, being first synthesized nearly a century ago. The development and implementation of the next generation of propellants will have to meet new and more stringent requirements of energy density, burn rate, stability, signature and hazards specifications, and formulations will likely be based on combinations of more than ten new oxidizers and energetic polymers. To provide some focal direction in what will be a lengthy (and otherwise risky) empirical development, a national energetic materials research program is emerging.

The goal of this national research program is to develop a robust, comprehensive chemical and physical model for the combustion of new polycyclic nitramines. The proposed program will provide a tool which can be used not only for interpreting experimental results, but for predicting quantitatively the effects of changing propellant design. Potential benefits include reductions, both in expensive laboratory and full scale testing, and in the time required for successful development. The development of such a model will require a fundamental quantitative understanding of the elementary chemical and physical processes in the gas, liquid and solid phases of propellant ignition and combustion. The currently proposed approach for development of this comprehensive model is based upon a hierarchical structure as shown in FIGURE 1 and consists of submodel testing and validation and the application of important new experimental and theoretical tools developed for and successfully used in other complex physicochemical problems. Among these tools are state-of-the-art experimental techniques in chemical physics and physical chemistry (e.g., laser spectroscopic techniques), state-of-the-art computational techniques in fluid mechanics, chemistry, and physics (largely due to the development of massively parallel computer architecture and algorithms), and systematic sensitivity analysis techniques, which link experimental and computational microscopic behavior to macroscopic observations.

It is important to recognize that the combustion of high energy density propellants is another example of complex physicochemical processes which have demanded the research community's attention in recent years. The combustion of hydrocarbons and the formation of atmospheric air pollution are two examples of complex phenomena where analog programs have contributed immensely to the understanding and control of such processes. The work of Melius (1988) on RDX combustion and of Yetter *et al.* (1988) on boron particle combustion are two examples of detailed modeling/sensitivity analysis studies on propellant combustion. With the transfer of knowledge from analog programs, the present program has a high probability of success.

A fundamental input to the overall program is the gas-phase nitrogen combustion chemistry and transport network simulation and validation subprogram at the base of FIGURE 1.

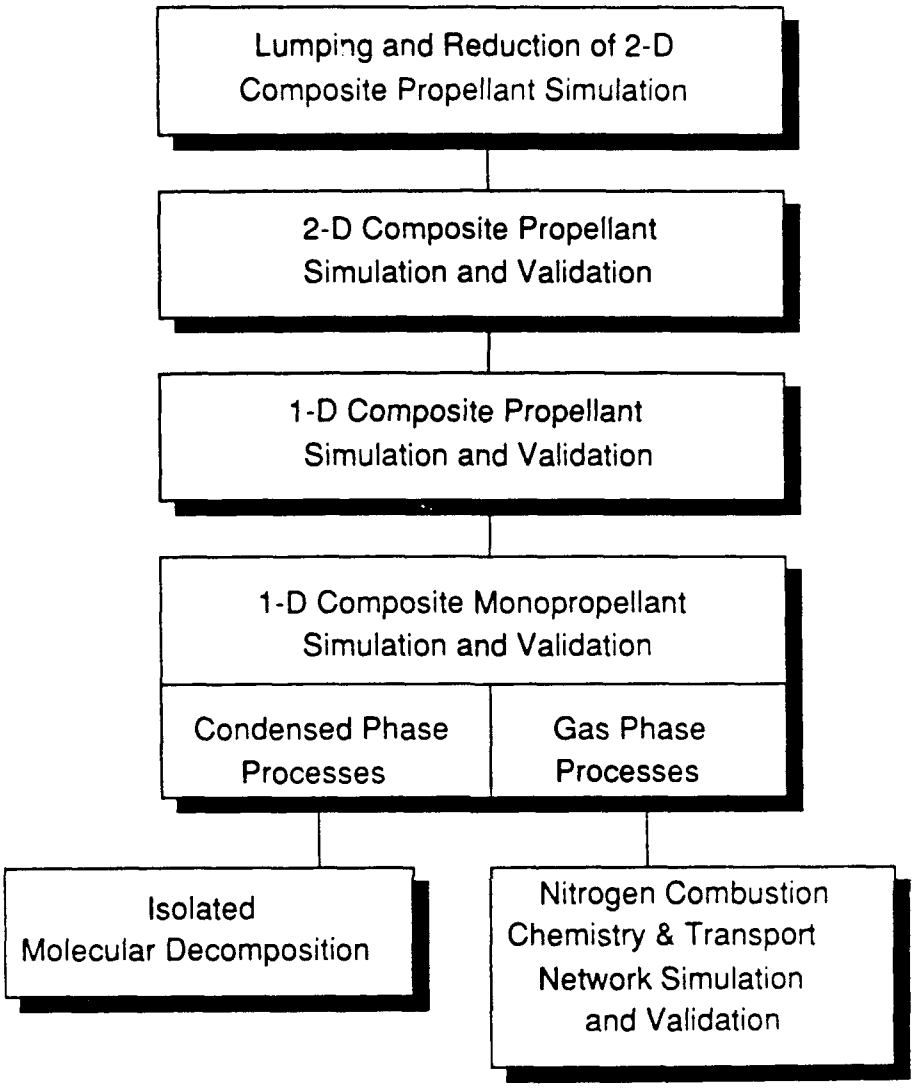

FIGURE 1. High Performance Propellant Combustion Simulation Research Program

The goal of this subprogram is to develop a detailed chemical/physical model for reaction and diffusion of the gas-phase species associated with the combustion process of energetic polycyclic nitramines and energetic polymers. Like the overall program, this subprogram can be subdivided into the hierarchy as shown in the flow chart of FIGURE 2. The proposed approach starts with developing a basic understanding of the gas- phase thermochemical, kinetic, and transport properties of key nitramine species and ends with the validation of a comprehensive reaction mechanism for the gas phase reaction of intermediate species. In this hierarchical approach, theory at the most fundamental level and at a semi-empirical level, interact with laboratory measurements of rate constants, product pathways and transport properties. From these pieces of information, a well founded chemical mechanism with associated rate constants is first derived and validated by comparison of model

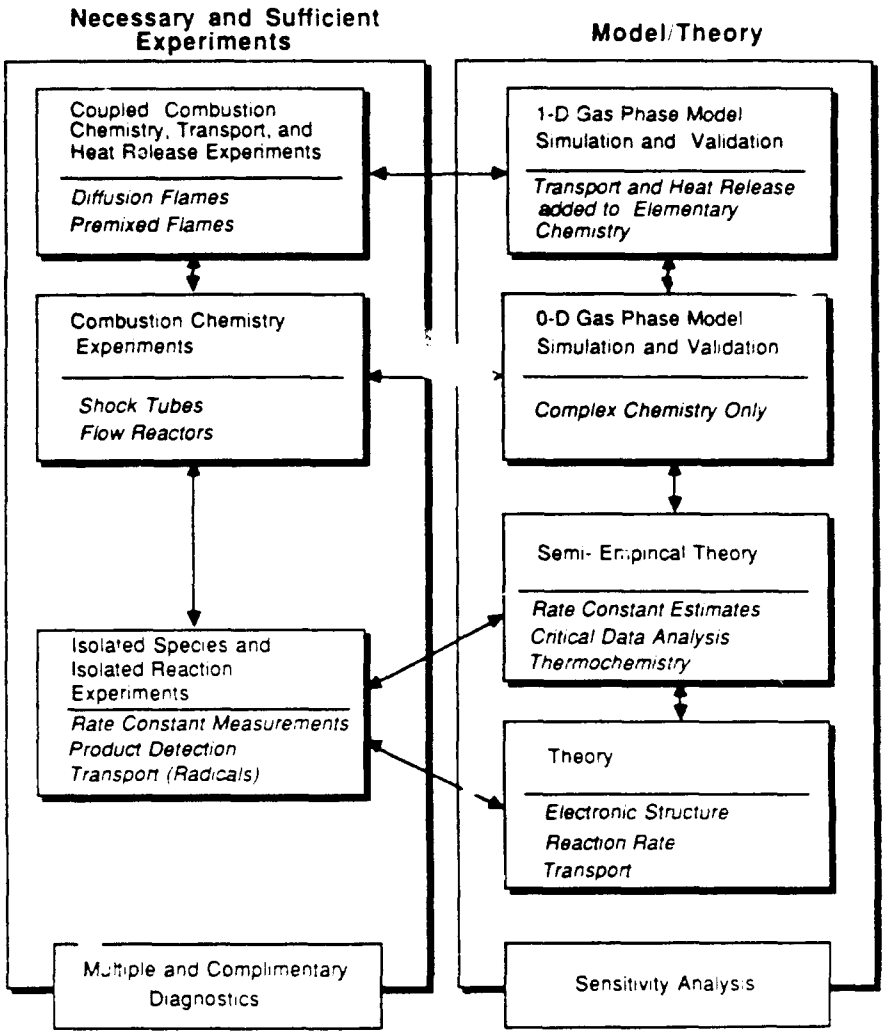

FIGURE 2. Nitrogen Combustion Chemistry and Transport Network Simulation and Validation

prediction with kinetic data from shock tubes and flow reactors. This accomplished, the effects of heat release and species/energy transport are included by simulation and validation of premixed and diffusion flames. Sensitivity analysis techniques are used at each level of theory and model development and validation. In particular, sensitivity analysis procedures are used to identify key species and reactions, and hence, provide an interactive and guiding tool between the elemental and mechanistic kinetic studies. In addition, multiple and complementary diagnostic techniques are applied to each of the experimental programs. The specific tasks of this subprogram include:

- determine via fundamental and semi-empirical theory the thermochemistry and transport properties of key species and the rate constants of key reactions.

- experimentally measure rate constants and reaction products of key reactions and transport coefficients of key species.
- perform critical review and analysis of thermochemical, kinetic and transport data of key species and reactions to yield well-founded reaction mechanisms.
- validate reaction mechanisms and associated rate parameters over well-defined and controllable temperature and pressure ranges with transport-free kinetic data from shock tube experiments and flow reactor experiments.
- validate combustion chemistry with simultaneous large heat release with data from gaseous premixed flames.
- validate transport properties with data from gaseous counter-flow diffusion flames.

The assembly and validation of detailed kinetic mechanisms is an important aspect of developing understanding of chemical processes occurring in propellant combustion. The resulting mechanisms provide useful tools in determining what elementary reactions require improved definition, in acting as benchmarks against which lumped chemistry models can be developed and tested, and in evaluating the interactions of chemistry and transport phenomena in simple one-dimensional systems. Moreover, comprehensive mechanisms, evaluated and validated over larger ranges in pressure, temperature, and equivalence ratio are required for simulating the more practical combustion environments where this gas phase chemistry is intimately coupled with chemical processes occurring at the material surface.

In the analog field of hydrocarbon combustion, the oxidation reaction consists primarily of the sequential fragmentation of the initial fuel molecule into smaller intermediate species, which are ultimately converted to final products, usually dominated by H_2O and CO_2. In many cases, these intermediate species can be treated as fuels themselves. For example, ethylene is an important intermediate of propane combustion and other higher hydrocarbons, but ethylene can also be a primary fuel. Carbon monoxide and hydrogen are common species which are observed during the oxidation of all hydrocarbons, and the same radical species H, O, OH, HO_2, HCO, and others are common to all hydrocarbon combustion. These characteristics can be used to great advantage in constructing reaction mechanisms for complex practical fuels. Reaction mechanisms can be developed systematically, beginning with the simplest species and reactions which are common sub-elements in the combustion of more complex species, and sequentially constructed by incorporating new species and reactions in order of increasing complexity. At each level, the newly added portions of the mechanism must be tested and validated by thorough comparison between numerically predicted and experimentally observed results. However, because of the sequential ordering, only those features which have been added need to be examined closely. This process is given further priorities by identification of the important features through application of sensitivity analysis and reaction flux analysis techniques.

The validation at each level of development of a reaction mechanism requires experimental data from several sources such as shock tubes, flow reactors, and static reactors. It is not sufficient to test a mechanism by comparison with a single experiment, because different elementary reactions can be dominant under different experimental conditions. For example, with many hydrocarbons, reactions between fuel molecules and H-atoms are

dominant in fuel-rich conditions, but much less important in fuel-lean conditions where reactions between fuel and O and OH radicals are most important. Furthermore, no single kinetics experiment covers the entire range of pressure/temperature/ residence time parameters which will be important under combustion conditions. Some reactions are negligible except under high temperature shock tube conditions, while others become unimportant for temperatures above 1000 *K*. Unless a mechanism is to be used only for a restricted class of applications under a specific set of system parameters, it must be validated by comparison with experimental data over wide ranges of physical conditions.

The three experiments mentioned above decouple the chemistry from transport phenomena and excessive heat release rates, and provide mechanistic kinetic data for different time scales of reaction. Typically, shock tubes cover 1-1000 μs and hence are used to study high temperature kinetics (T > 1000 *K*). Flow reactors have time scales typically between 10 and 1000 *ms* and are used to study kinetics at intermediate temperatures (800 *K* < T < 1200 *K*) while static reactors have a time scale between 0.1 and 1000 *s* and are used to study kinetics at low temperatures (T < 800 *K*).

The approach for mechanism development discussed above for hydrocarbon oxidation is also applicable to the construction of reaction mechanisms for the gas-phase intermediates of propellant combustion. An important component to this process not discussed here is the experimental and theoretical studies on individual species and reactions, described in the bottom half of FIGURE 2. Such studies provide the elemental parameter input necessary for mechanism development. These two types of kinetic studies, that is, those devoted to complex reactions and those devoted to isolated reactions, must be conducted interactively for efficient and successful model development. For example, the rates of all possible elementary reactions cannot be practically measured in the laboratory; however, mechanistic studies combined with sensitivity analysis may be used to pinpoint and/or to place priority on those individual reactions which require the most attention.

Once a gas-phase kinetics model has been developed, validation of coupled gas-phase heat release rates and gas-phase transport is required to complete the development and validation of the entire gas-phase thermochemical, kinetics and transport model. The procedure is again hierarchical and is shown schematically in FIGURE 3. Data from premixed flames are necessary to validate heat release rates and flame speed predictions. In premixed flames, kinetics and transport are of almost equal importance; however, the system is almost entirely driven by the heat release and hence the temperature profile through the flame. The ability to deconvolute the kinetics, which produce this heat release, is very difficult due to simultaneous transport processes and the high sensitivity of measured observables to the temperature measurements. Data from diffusion flames are necessary to validate transport and extinction phenomena, in addition to gas- phase kinetics and heat release rates.

The objectives of this research program are to obtain kinetic data from flow reactor experiments and to develop and validate reaction mechanisms for gas-phase intermediates important to the combustion of energetic polycyclic nitramines and energetic binders.The inherent nature of the research requires: (1) an experimental effort for determining reactant, intermediate, and product species profiles as a function of reaction time in a flow re-

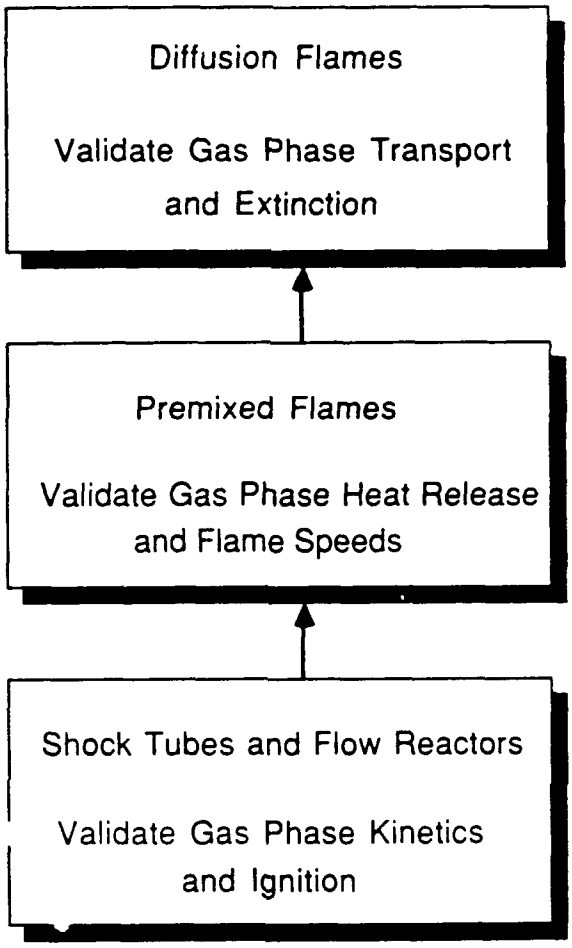

FIGURE 3. Hierarchical Development and Validation of Gas Phase Model

actor. (2) comprehensive reaction mechanism development and accompanying computer modeling, (3) application of existing and developing sensitivity analysis techniques to extract the maximum information from the first two parts of the research, (4) a research effort coordinated and integrated with other laboratories studying similar, yet complimentary, gas-phase kinetics, and (5) coordinated efforts with other laboratories to interface the gas-phase mechanisms developed with heterogeneous reaction chemistry and solid propellant surfaces.

1.2 Program Overview and Status

The experimental aspects of this work are being conducted in a variable temperature (600 $K < T < 1200\ K$), variable pressure (1 *atm* < P < 18 *atm*) flow reactor with residence times ranging from 10 *ms* to 10 *s*. A second variable temperature, atmospheric pressure reactor ($800\ K < T < 1200\ K$) is also available for use. The measurement of reactant, intermediate, and product species concentrations as a function of reaction time via continuous sampling and thermal quenching provide not only substantial definition of the phenomenology of reaction mechanisms, but a much more constrained set of pure kinetic data than can be derived from flame and shock tube experiments. Analytical detection and quantification of stable species includes on-line analysis by Fourier transform infrared. In addition, CO and CO_2 concentrations are measured continuously by non-dispersive infrared, NO and NO_2 concentrations by chemiluminescence, and O_2 concentrations by thermomagnetic analysis. Off-line analysis of stable species includes gas chromatography and gas chromatography/mass spectrometry. Measurement of OH radical concentrations are obtained by line of site absorption and laser induced fluorescence techniques. Temperature measurements are obtained by fine wire silica coated Pt6%Rh/Pt30%Rh thermocouples. Velocity, and hence relative reaction residence times, are obtained from reacting flow pitot static probe measurements and non-reacting flow hot wire measurements.

The modeling aspects of the program emphasize the use of hierarchical reaction mechanism construction and validation along with reaction flux and gradient sensitivity analysis. Sensitivity analysis is used to identify key species and reactions, and hence, provide an interactive tool for coordinating experiment and model development.

Kinetic mechanistic studies are utilized for understanding the experimental observations performed as part of this program as well as for developing comprehensive reaction mechanisms for use in a general propellant combustion model. Construction of comprehensive reaction mechanisms is to be carried out in conjunction with other gas-phase experimental and modeling programs which use shock tubes, premixed flames, and diffusion flames as a source of kinetic data. Each of these experiments provide kinetic data that is complimentary to flow reactor data, which collectively provide the necessary data for developing and validating the most complete comprehensive model, for use in both homogeneous and transport-coupled situations.

The chemical systems of interest include the fuels, H_2, CO, CH_2O, CH_4, C_2H_4, HCN and NH_3 and oxidizers NO_2, N_2O, and NO. Flow reactor studies will be carried out with dilute combinations of fuel and oxidizer chosen from this list, reacting in a bath of nitrogen. The selection of these fuels and oxidizers is based on existing preliminary experimental and theoretical evidence that HCN, CH_2O, N_2O and NO_2 are major gas-phase intermediates of polycyclic nitramine combustion, each being produced near or at the surface of the burning propellant. Ammonia is a convenient source of NH_2 and NH radicals, both of which are important unstable intermediates in the oxidation and decomposition of nitramines. Ethylene and methane are selected as representative gas-phase intermediates produced from the combustion of energetic binders. The proposed hierarchical structure among the fuels follows three paths: a reaction sequence of stable carbon species, C_2H_4 -> CH4 -> CH_2O -> CO/H_2O -> H_2, and two reaction sequences of stable fuel bound nitrogen spe-

cies, HCN -> CO/H_2O-> H_2 and NH_3 -> H_2. Here the kinetics of each system to the right of the other is a submechanism of the former. The oxidizer nitrogen chemistry typically follows the sequence NO_2 -> NO -> N_2O -> N_2. Studies will begin with the simplest systems and proceed towards the more complex.

The result of this work will be state-of-the-art detailed reaction mechanisms validated over the temperature and pressure ranges of the flow reactor experiments for the chemical systems described above. With results from other gas-phase kinetic experiments, a single comprehensive reaction mechanism may be developed for use in 1-D and 2-D composite propellant combustion models which include coupled gas-phase/heterogeneous chemistry.

During the past year, a Nicolet Model 730 FTIR was installed and calibrated for the measurement of oxides of nitrogen, simple hydrocarbons, carbon oxides and water. Under other funding, a continuous selective analytical technique has also been developed for molecular hydrogen. Experiments and modeling calculations were conducted on the kinetics of N_2O and NO_2 decomposition (1000 *K* -1100 *K*, 3 *atm.* - 6 *atm.*), and on the reactions of H_2 with N_2O (925 *K* - 1073 *K*, 1 *atm.* - 3 *atm.*) and H_2 with NO_2 (803 *K* - 873 *K*, 3 *atm.*)

1.3 Report Outline

Section 2.0 presents the flow reactor experiment. A discussion of the modifications made to this system that were required in order to study the kinetics of nitrogen oxidizers is given, as well as the procedures used to measure and quantify the concentrations of the oxides of nitrogen. A discussion of the modeling approach is given in Section 3.0. The current reaction mechanism is also described in this section. In Section 4.0, a description of the studies on N_2O decomposition and on its reaction with H_2 are given. Section 5.0 presents the results of kinetic studies on NO_2 decomposition and its reaction with H_2. Finally, Section 6 describes the current and on-going research.

2.0 FLOW REACTOR EXPERIMENT

2.1 The Atmospheric and Variable Pressure Flow Reactors

Flow reactor experiments are unique in providing experimental data in a range of conditions typically not accessible in shock tubes and static reactors yet still of significant importance to propellant combustion. From such experiments, the evolution of stable reactants, intermediates and product concentrations for chemical reacting systems are defined in considerable detail producing highly constrained sets of data for model development. In fact, this technique (described in detail in APPENDIX A) has been the source of much of the previous intermediate temperature, atmospheric pressure data for the oxidation of methane, ethylene, propane, n-butane, carbon monoxide/hydrogen, octane (Hautman, 1981; Proscia, 1983; Westbrook and Pitz, 1984; Pitz, *et al.*, 1984; Westbrook *et al.*, 1983; Westbrook and Dryer, 1984; Yetter, 1985; Brezinsky and Dryer, 1985, 1986; Dryer and Brezinsky, 1986; Axelsson *et al.*, 1988; Dryer, 1989) and simple aromatics (Brezinsky, 1985; and subsequent work of Prof. I. Glassman and his colleagues). These data have

provided not only phenomenological insights into mechanisms for pyrolysis and oxidation, but a source of information for validation of detailed mechanisms, and a means to study the intimate coupling of elementary reactions.

The variable pressure flow reactor accesses a range of pressures (0.1 to 28 atmospheres by design, 1.0 to 18 atmospheres in present operation), and a wider range of temperatures (from as low as 600 *K* to 1200 *K*) with improved experimental control and diagnostics, in comparison to those of the atmospheric pressure flow reactor (APPENDIX A). Available reaction times as short as 50 milliseconds and as long as 10,000 milliseconds are possible, all with the same experimental method, and without having to consider heterogeneous wall effects on the measured homogeneous kinetics. In addition to the pressure range now accessible in this system, several other new experimental features have been incorporated into this system. The addition of a Nicolet Model 730 FTIR permits on-line measurement of most of the IR absorptive stable species of interest under this research effort to determine levels of about 0.1 *ppm*. The new design of the high pressure flow reactor also allows for improved optical access, permitting simultaneous insitu optical diagnostic detection of unstable species. The integration of the entire experiment (experimental operation and data acquisition) into a closed loop control computer based system allows for more frequent experiments and improved data collection.

The upper residence time limit criteria for flow reactors is the maintenance of convective residence times which are short in comparison to diffusion times to the reactor wall surface. This limiting criteria is strongly influenced by the selection of the flow reactor diameter. Estimating the order of the diffusion time to the wall as

$$\tau_d = d^2 / 4\ D$$

where d is the diameter of the reactor tube and D is the mass diffusion coefficient, and the convective residence time as

$$\tau_c = L/u$$

where L is the length of the reactor duct and u is the mean flow velocity. $\tau_d >> \tau_c$ when

$$(Re)(Sc) >> 4L/d$$

where *Re* designates the flow Reynolds number based on the reactor duct diameter and *Sc* designates the Schmidt number of the carrier gas. For the present parameter conditions, this translates to

$$(Re)(Sc) >> 40$$

As the Schmidt number is the order of one, this means the flow Reynolds number should be much larger than 40 to meet this condition. The reactor is intended to be run only at Reynolds numbers greater than about 1000. As the duct L/d downstream of the mixer section will always be less than 10, the flow is not fully developed. As the boundary layer develops at the duct surface, radially uniform conditions continue to exist near the flow centerline. As the flow field further develops, axial velocity will change as a function of

distance from the mixer section. Axial velocity profiles must therefore be defined in order to determine the relative reaction time as a function of distance from the mixer to the sampling position.

However, very important implications result from these observations, particularly at increased operating pressures. FIGURES 4 and 5 show Reynolds number of the flow for a 10 *cm* diameter reactor duct as a function of available reaction time for various operating pressures and temperatures. Note that at higher pressures and lower reaction temperatures, the reaction test times at Reynolds numbers exceeding 1000 cover a range from 10 milliseconds to more than 10,000 milliseconds. This new facility therefore presents the possibility of studying kinetic issues over a very range of conditions, including a temperature range previously available only in static reactors.

One of the basic design principles of static reactors is that diffusive transport is rapid with regard to chemical reaction and energy release so that the local conditions within the reactor remain homogenous, and isothermal. Reaction times under these conditions are typically in excess of many tens of seconds, and thus, diffusion of radical and unstable molecular intermediates to surfaces result in perturbations of the gas phase chemistry. There are no such surface effects in the variable pressure flow reactor.

The design concept of the variable pressure flow reactor is based on fixing the diagnostic sampling position, and moving the point of fuel injection relative to this location to vary the relative reaction time one wishes to observe. The approach is very similar to that which is normally performed in the study of pre-mixed laminar one dimensional flames where the burner rather than the diagnostic sampling position is moved. This approach not only permits very short gas sampling residence times to continuous, on-line diagnostic instruments (important for on-line measurement of low-stability molecular species such as aldehydes and other oxygenates), but simple accommodation of optical diagnostics at the sampling location. Crossed-beam optical access ports (normal to the flow direction) are positioned at the same location at which a hot water cooled, wall convection quenched, gas sampling probe and silica coated thermocouple probe are axially located. Optical diagnostic measurements of OH using existing line resonance absorption or fluorescence techniques (Linteris, 1991) can be much more easily accomplished than in the atmospheric pressure flow reactor, and other insitu optical measurements, including insitu FTIR and other resonance absorption measurements can also be added to the facility in the future.

A schematic diagram of the variable pressure flow reactor is given in FIGURE 6. Nitrogen carrier gas with oxidant flows from left to right in the figure. Fuel, along with about 10%of the total nitrogen carrier flow is injected into the carrier and oxidizer stream at a mixer on the left end of a conical silica foam diffuser. The mixer is jet stirred and has a nominal turnover time of about 0.5% of the total test time. The flow reactor is operated as a steady, isobaric flow device and the time from mixing to sample position is varied by moving the mixer / diffuser assembly along the quartz test tube. At the right end is the fixed sample location.

The shell is made of 12" standard weight carbon steel pipe and is ASME stamped for operation from full vacuum to 30 *atm* and 245 *K* to 533 *K*. The pressure shell is designed to

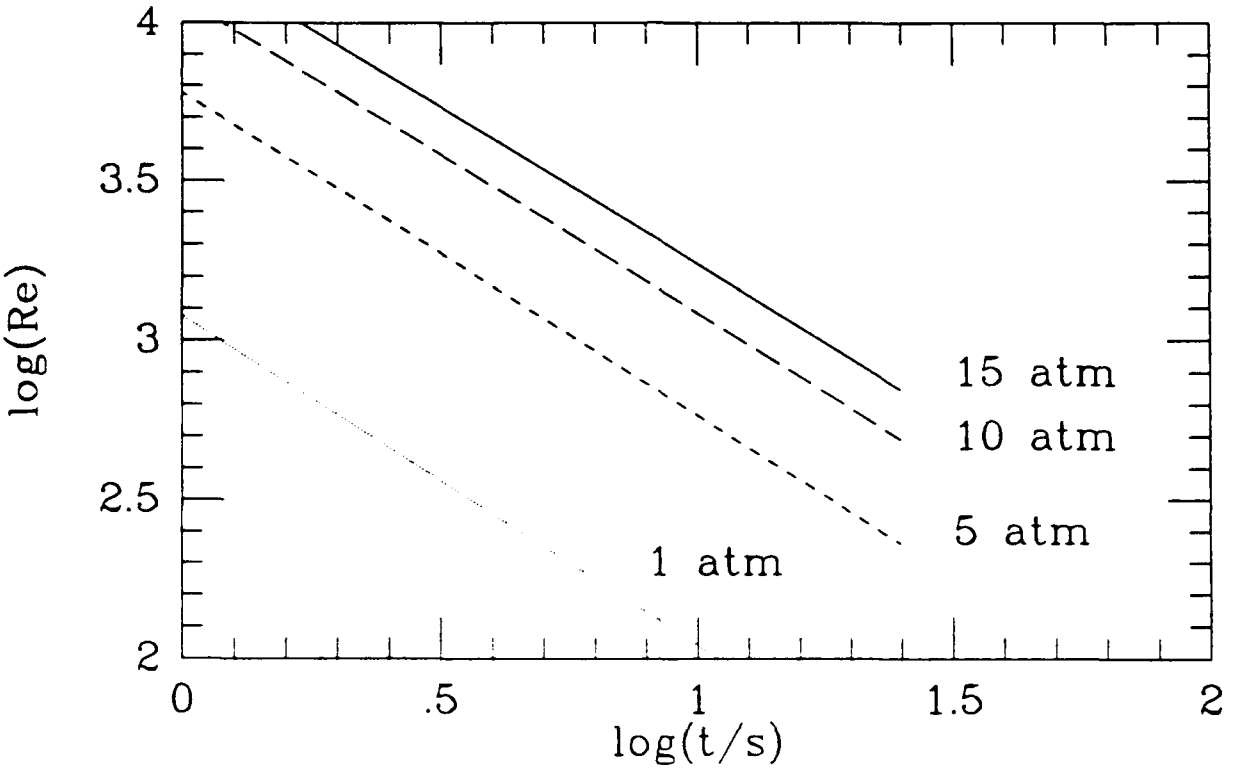

FIGURE 4. Operational Reaction Test time as a Function of Flow Reynolds Number and Operating Pressure for a 10 cm Diameter Reactor Duct

enclose not only the reactor section (the reactor duct heaters and insulation), but also the positioning mechanism and fuel vapor injection probe which axially locates the fuel/carrier mixing section relative to the sampling position. This design results in very low thrust to move probes (due to pressure drop across flanges) and eliminates the need for critical dynamic seals. Since all flanges are at lower temperature, there is also no need for exotic materials of construction to be used for the pressure shell nor elaborate designs required to maintain pressure seals.

The reactor duct itself is a 173 *cm* long, 2 *mm* wall thickness, 10.16 *cm* inside diameter, fused silica tube which extends from a Inconel mating flange at the fuel injection probe entrance to a similar mating flange located at the entrance to the exhaust port of the reactor

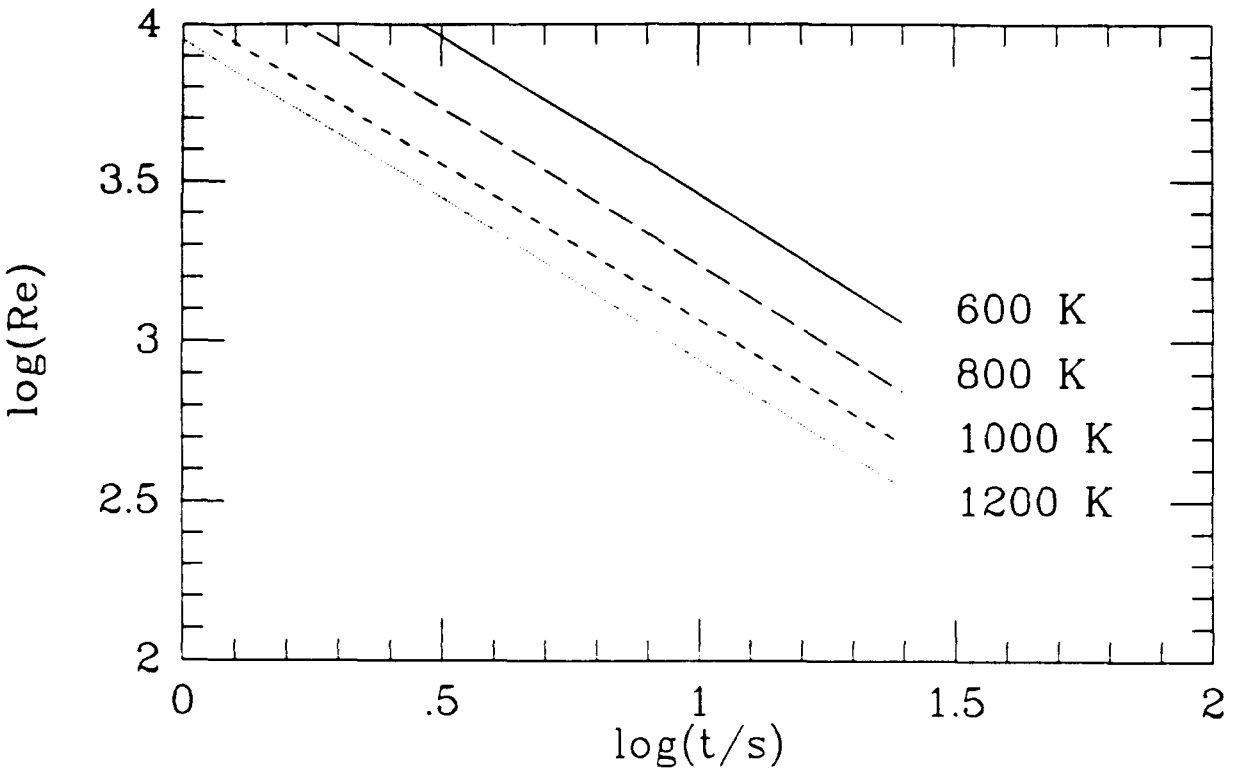

FIGURE 5. Operational Reaction Time as a Function of Flow Reynolds Number and Flow Temperatures and 15 Atmosphere Operating Pressure for a 10 cm Diameter Reactor Tube

shell. A maximum of about 100 *cm* and a minimum of 1 *cm* of axial distance from the exit of the mixing section to the sampling position are possible. In principle, reactor duct diameter should be able to be reduced to as small as 5 *cm* inside diameter by replacing the inconel mating flanges, the reactor duct itself, and installing a smaller diameter mixing section. The carbon steel shell is manufactured in two separate parts in order to accommodate such changes.

A cross section of the fuel mixer and diffuser is shown in FIGURE 7. The mixer section is approximately 47 *cm* long and is machined from a low porosity, silica foam block to an outside diameter about 0.1 *mm* less than the nominal 10.16 *cm* inside diameter of cylindrical reactor duct. The interior contour of the mixer section is shaped as a converging/di-

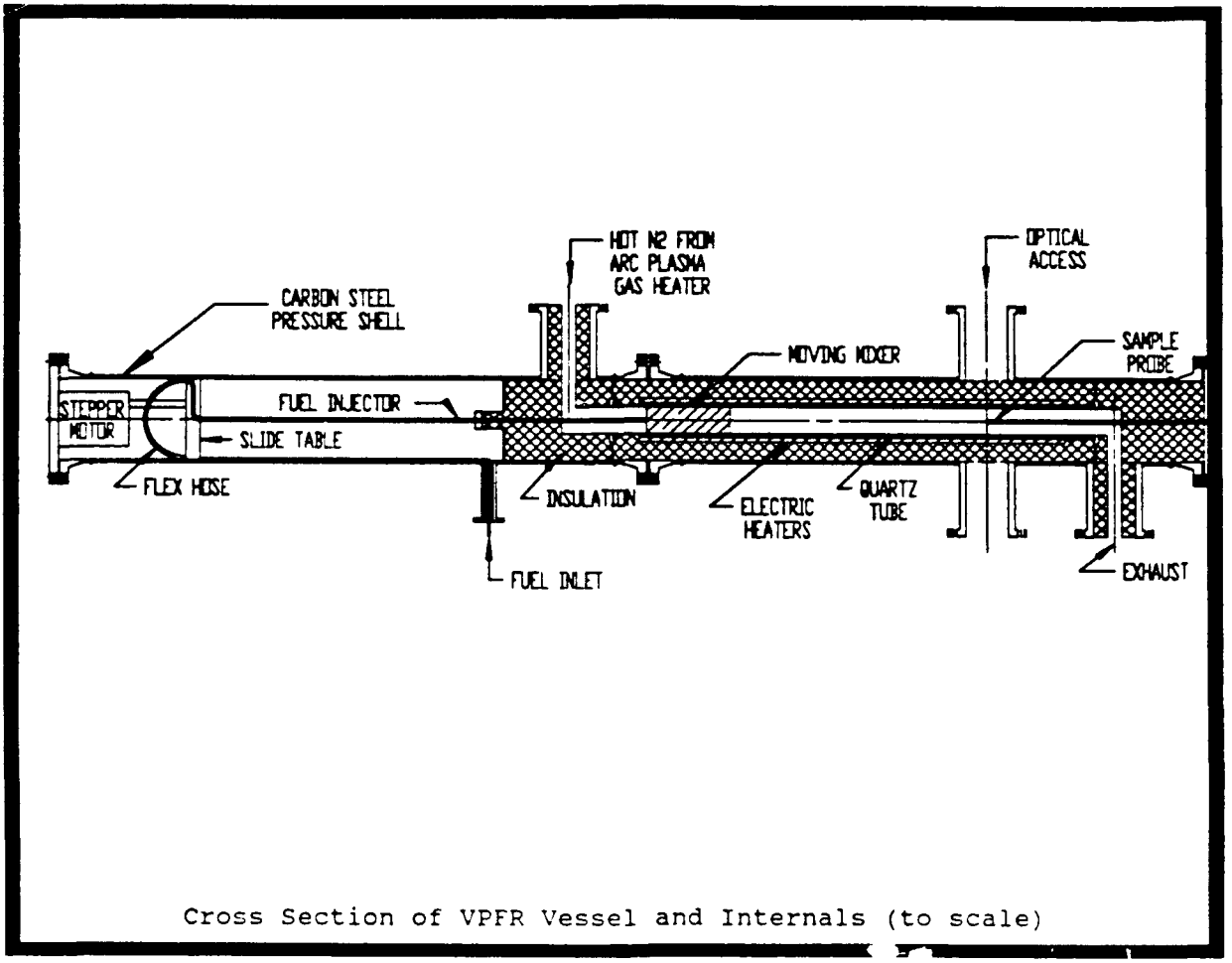

FIGURE 6. Schematic of variable pressure flow reactor design

verging nozzle with a throat diameter of 2.5 *cm* and an expansion half angle of 7 degrees. Flow resistance through the long annular space between the mixer section and reactor duct wall is very large in comparison to that through the central venturi and nearly all of the carrier flow therefore passes through the central venturi. One inch long ceramic fiber piston ring seals are added at both the upstream and downstream ends to minimize leakage between the diffuser and the quartz test tube. The mixer - diffuser section consists of a central round baffle plate which forces the nitrogen-oxidizer flow out to the reactor tube wall and then radially inward through a gap between the plate and the upstream end of the diffuser. Fuel and diluent nitrogen are delivered to the mixer through a fuel vapor injection probe, which is used also to move the diffuser. The fuel vapor injection probe is partially insulated from the carrier flow to prevent premature pyrolysis reactions of the nitrogen di-

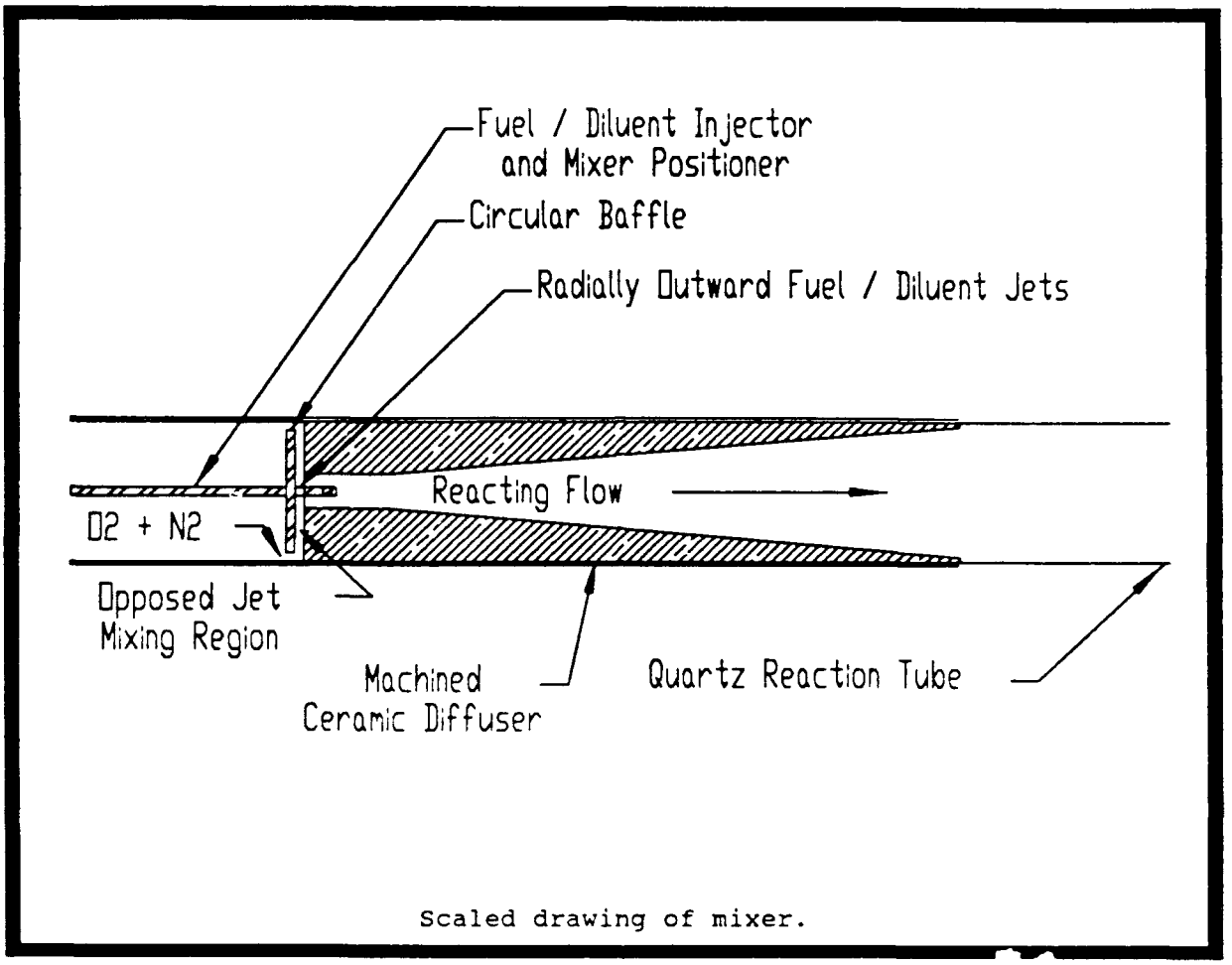

FIGURE 7. Schematic of mixer and diffuser section

luted fuel vapor inside the probe from occurring. All fuels are premixed into varying amounts of added nitrogen diluent to reduce residence time within the fuel injection probe. The injector for the present experiments was fabricated from a 316 stainless steel 6.35 *mm* outside diameter *X* 0.9 *mm* thick wall tube. The fuel-diluent flow is then injected radially outward into this radially inward flow through eight 0.25 *mm* diameter jets equally spaced around the circumference of the injector tube. All gas flows are measured with Teledyne-Hastings mass flow meters with a maximum range of uncertainty in any gas flow estimated to be about 2% of full scale, which for the present experiments translates into an uncertainty range of not more than 6% for the nitrogen and oxidizer flows.

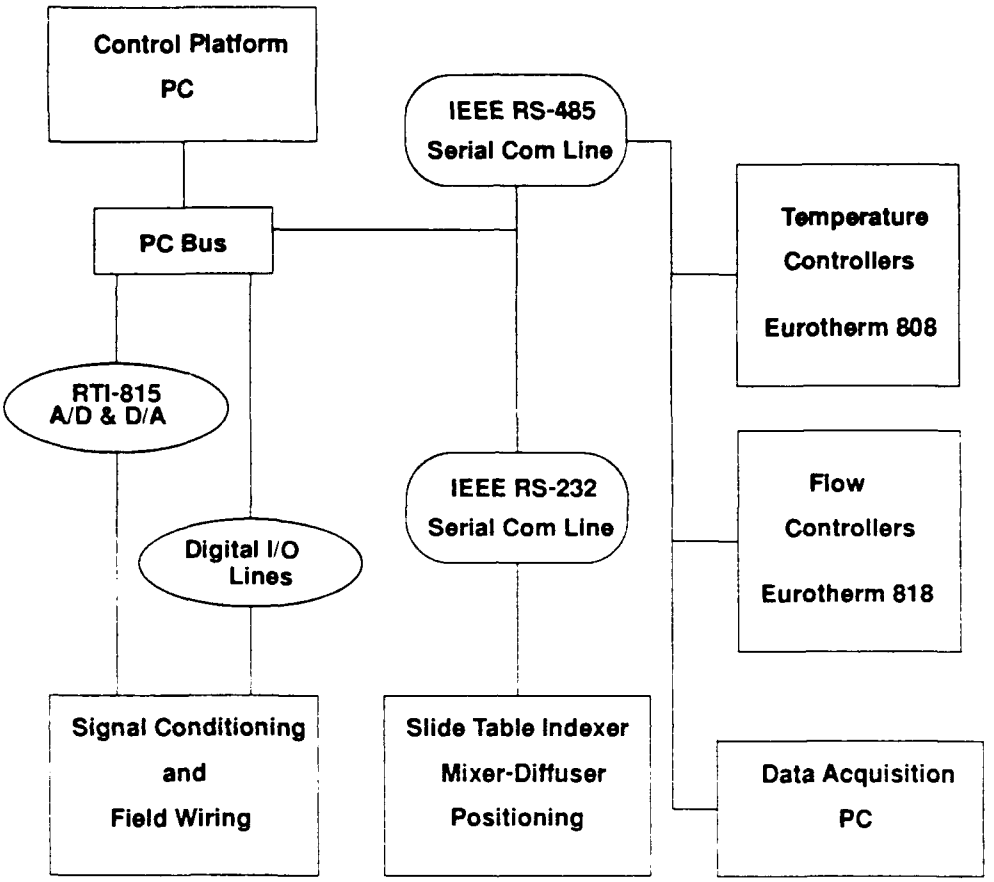

FIGURE 8. Block Diagram of the Control System for the Variable Pressure Flow Reactor

Because of the relatively high heating rates involved (tens of *kw*), as well as the temperatures involved in some of the systems to be studied (as high as 1,100 *C*, the limitation of the quartz test tube), an arc plasma gas heater is used to heat the carrier gas. The arc plasma torch heater is similar to that used for the last fifteen years at Princeton. A new microprocessor-based flow and arc power control system has been designed to vary the plasma power input and thermal efficiency for controlling the carrier flow temperature, as monitored at the fuel/carrier mixer location (thus radiation losses to the fuel injection probe from the carrier gas do not affect the inlet carrier temperature). Automated control systems represent another important design improvement, since the precision of the quasi-steady operation of a flow reactor, particularly its temperature field, affect the accuracy of the kinetic measurements. To our knowledge other flow reactor systems have not yet developed

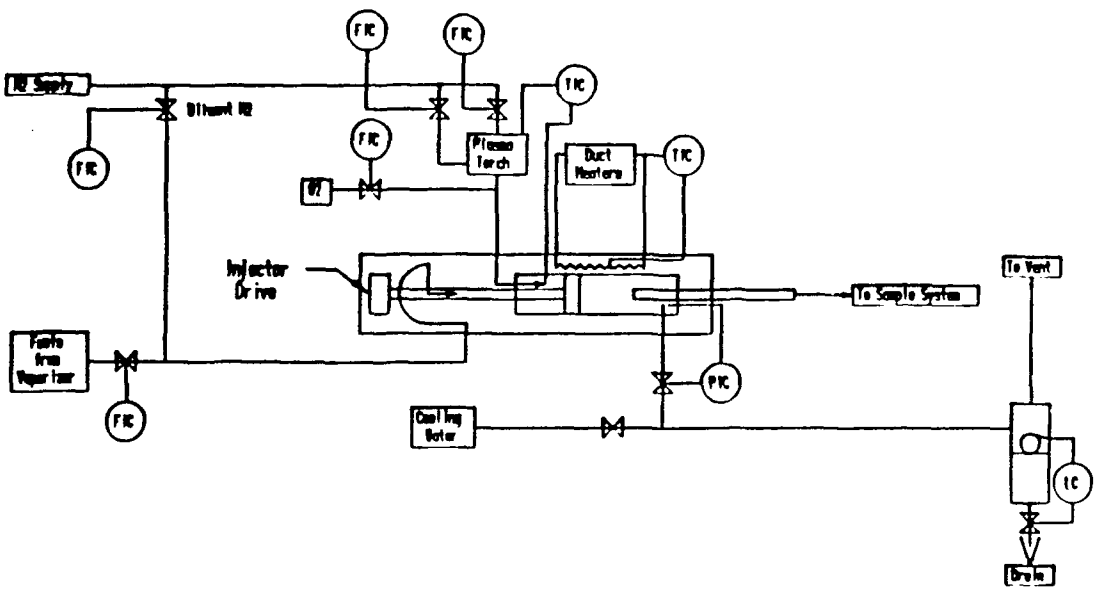

FIGURE 9. Gas Flow Control Schematic for the Variable Pressure Flow Reactor

or implemented integrated controls. A 35 *kw* electric resistance gas heater has been developed to replace the arc plasma gas heater to operate at low flow (less than 5 *g/s* total), low duty (less than 10 *kw*), high pressure (above 10 *atm*) conditions. FIGURE 8 shows schematically the control approach used in the new reactor facility design, while FIGURE 9 shows the flow systems design. All flows are monitored by electronic mass flow meters and positioning of motor driven metering valves are controlled by Proportional - Integral - Derivative (PID) Controllers which sense the mass flow meter output. Similar closed loop controllers are used to control all heater temperatures and the flow reactor operating pressure. Operating pressure of the reactor is controlled by closed loop control of a high temperature back pressure valve in the exhaust flow section. The PID controllers may be

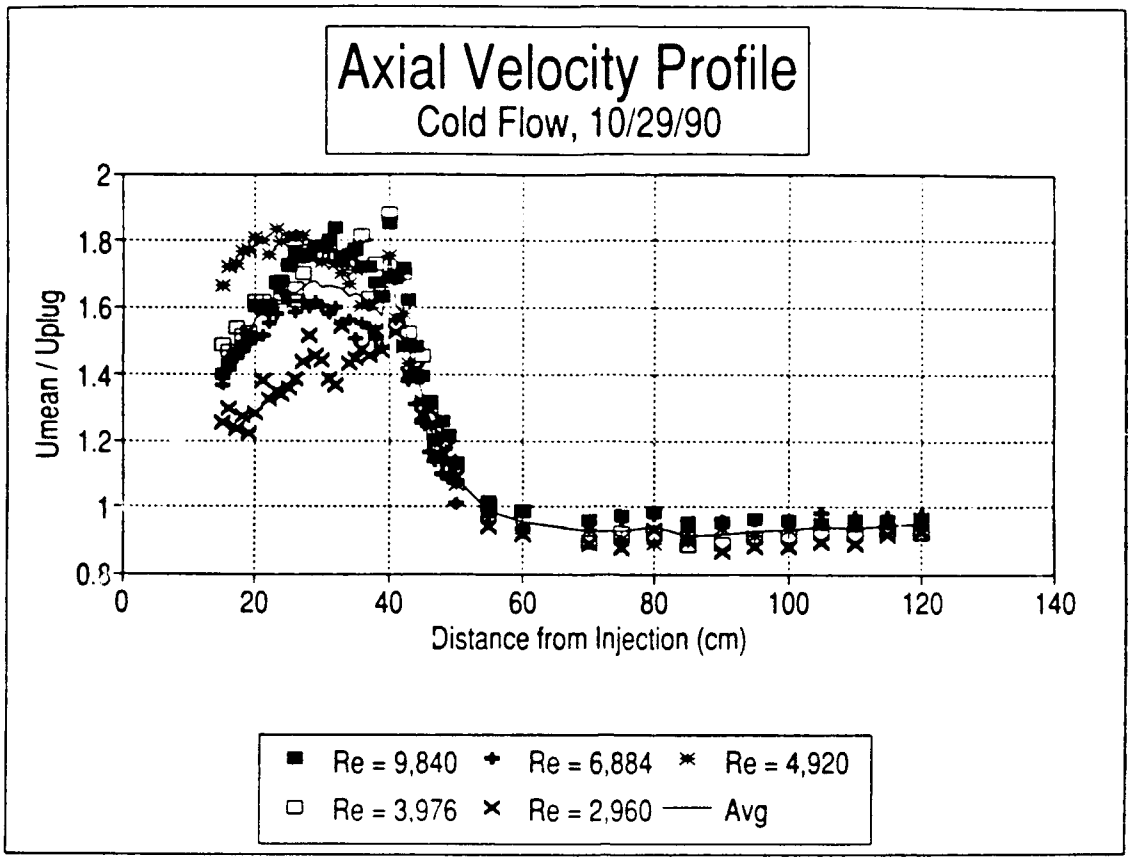

FIGURE 10. Normalized centerline velocity profile from hot wire anemometry measurements

manually operated. Each controller is also linked to a IBM/PC/AT microprocessor via a RS-485 port connection so that all control parameters may be read or altered by the PC.

In order to translate flow reactor position into reaction time, the mean velocity distribution along the centerline is required. The centerline velocity profile is measured with a TSI Model 1750 hot wire anemometer. These measurements are performed in the reactor under cold flow conditions. Typical mean velocity measurements are reported in FIGURE 10. The corresponding root mean square velocities (U_{rms}) are reported in FIGURE 11. The U_{rms} measurements show that the turbulence is decaying over the length of the reactor. However, examination of FIGURE 10 shows that the flow in the diffuser and test section is nearly plug flow. The reaction time is obtained by integration of the test section velocity profile. An effective flow area table for the diffuser and test section is constructed from the cold flow hot wire anemometry velocity survey. Effective flow areas from this table, along with the measured flow rates, temperatures and pressures are used to obtain the local values of $u(x)$. Residence time is then obtained by numerically integrating

$$t = \int_0^x \frac{dx}{u(x)} .$$

The maximum uncertainty in reaction time, including the mixing time (0.5%), the uncertainty in the velocity survey (6%), the uncertainty in flow measurements (6%), the uncertainty in probe position (0.4%), and the sample quench time is +/- 7%.

The sample temperature is measured with a silica coated Pt6%Rh/Pt30%Rh thermocouple. The total estimated uncertainty in temperature measurement, including allowance for

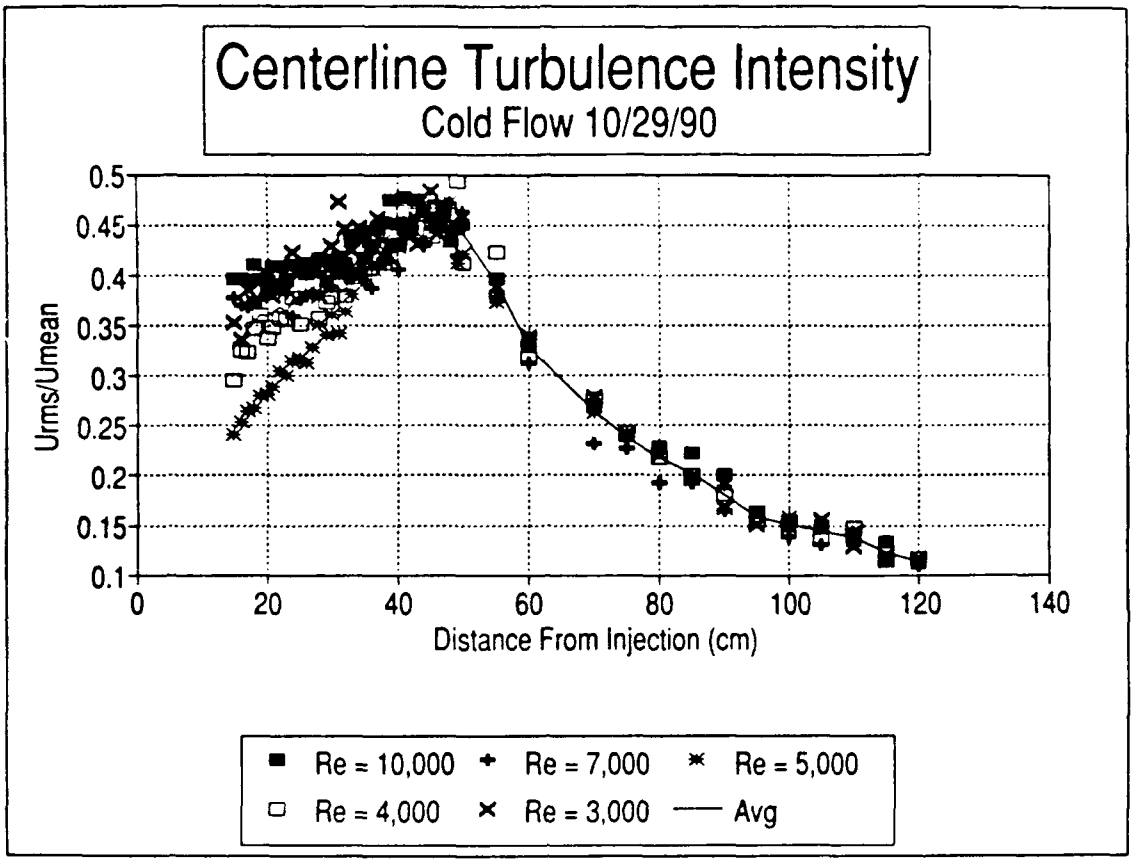

FIGURE 11. Centerline turbulent intensity profile from hot wire anemometry measurements

radiation errors due to the proximity of the cold sample probe is estimated at +/- 10 *K*. The relative uncertainty in temperatures within an experiment are estimated to be +/- 1 *K*.

A hot water cooled, stainless steel sample probe is mounted in the reactor end flange and is used to continuously extract and convective quench a small portion of the reacting gases. Quench times estimated for atmospheric pressure flow reactor operation at 1 *atm* are of the order of 0.0005 *s* for quench to 600 *K* to 0.002 *s* for quench to 400 *K* (not more than 2% of total test time). These estimates are based on a finite difference model that was calibrated with actual temperature measurements (Emdee, 1988). The quench time scales with the characteristic time for diffusion of energy from the centerline of the sample tube to the wall of the sample tube, and thus, the quench time is proportional to the experimental pressure. Because kinetic times are typically inversely proportional to the pressure, the quench times are estimated to be of the order of 1% of the test times at all pressures. From the probe, the gas sample flow is sent to a FTIR, a continuous electrochemical analyzer for O_2, continuous NDIR analyzers for CO and CO_2, and to a continuous selective detector for H_2. A diagram of the sample train is given in FIGURE 12. Data acquired by these instruments is forwarded to an a/d board interface and recorded on a hard disk based microprocessor system. As in the atmospheric pressure flow reactor, this continuous sampling and analysis system will also accommodate intermittent sample trapping for gas chromatographic analysis. A gas sampling and storage technique for interfacing with gas chromatographs and gas chromatograph/mass spectrometers, developed here for the AFPR and used extensively in our previous work, continues to be available.

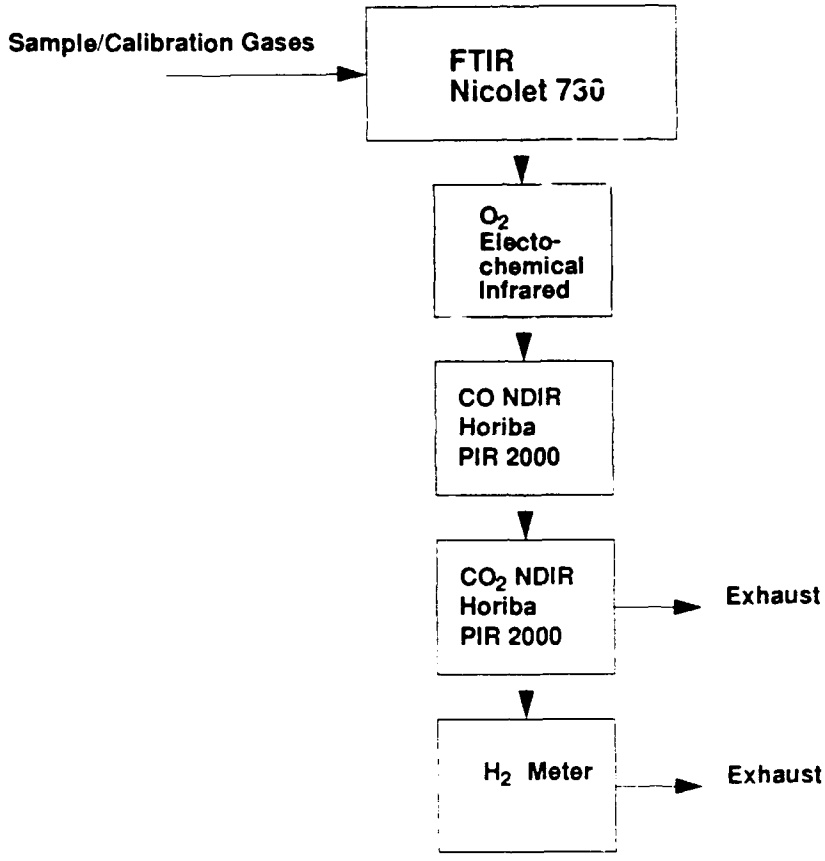

FIGURE 12. Schematic of sample train

Species and temperature profiles are obtained by positioning the diffuser - mixer section at equally spaced locations along the length of the reactor centerline. About 2.5 minutes of time is required for the sample flow to purge the 0.5 liter FTIR gas cell. Stabilization of the oxygen, carbon monoxide, carbon dioxide concentrations as indicated by the on line analyzers, which are upstream of the FTIR in the sample line, provides verification of adequate purging. The FTIR purge time is currently the factor that limits the data collection rate.

The variable pressure flow reactor facility is located immediately adjacent to a laser diagnostic facility (developed under a DOE University Research Initiative grant) which has already been used to make laser resonance absorption and fluorescence measurements of

OH in the atmospheric pressure reactor (Linteris, 1991). Adaptation of this facility to the variable pressure flow reactor involves primarily optics development for transferring the laser beam to the facility and mating window designs for the reactor shell, and should be completed within the coming year.

2.2 Flow reactor modifications for N_2O and NO_2

A number of modifications to the apparatus and experimental procedure have been necessary for studies with N_2O and NO_2 as oxidizers. First, both N_2O and NO_2 decompose slowly at the conditions under study here (see the discussion later in this report). Consequently, their addition to the carrier gas upstream of the mixer-diffuser section was not acceptable. This difficultly for the present studies was overcome by introducing the N_2O and NO_2 through the fuel injector right at the mixer. Thus, when the H_2 reaction was studied, H_2 was added upstream of the mixer-diffuser section.

Second, because of the large mass flows of N_2 required in the system (e.g. 35 *g/s*), nitrogen is stored as a liquid and vaporized prior to its introduction into the reactor. Small quantities of molecular oxygen (typically less than 30 *ppm*) may be present in the flow, which will be shown later to affect the kinetics of the N_2O system. This problem was reduced by the addition of the H_2 upstream of the mixer, allowing time for the O_2 to be consumed by the H_2 prior to N_2O or NO_2 injection.

The third and most serious problem was the present choice of construction material utilized for the baffle plate and the injector tube itself stainless steel). Hot stainless steel surfaces can act as a catalyst for NO_2 particularly at surface temperatures higher than approximately 930 K. For the present set of experiments with NO_2, this temperature was an upper limit. The mixer-diffuser section has been redesigned and all of the stainless steel components are currently being replaced with quartz.

2.3 Measurement of Oxides of Nitrogen and Water Vapor

A Nicolet Model 730 fourier transform infrared analyzer (FTIR) is used to measure the oxides of nitrogen and water vapor for the current results and will be used for measurement of other reactants in future studies, e.g., compounds containing up to four carbon atoms. On-line FTIR should also be able to measure accurately some species which cannot be stored (without chemical stabilization) for later off-line analysis using gas chromatographs, etc., such as hydrogen peroxide, formaldehyde, and other oxygenates.

The analyzer has a 0.5 liter gas cell with a optical path length of 8 *m*. A liquid nitrogen-cooled MCTA detector is used to measure spectral absorbance with a resolution of 0.5 cm^{-1}. Multivariate least squares fit software is used for quantification of the spectral data.

Calibrations for NO, N_2O and NO_2 were obtained by measuring absorbance for different concentrations of each compound in nitrogen (minimum of three) from calibrated gas cylinder bottles supplied by MATHESON. Examples of spectral calibration data are given in FIGURES 13-15 for 7260 *ppm* of N_2O in N_2, 500 *ppm* NO in N_2, and 2996 *ppm* of NO_2 in N_2, respectively.

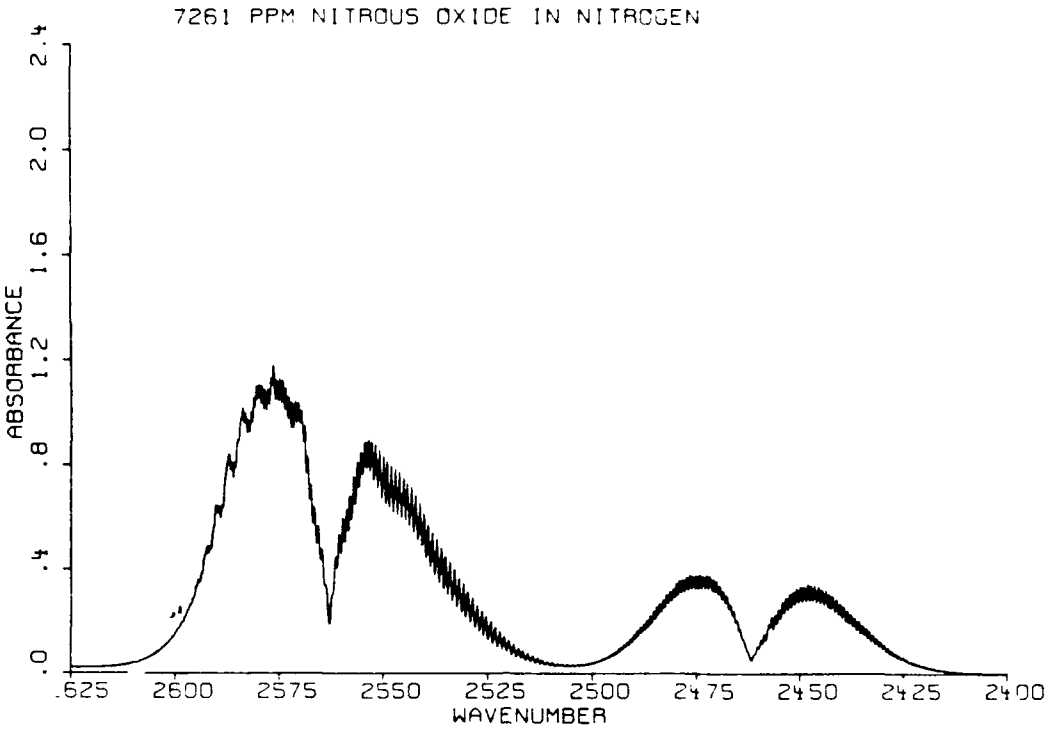

FIGURE 13. Absorbance Spectrum from Nitrous Oxide in Nitrogen

The FTIR has also allowed measurement of water vapor concentration. This measurement is important because it permits closure of the hydrogen atom mass balance, which is typically not available in most kinetic studies. Water calibrations were made from the catalytic oxidation of a known amount of H_2 in an O_2/N_2 mixture. An example of the spectra for 4000 *ppm* of H_2O in N_2 is given in FIGURE 16.

An example of the spectra from an actual H_2/N_2O experiment is reported in FIGURE 17 illustrating the well resolved spectra. All of the spectra reported here were obtained with 32 scans.

2.4 Measurement of Molecular Hydrogen

Molecular hydrogen is present in most combustion processes in concentrations from parts per million (*ppm*) to several percent by volume. However, hydrogen is inherently difficult to quantify in multi-component mixtures. The significance of the hydrogen molecule, as either a primary fuel or an intermediate in hydrocarbon oxidation, makes its measurement very important. Existing direct methods of hydrogen detection include gas chromatography with a thermal conductivity detector (TCD); however they require collection of individual gas samples and relatively long analysis times. Under other support, a new technique has been developed to continuously measure the amount of hydrogen in the flow of a gaseous mixture. A detailed description of the system will be available following a patent evaluation on the device (which is presently underway).

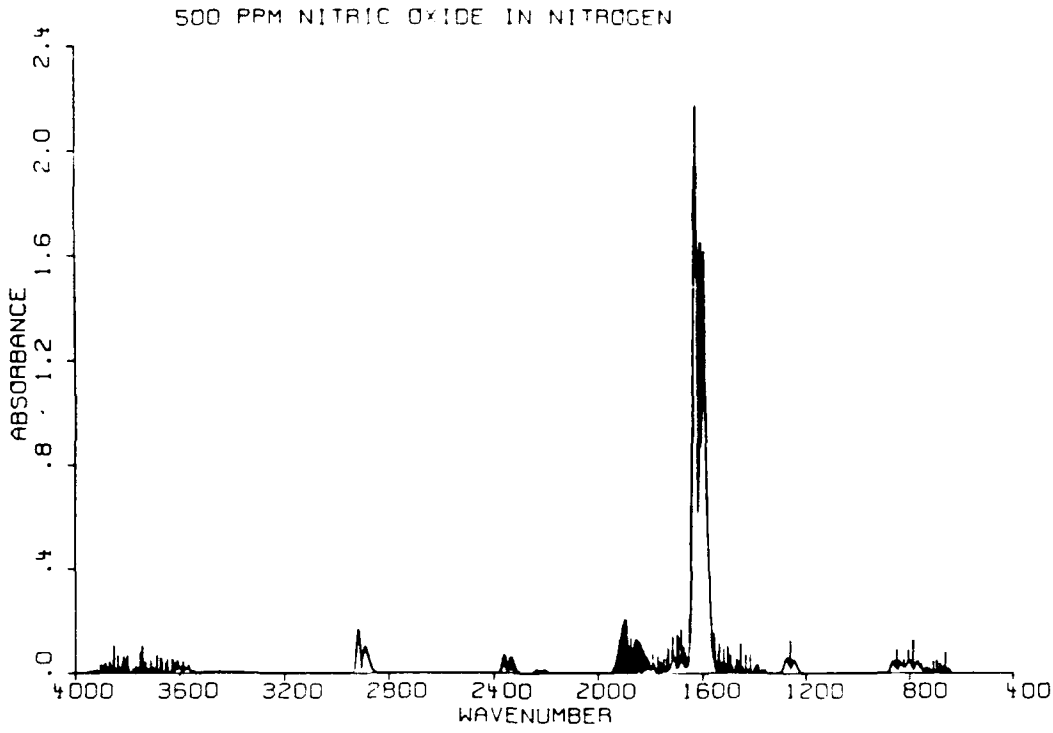

FIGURE 14. Absorbance Spectrum of Nitrogen Oxide in Nitrogen

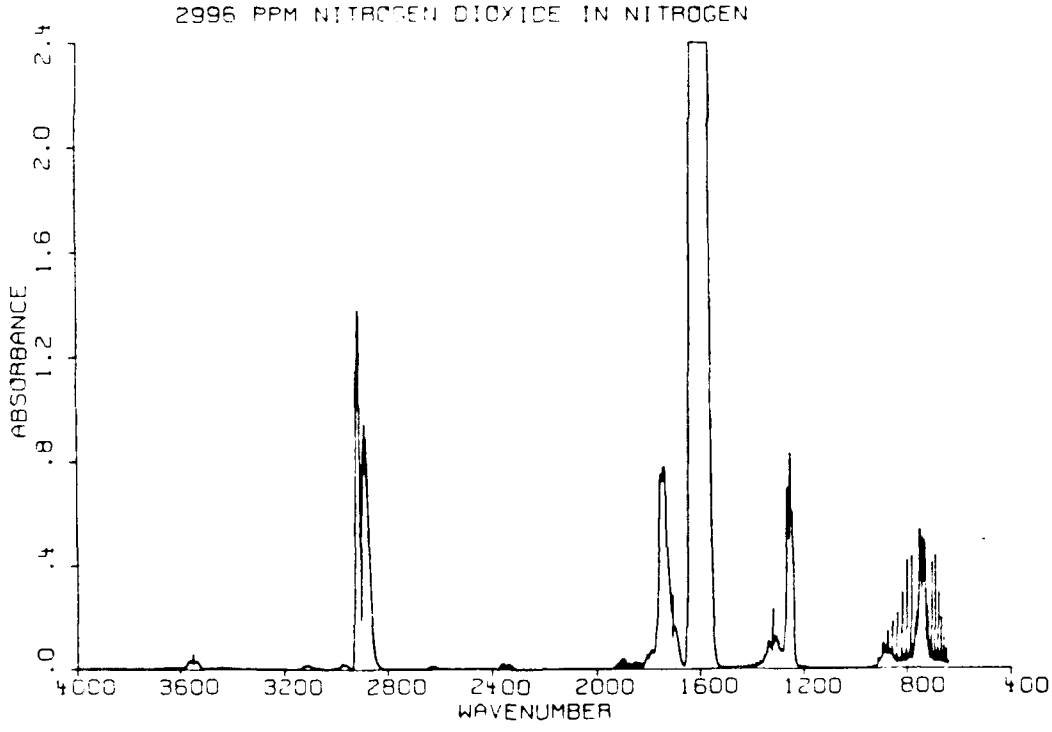

FIGURE 15. Absorbance Spectrum of Nitrogen Dioxide in Nitrogen

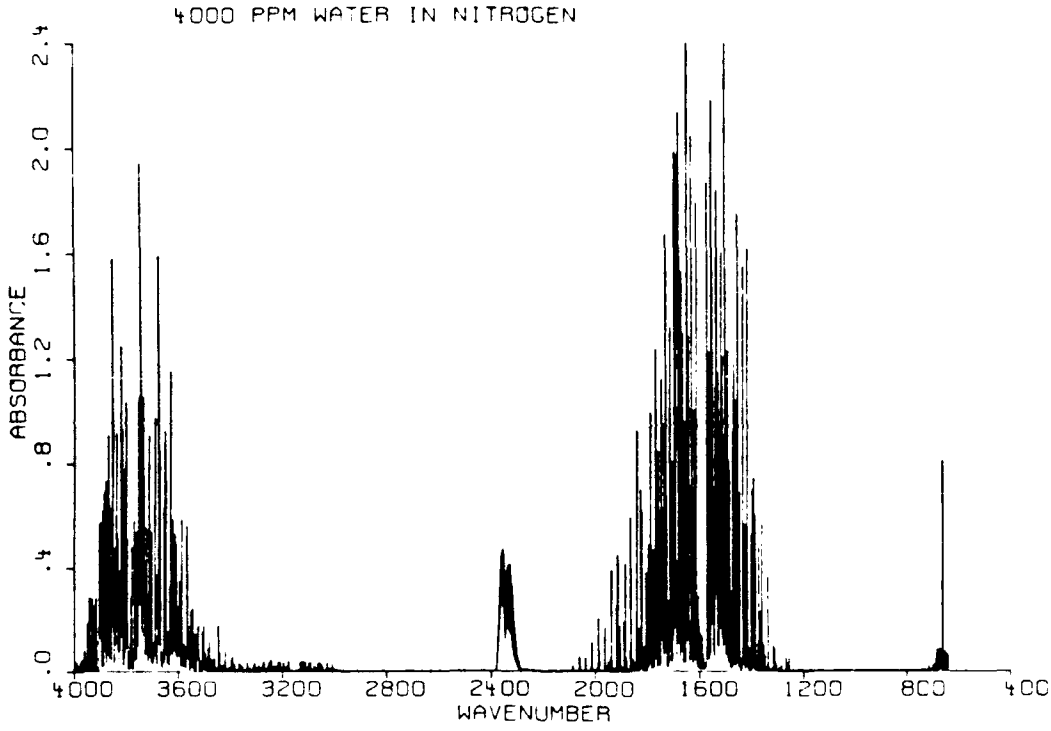

FIGURE 16. Absorbance Spectrum of Water in Nitrogen

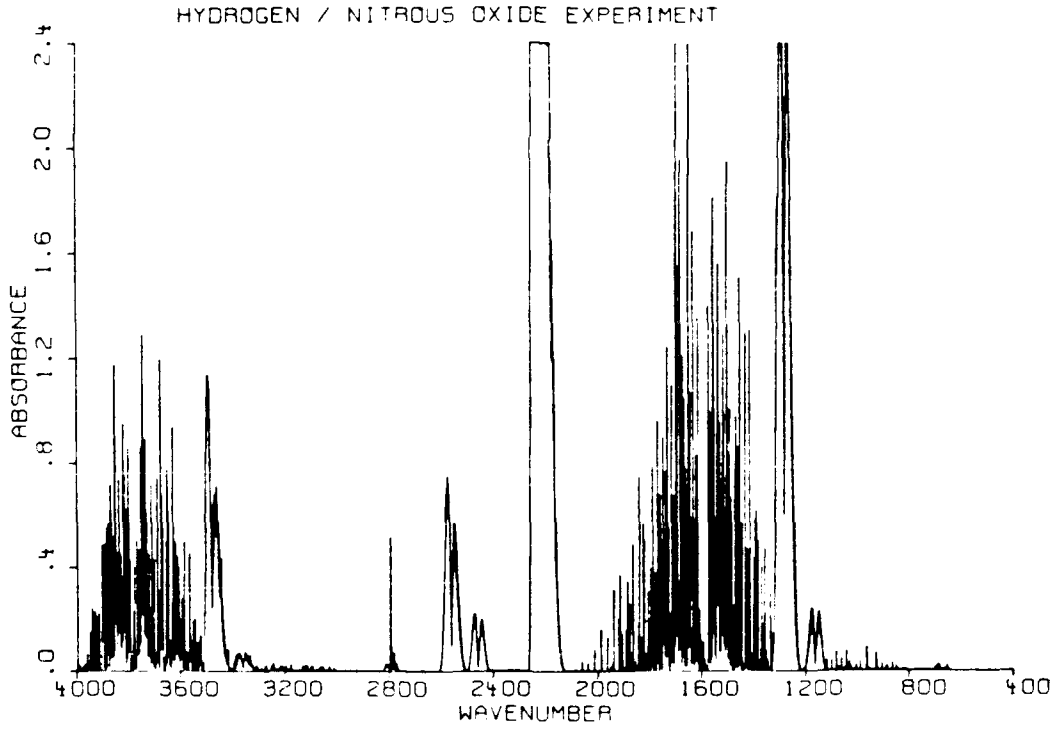

FIGURE 17. Absorbance Spectrum from Hydrogen / Nitrous Oxide Experiment

3.0 MODEL DEVELOPMENT AND VALIDATION

3.1 Flow Reactor Model and Sensitivity Analysis Equations

3.1.1 Model Equations

In the case of the flow reactor, convective transport is large relative to the diffusive transport as a result of operation with high through-put velocities, and thus the longitudinal gradients are small. This assumption reduces the steady, one-dimensional conservation equations of mass, species, and energy to the following

$$M = \rho u A \qquad \text{(EQ 1)}$$

$$M\frac{dY_k}{dx} = A\omega_k W_k \qquad \text{(EQ 2)}$$

$$M\frac{dT}{dx} = -\frac{A}{C_p}\sum_{k=1}^{K}\omega_k h_k W_k \qquad \text{(EQ 3)}$$

In these equations x denotes the independent spatial coordinate; M, the mass flow rate; T, the temperature; Y_k, the mass fraction of the kth species; ρ, the mass density; W_k, the molecular weight of the kth species; C_p the constant pressure heat capacity of the mixture; h_k, the specific enthalpy of the kth species; and A, the cross sectional area of the reactor tube.

Assuming M and A as constants and equating the convective derivative ud/dx to the unsteady term d/dt, the above equations can be rewritten as,

$$\frac{dY_k}{dt} = \frac{\omega_k W_k}{\rho} \qquad \text{(EQ 4)}$$

with $k=1,....K$, and,

$$\frac{dT}{dt} = \left(-\frac{1}{\rho C_p}\right)\sum_{k=1}^{K}\omega_k h_k W_k \qquad \text{(EQ 5)}$$

If the flow reactor is operated with dilute mixtures, the exothermicity of the mixture is small and the system remains nearly isothermal. Under these conditions, the energy equation is eliminated from the above set.

3.1.2 Sensitivity Analysis

The role of sensitivity analysis is to probe the relationships between the model parameters and the solutions to the governing equations; that is, the spatial or time dependent species concentrations, temperature, velocity, etc. In essence, a sensitivity analysis to the above flow reactor model allows questions to be answered concerning (1) interpretation and

analysis of models (2) relationships between model parameters and experiment and (3) inversion problems. Typical of these questions may be the following:

- What steps are significant in the mechanism?
- What role might a particular observation play regarding identification or determination of a particular rate constant?
- Can alterations in one part of a mechanism be compensated for by changes elsewhere while leaving the observations fixed?
- Are different observations in the same chemical system truly independent?
- What physical content resides in identifiable features of concentration or thermal profiles?
- How can one establish the role of initial species or possibly the effect of the induction of species during the reaction?
- By what pathway through the mechanism does one species control the behavior of others?
- How do the various rate constants work in concert to have major or minor influences on combustion phenomena?
- Can the role of missing reactions or steps in a mechanism be assessed?
- How may one quantitatively reduce the number of rate constants or transport coefficients in a reactive system?
- Can systematic means be found to lump combustion systems?
- How do statistical errors in the model input propagate to laboratory observations?
- When inverting laboratory data by residual minimization, what correlations are produced among the data and/or parameters?

The governing flow reactor equations described in the last section can be generalized as

$$\boldsymbol{F}(\boldsymbol{O}, \alpha) = 0 \qquad \text{(EQ 6)}$$

where $\boldsymbol{O}$ represents the vector of N dependent variables, and the vector α of length M represents the system parameters such as activation energies, preexponential factors, and other quantities that enter the differential equations.

In a sensitivity analysis, the quantities of natural interest are the first order sensitivity coefficients

$$S_{ij} = \frac{\partial O_i}{\partial \alpha_j} \qquad \text{(EQ 7)}$$

which provide a direct measure of how the *jth* parameter controls the behavior of the *ith* dependent variable at point x and time t. The appropriate equations for these quantities can be derived by differentiating EQ 4 with respect to α_j. Noting that the functional vector $\boldsymbol{F}$

depends on α both explicitly and implicitly through the solution vector $\boldsymbol{O}$, differentiation of EQ 6 yields

$$\frac{d}{d\alpha_j}\boldsymbol{F}(\boldsymbol{O}(\alpha),\alpha) = \frac{\partial \boldsymbol{F}}{\partial \boldsymbol{O}}\frac{\partial \boldsymbol{O}}{\partial \alpha_j} + \frac{\partial \boldsymbol{F}}{\partial \alpha_j}. \qquad \text{(EQ 8)}$$

($j=1,2,\ldots,M$). Recalling that the Jacobian matrix is given by $J = \partial \boldsymbol{F}/\partial \boldsymbol{O}$, we have

$$\boldsymbol{J}\frac{\partial \boldsymbol{O}}{\partial \alpha_j} = -\frac{\partial \boldsymbol{F}}{\partial \alpha_j}. \qquad \text{(EQ 9)}$$

($j=1,\ldots,M$). Solution of these equations is generally obtained with the simultaneous solution of the governing equation. In the present work, the kinetic equations and sensitivity equations were solved using SENKIN (Kee *et al.*, 1990).

The gradients studied in the present work include the sensitivities of the temperature and species mass fractions with respect to variations in the kinetic parameters of the mechanism. For example, the responses of observable O_i to variations in the forward and backward rate constants, k_f and k_b are,

$$\frac{\partial O_i}{\partial \ln k_f} \text{ and } \frac{\partial O_i}{\partial \ln k_b}.$$

Because of the principle of detailed balancing, the forward and reverse rate constants are related through the equilibrium constant. In a sensitivity analysis, if k_f is perturbed and k_b is held constant, the equilibrium constant, K, is simultaneously varied by the same amount. Posing the original problem in terms of K and k_f, the latter which we define here as k_{net} to differentiate it from the original problem with k_f and k_b as the variables, yields another set of sensitivity gradients. These gradients are obtainable from the original set of sensitivities. It can easily be shown that the sensitivity of observable O_i to k_{net} equals,

$$\frac{\partial O_i}{\partial \ln k_{net}} = \frac{\partial O_i}{\partial \ln k_f} + \frac{\partial O_i}{\partial \ln k_b} \qquad \text{(EQ 10)}$$

and the sensitivity of O_i to the equilibrium constant K is

$$\frac{\partial O_i}{\partial \ln K} = -\frac{\partial O_i}{\partial \ln k_b} \qquad \text{(EQ 11)}$$

Note that if the reverse rate constant is as important as the forward rate constant and opposite in sign, the net sensitivity equals zero. In many situations, this is a good indication that the reaction is microscopically balanced and that the important parameter is the equilibrium constant.

3.2 Chemical Systems and the Modeling Approach

The proposed hierarchical structure of chemical systems of importance to propellant combustion is shown in FIGURE 18. Both HCN and CH_2O are expected to be major gas-phase

intermediates of polycyclic nitramine combustion. Decomposition of RDX through concerted detrimerization or initial N-NO_2 bond fission has been shown to yield N_2O and CH_2O at low temperatures and HCN and NO_2 at high temperatures. In recent T-jump experiments of Brill (1991) for HMX decomposition, N_2O and NO_2 were observed to proceed all other gas phase species from the surface. The ratio of N_2O to NO_2 was found to decrease with increasing temperatures, being approximately equal for temperatures of 300-350°C, which is near the surface temperature of a burning propellant. Although the ratio of CH_2O to HCN was not observed to follow this trend, both HCN and CH_2O are important gas-phase reactants. They are also important intermediates in RDX combustion as shown in FIGURE 19 for the 0.5 *atm* pressure RDX flame model results of Melius (1985). Note from FIGURE 19, that CH_2O is consumed very rapidly and prior to the gas-phase temperature rising above 1200 K (not shown in this figure). Furthermore, note that both CH_2O and HCN are nearly consumed within 1 *mm* from the flame surface. Both of these facts emphasize the importance of flow reactor experiments, i.e., the chemistry near the propellant surface is well within the temperature range of the flow reactor, and second, the high convective flows of the flow reactor will spread the reaction out over approximately a meter in length, thus providing excellent spatial resolution with which to obtain accurate kinetic data. The model analysis of RDX flames by Melius also shows that the reaction paths follow the hierarchy as shown in FIGURE 18. In particular, the $CO/H_2O/NO_2$ reaction mechanism is a submechanism of both the CH_2O/NO_2 and the HCN/NO_2 systems, and the H_2/NO_2 reaction is a submechanism of the $CO/H_2O/NO_2$ system.

Preliminary experimental results by Parr (1989) on polycyclic nitramine flames has indicated that the interaction between an energetic binder and the polycyclic nitramine significantly affects ignition and combustion kinetics, much more than with HMX. Consequently, an understanding of the gas-phase kinetics of binder intermediates, such as C_2H_4 and CH_4, is also of importance. Assuming that the dominant route for CH_3 radicals is reaction with NO_2 and not itself, the methane reaction may be considered a submechanism of C_2H_4. However, under fuel-rich conditions, methyl radicals can be expected to recombine to form ethane, and hence the hierarchical structure of FIGURE 18 would have to be modified accordingly.

The nitrogen oxidizers typically follow the path of NO_2 -> NO -> N_2O-> N_2. Consequently, both NO and N_2O as oxidizers are submechanisms of the systems reported in FIGURE 18.

A proposed reaction grid for RDX combustion is presented in FIGURE 20 (Alexander *et al.*, 1989). There are over 700 possible interactions between the proposed species. Many of these interactions may be discarded based on thermochemical and structural considerations. Note that the reaction systems presented in FIGURE 18 provide the necessary building blocks to systematically develop and validate the RDX reaction mechanism. With the exception of the last block, these reaction systems are also the building blocks necessary for constructing the reaction mechanisms of the polycyclic nitramines of interest here.

As indicated in FIGURE 18, the smallest submechanism is the H_2/NO_2 reaction system, which is shown in FIGURE 20 to consist of the well known H_2/O_2 system and species and

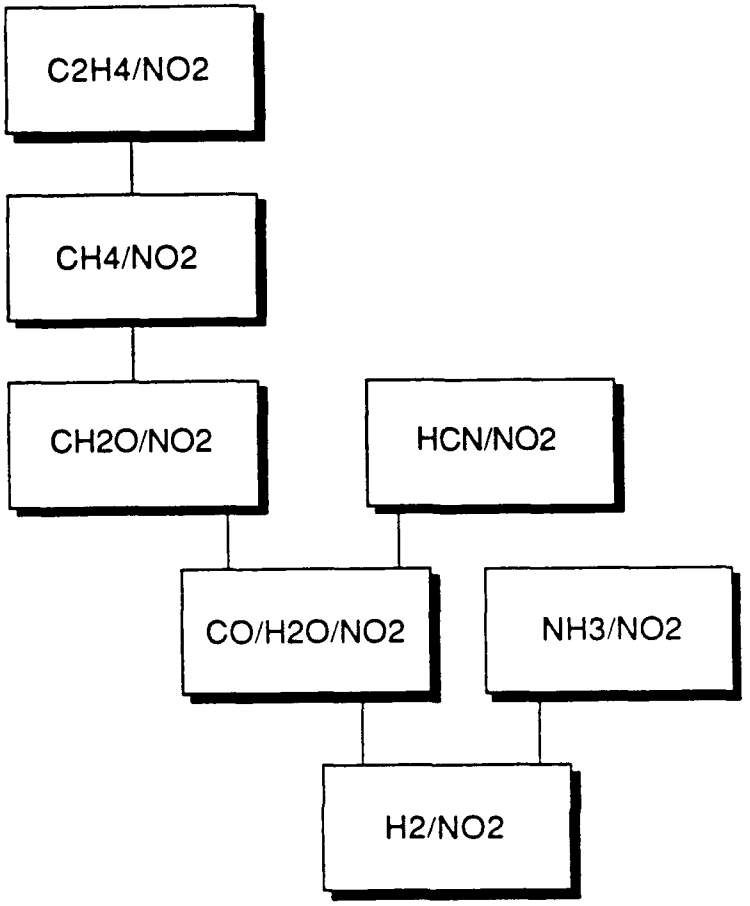

FIGURE 18. Hierarchical Development and Validation of Gas Phase Reaction Mechanisms

reactions important to NO_x formation and destruction. Hence a sound foundation already exists on which to build larger mechanisms.

Using the HCN/NO_2 reaction mechanism of Thorne and Melius (1989) and retaining only those species and reactions listed in the H_2/O_2 and NO_x formation and destruction mechanism of FIGURE 20, a series of hypothetical calculations were performed on H_2/NO_2 to simulate experiments in flow reactors, shock tubes and premixed flames.

The results for an equal molar mixture of H_2 and NO_2 in nitrogen (flow reactor, $T_1 = 1200$ *K*, 1 *atm*), in argon (shock tube, $T_1 = 2200$ *K*, P = 1 *atm*), and without diluent (premixed flame, $T_1 = 298$ *K*, P = 0.1 *atm*) are shown in FIGURE 21. The model predicts that experi-

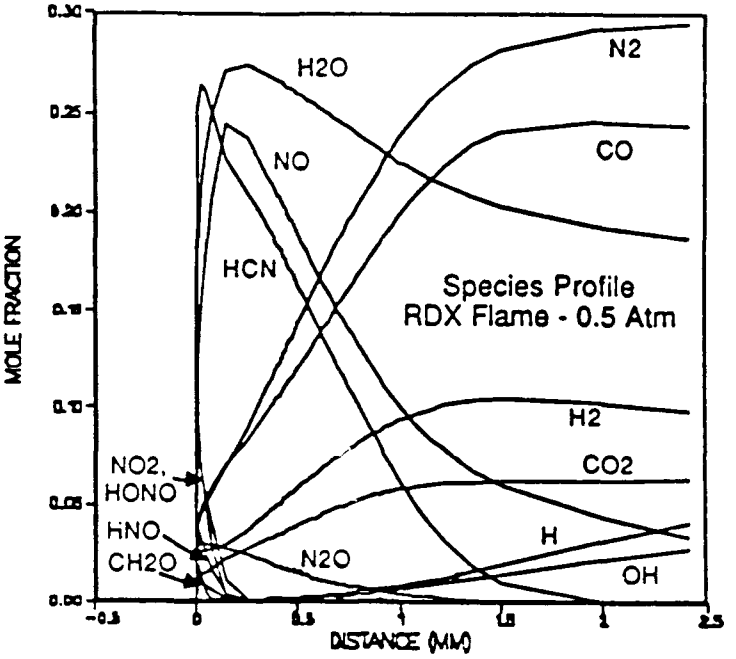

FIGURE 19. Simulated Structure of RDX Combustion (from Melius, 1988).

ments are possible in each device, which will ultimately lead to validation of the model. Compare the spatial dependence of the flow reactor and premixed flame. The results of a sensitivity analysis for the three experiments are presented in FIGURE 22. Note that the combination of reactions important to the shock tube and flow reactor are the same as those important to the flame. However, for the flame, diffusivities of radicals and energy (although not listed in FIGURE 22) were equally important parameters in the model, and hence model validation in the flame includes both transport and chemistry. The circled reactions in FIGURE 22 indicate the well studied H_2/O_2 reactions. The other reactions are from the NO_x formation and destruction mechanism, some of which have rate constants not as well known.

In FIGURE 23, sensitivity analysis results are presented for HCN/NO_2 mixtures, obtained from corresponding kinetic calculations of flow reactor, shock tube and premixed flame experiments. The circled reactions include all the reactions which were important in the H_2/NO_2 studies. Note again that the reactions important to the flame are the same as those important to the combined shock tube and flow reactor studies. Also note that the total number of important reactions to both HCN/NO_2 and H_2/NO_2 mixtures is small compared to the total number of possible kinetic interactions as described in FIGURE 20.

Lastly, FIGURE 24 presents the reactions which govern the RDX burn rate (Melius, 1988). The circled reactions include all those found important to the HCN/NO_2 and H_2/NO_2 mixtures. Note that with the exception of N+OH = NO+H (which would likely show up as important in other proposed mixtures to study, e.g., H_2/NO mixtures), the only unknown

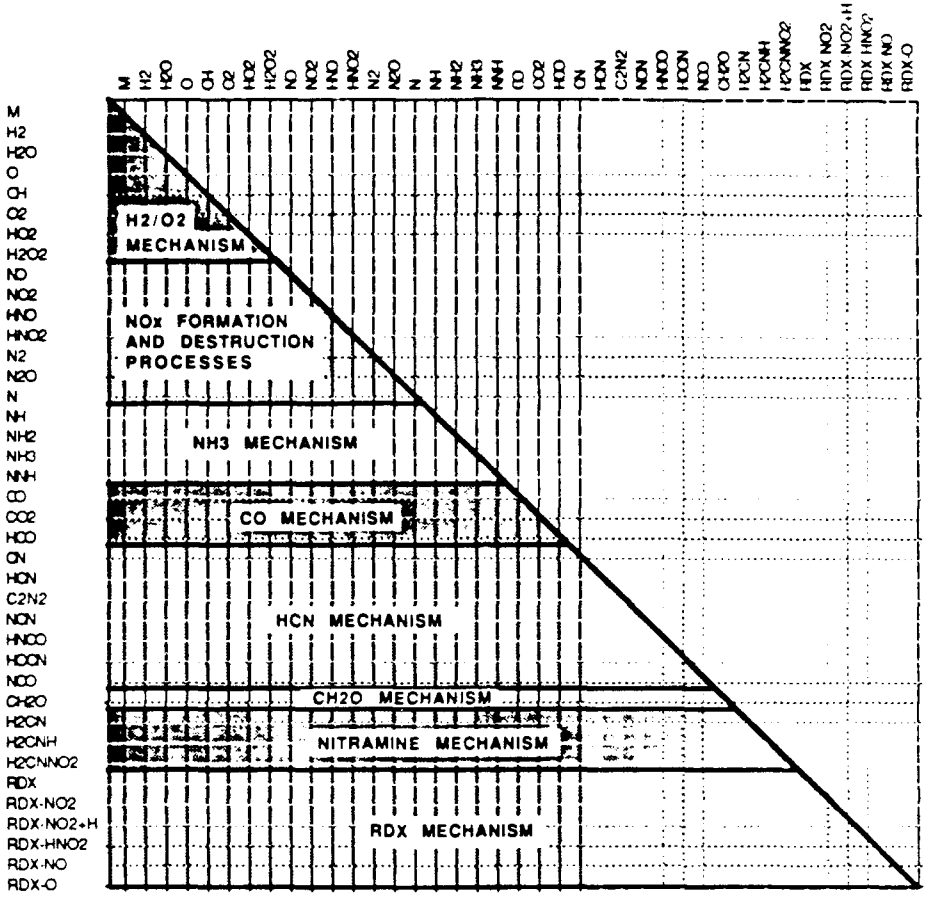

FIGURE 20. Reaction Grid for RDX Decomposition

reactions of importance to the RDX burn rate are the initial decomposition reactions of RDX.

Although the results of FIGURES 22-24 are preliminary and not comprehensive, they do emphasize the importance of systematic construction of reaction mechanisms and the importance of mechanism development via kinetic data from different types of experiments.

In summary, FIGURE 18 reports the hierarchical structure of the proposed research, starting with experiments and model development and validation for H_2 systems and then subsequently proceeding towards C_2H_4 and HCN. Several of these systems, either with NO_2 or N_2O as oxidizers, have been studied. However, most of the recent studies have been

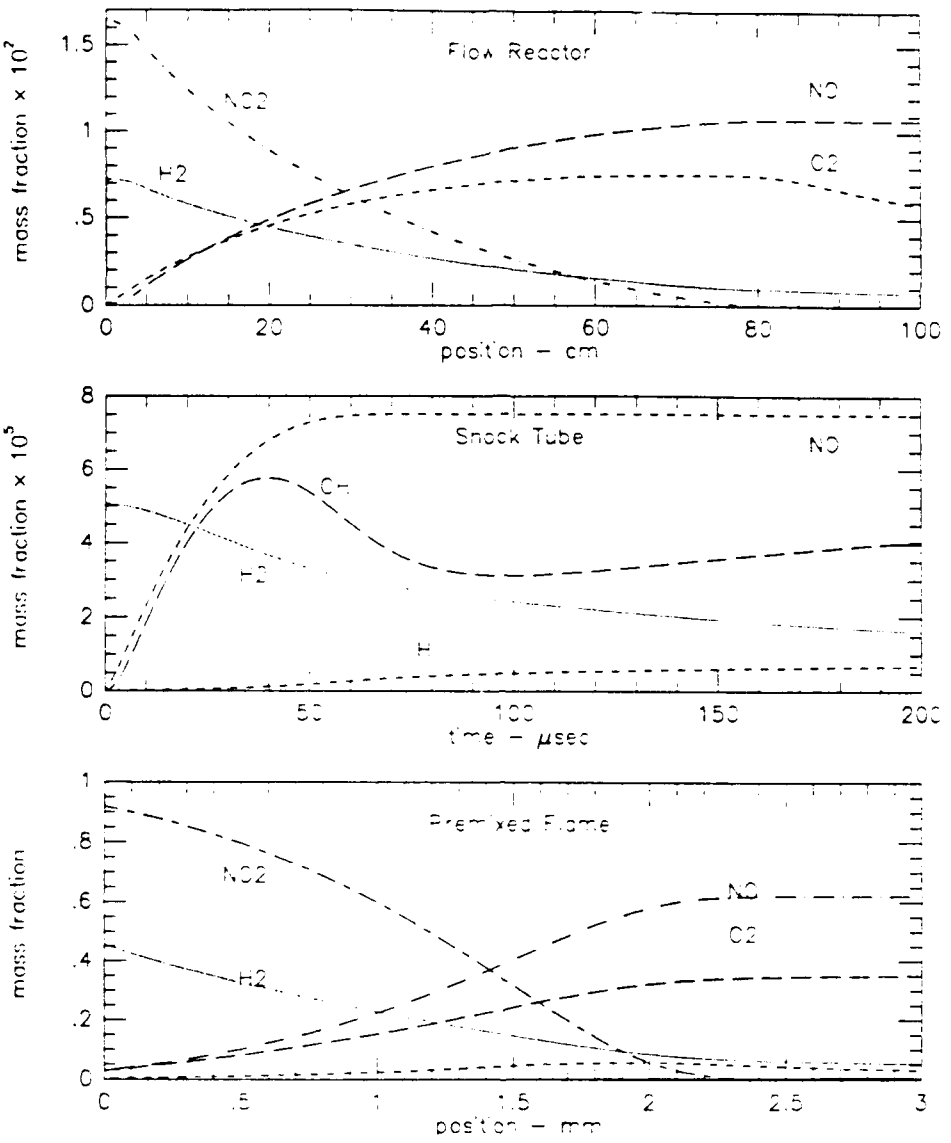

FIGURE 21. Simulated Experiments with H_2 NO_2 Mixtures

conducted in premixed flame configurations (see for example, Branch *et al.*, 1989a and 1989b, Cattolica, R. *et al.*, 1982, Miller and Bowman, 1989). Even less work has been conducted on these mixtures in shock tubes (see for example Lin, 1989). At present, flow reactor data on the kinetics of these mixtures is virtually non-existent, as is gas-phase kinetic data above one atmosphere pressure. Such data will be of significant importance to the success of the overall energetic materials research program.

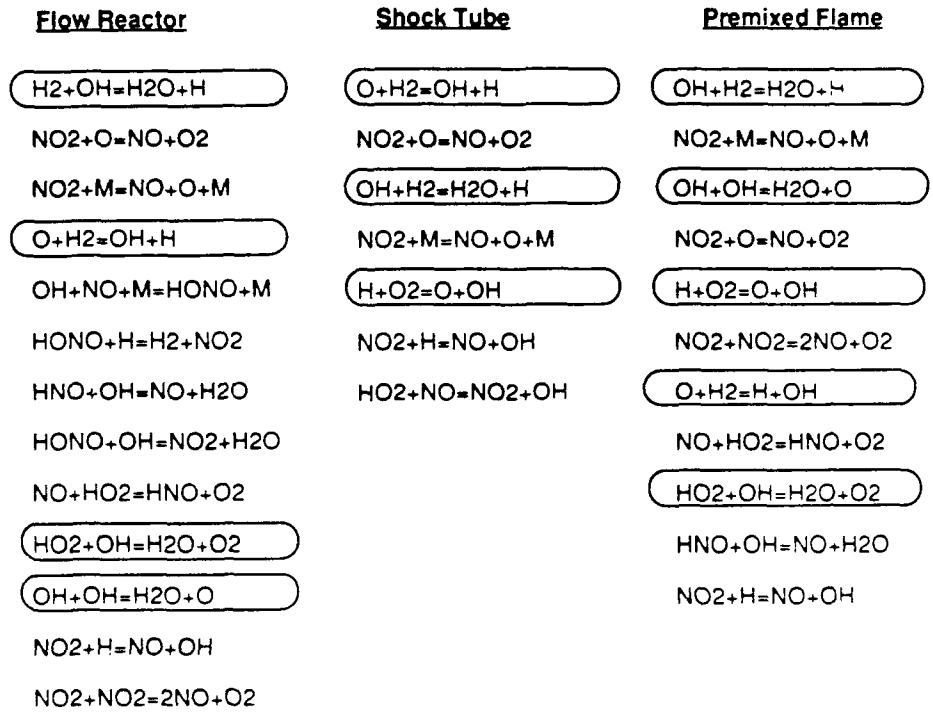

FIGURE 22. Reactions with High Sensitivity in H2/NO2 Mixtures

3.3 Reaction Mechanism for $H_2/NO_2/N_2O$ Kinetics

The initial $H_2/NO_2/N_2O$ reaction mechanism has been constructed by starting with a comprehensive reaction mechanism for H_2/O_2 kinetics. TABLE 1 contains the standard enthalpies of formation $\Delta H_{f,298}$, entropies and specific heats for the atomic and molecular species considered in the H_2/O_2 submechanism. All of the data are from the JANAF Tables (1985) with the exception of the heat of formation for HO_2, which is from Hills and Howard (1984). The temperature dependencies of the data are stored as polynomial fits in the format of the NASA chemical equilibrium program (Gordon and McBride, 1971). The polynomial coefficients for all species except HO_2 are from Kee *et al.* (1987). The polynomial coefficients for HO_2 were obtained using the THERM code of Ritter and Bozzelli (1987)

Flow Reactor	Shock Tube	Premixed Flame
HCN+O=NCO+H	HCN+O=NCO+H	N2O+M=N2+O+M
NO2+M=NO+O+M	NO2+M=NO+O+M	HCN+O=NCO+H
CN+O2=NCO+O	NCO+M=N+CO+M	NCO+M=N+CO+M
CO2+N=NO+O2	NO2+O=NO+O2	N+NO=N2+O
H+O2=OH+O	NCO+NO=N2O+CO	[illegible]+M=NO+O+M
HCN+O=NH+CO	H+O2=OH+O	NO2+O=NO+O2
HCN+OH=CN+H2O	N+NO=N2+O	CO+OH=CO2+H
NH2+NO=NNH+OH	CN+O=CO+N	NCN+OH=HCN+NO
CN+HCN=C2N2+H	CN+OH=NCO+H	HCN+OH=CN+H2O
NH2+NO=N2+H2O		NH+OH=HNO+H
HOCN+H=HNCO+H		H+OH+M=H2O+M
HNCO+H=NH2+CO		
CN+N2O=NCO+N2		
HCN+OH=HNCO+H		
HCN+OH=HOCN+H		

Flow reactor and shock tube sensitivities were determined with respect to the HCN mass fraction. Premixed flame sensitivities are from Thorne and Melius (27th JANNAF Combustion Meeting) and were determined with respect to the mass burning rate.

FIGURE 23. Reactions with High Sensitivity in HCN Mixtures

The reaction mechanism, consisting of 19 forward and reverse elementary reactions is listed in TABLE 2. The forward rate constants are all literature values (see Yetter *et al.*, 1991). Backward rate constants are computed from the forward rate constants and equilibrium constants. The temperature range listed in the table covers the domain over which the forward rate constant parameters were derived. For many of the reactions, this is also a good indication of the range of experimental data.

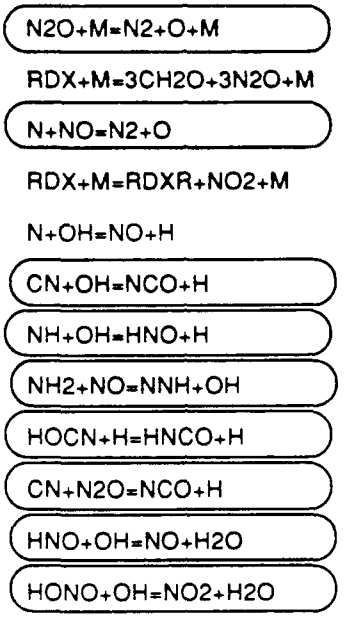

The results are from Melius (25th JANNAF Combustion Meeting). The sensitivities are evaluated with respect to the mass burning rate.

FIGURE 24. Chemical Reactions Governing RDX Burn Rate

TABLE 1. H_2/O_2 Thermochemical Parameters[a]

SPECIES	$\Delta H_{f,298}$	S_{298}	$C_{p,300}$	$C_{p,400}$	$C_{p,500}$	$C_{p,600}$	$C_{p,800}$	$C_{p,1000}$	$C_{p,1500}$
H	52.10	27.39	4.97	4.97	4.97	4.97	4.97	4.97	4.97
O	59.56	38.47	5.23	5.14	5.08	5.05	5.02	5.00	4.98
OH	9.32	43.88	7.15	7.10	7.07	7.06	7.13	7.33	7.8
H_2	0.00	31.21	6.90	6.96	7.00	7.02	7.07	7.21	7.73
O_2	0.00	49.01	7.01	7.22	7.44	7.65	8.07	8.35	8.72
H_2O	-57.80	45.10	8.00	8.23	8.44	8.67	9.22	9.87	11.26
HO_2	3.00	54.43	8.36	8.95	9.48	9.96	10.75	11.37	12.34
H_2O_2	-32.53	55.66	10.41	11.44	12.34	13.11	14.29	15.21	16.85

[a] units are *kcal/mol* for $\Delta H_{f,298}$ and *cal/mol-K* for S and C_p

Recombination/dissociation reaction rate parameters are reported for N_2 as the bath gas. The collision efficiencies of species other than N_2 were accounted for by including chaperon efficiencies in the total concentration [M] as described in the bottom of TABLE 2 (Warnatz, 1985). In this mechanism, it is assumed that third body efficiencies, although different among the species, are the same for each recombination/dissociation reaction.

The uncertainty factor (UF) is defined by $k_{max} = k \times UF$ and $k_{min} = k/UF$. The uncertainties placed on each rate constant were derived from Tsang and Hampson (1986) and Warnatz (1985) and are intended to cover the temperature ranges reported.

The species and reactions added to the H_2/O_2 mechanism to account for N_2O or NO_2 as an oxidant of H_2 are reported in TABLES 3 and 4, respectively. The species included were obtained from a chemical kinetic data base for propellant combustion recently generated by Tsang and Herron (1990). All of the thermodynamic data and the polynomial coefficients are from Kee *et al.* (1987). The mechanism includes all the reactions involving the species NO, NO_2, HNO, HONO, and N_2O and their recommended rate constants as reviewed by Tsang and Herron (1990). Two exceptions to this are the rate constants for the reaction between NO_2 and H and between N_2O and OH. The reaction between NO_2 and H has been recently studied by Ko and Fontijn (1991) over the temperature range 296 - 760 K and we have adopted their experimental evaluation here. For the reaction between N_2O and OH, Tsang and Herron place an upper limit on this reaction and suggest two product channels. The second endothermic channel forms HNO and NO ($\Delta H_{R,298}$=16.45). The rate constant recommended was 8.43×10^{12} exp(-9935/RT). As described below, the rate of this reaction at 1000 K was found to be too large, when using only the first channel ($\Delta H_{R,298}$=-25.93). The rate used by Miller and Bowman for this reaction is about a factor of three lower at this temperature and is used here. The second channel is included in the mechanism, however the rate constant is specified for the backward reaction and is from Thorne and Melius (1989).

TABLE 2. H_2 O_2 Reaction Mechanism

	ΔH_{298}	$\log(A_f)$	n_f	$E_{a,f}$	UF	T_{RANGE}
H_2-O_2 Chain Reactions						
1. $H+O_2 = O+OH$	16.77	14.28	0.00	16.44	2	962-2577
2. $O+H_2 = H+OH$	1.86	4.71	2.67	6.29	1.5	297-2495
3. $OH+H_2 = H+H_2O$	-15.02	8.33	1.51	3.43	1.5	250-2581
4. $OH+OH = O+H_2O$	16.87	4.09	2.62	-1.88	2.5	250-2000
H_2-O_2 Dissociation/Recombination Reactions						
5. $H_2+M = H+H+M$	104.1	19.66	-1.40	104.38	3.0	600-2000
6. $O+O+M = O_2+M$	-119.1	15.79	-0.50	0.00	1.3	2000-10000
7. $O+H+M = OH+M$	-102.3	18.67	-1.00	0.00	10.0	-----
8. $H+OH+M = H_2O+M$	-119.2	22.35	-2.00	0.00	2.	1000-3000
Formation and Consumption of HO_2						
9. $H+O_2+M = HO_2+M$	-49.07	19.83	-1.42	0.00	3.	200-2000
10. $HO_2+H = H_2+O_2$	-55.07	13.82	0.00	2.13	2.	298-773
11. $HO_2+H = OH+OH$	-36.44	14.23	0.00	0.87	2.	298-773
12. $HO_2+O = OH+O_2$	-53.22	13.24	0.00	-0.40	1.2	200-400
13. $HO_2+OH = H_2O+O_2$	-70.09	16.16	-1.00	0.00	2.	298-1400
Formation and Consumption of H_2O_2						
14. $HO_2+HO_2 = H_2O_2+O_2$	-38.51	12.48	0.00	1.39	3.	650-800
15. $H_2O_2+M = OH+OH+M$	51.14	17.08	0.00	45.50	2.	700-1500
16. $H_2O_2+H = H_2O+OH$	-68.02	13.00	0.00	3.59	3.	283-800
17. $H_2O_2+H = H_2+HO_2$	-17.56	13.68	0.00	7.95	5.	250-800
19. $H_2O_2+OH = H_2O+HO_2$	-32.57	12.85	0.00	1.43	2.	98-800

[a] units are *cm³-mole-s-kcal*, $k = AT^n \exp(-E_a/RT)$

[b] $[M] = [N_2]+[H]+[O]+[OH]+2.5[H_2]+[O_2]+12[H_2O]+[HO_2]+[H_2O_2]+1.9[CO]+3.8[CO_2]+[HCO]$

In addition, a few reactions have been added to the present system that were not reviewed by Tsang and Herron, which appear in mechanisms developed by Miller and Bowman for predicting NO_x formation and destruction and by Thorne and Melius for predicting HCN/NO_2 kinetics.

The pressure dependence of unimolecular reactions is based on the relation of Troe (1977). The second order rate constant, k_0, the first order rate constant, k_{inf}, and the broadening factor, F_c, are also from Tsang and Herron.

The formation of NH in H_2/N_2O systems has been suggested by Danby and Hinshelwood (1940) and later by Baldwin *et al.* (1975). Baldwin *et al.*, who observed NO production near 870 K in bulb experiments attributed the NO to a second channel of the H + N_2O reaction

$$H + N_2O \rightarrow NH + NO \qquad \Delta H_{298} = 34.1 \text{ kcal/mol}$$

$$H + N_2O \rightarrow N_2 + OH \qquad \Delta H_{298} = -62.2 \text{ kcal/mole}$$

The initial mechanism did not include the endothermic channel because NO was not observed in the H_2/N_2O experiments. However, to check the importance of this channel and the subsequent reactions which consume NH, reactions 53 - 73 in TABLE 4 were included, which are from Miller and Bowman and Thorne and Melius. Reactions involving HN_2, HN_3, and NNH were not included because there is little likelihood that these species play any significant role in the H_2/N_2O and H_2/NO_2 systems of this work.

TABLE 3. Nitrogen Species and Thermochemical Parameters[a] added to the H_2/O_2 System

SPECIES	$\Delta H_{f,298}$	S_{298}	$C_{p,300}$	$C_{p,400}$	$C_{p,500}$	$C_{p,600}$	$C_{p,800}$	$C_{p,1000}$	$C_{p,1500}$
NO	21.58	50.35	7.11	7.19	7.31	7.45	7.82	8.14	8.54
NO_2	7.91	57.34	8.83	9.64	10.33	10.93	11.89	12.49	13.17
N_2O	19.61	52.55	9.27	10.18	10.94	11.56	12.51	13.12	13.94
HNO	23.80	52.73	8.26	8.84	9.36	9.84	10.76	11.48	12.49
HONO	-18.34	59.59	10.88	12.27	13.39	14.31	15.67	16.56	17.89
$HONO_2$	-30.18	63.17	12.34	14.70	16.60	18.12	20.30	21.70	23.45
NO_3	17.00	60.37	11.31	13.32	14.90	16.10	17.59	18.27	19.10
N	112.96	36.61	4.97	4.97	4.97	4.97	4.97	4.97	4.97
NH	85.21	43.30	6.96	6.98	7.00	7.04	7.21	7.48	8.06

[a] units are *kcal/mol* for $\Delta H_{f,298}$ and *cal/mol-K* for S and C_p

TABLE 4. NO_2-N-O Reaction Mechanism Added to the H_2-O_2 System

		A_f	n_f	$E_{a,f}$	Ref.
NO Reactions					
20. NO+M=N+O+M		0.145E+16	0.000	148400.000	Tsang and Herron (1990)
21. NO+O=NO_2	k(*inf*)	0.130E+16	-0.750	0.000	Tsang and Herron (1990)
	$k(0,N_2)$	0.472E+25	-2.870	1552.000	$F_c(N_2)$ =0.95-10^{-4}T
22. NO+O=O_2+N		0.181E+10	1.000	38750.000	Tsang and Herron (1990)
23. NO+H=HNO	k(*inf*)	0.152E+16	-0.410	0.000	Tsang and Herron (1990)
	$k(0,N_2)$	0.896E+20	-1.320	735.200	$F_c(N_2)$ = 0.82
24. NO+H=N+OH		0.169E+15	0.000	48800.000	Tsang and Herron (1990)
25. NO+OH=HONO	k(*inf*)	0.199E+13	-0.050	-7.213	Tsang and Herron (1990)
	$k(0,N_2)$	0.508E+24	-2.510	-67.560	$F_c(N_2)$ = 0.62
26. 2NO=N_2+O_2		0.130E+15	0.000	75630.000	Thorne and Melius (1989)
27. NO+HO_2=HNO+O_2		0.200E+12	0.000	2000.000	Thorne and Melius (1989)
NO_2 Reactions					
28. NO_2+H_2=HONO+H		0.241E+14	0.000	28810.000	Tsang and Herron (1990)
29. NO_2+O=O_2+NO		0.391E+13	0.000	-238.400	Tsang and Herron (1990)

30. $NO_2+O=NO_3$	k(*inf*)	0.133E+14	0.000	0.000	Tsang and Herron (1990)
	$k(0,N_2)$	0.149E+29	-4.080	2468.000	$F_c(N_2) = 0.79\text{-}1.8\times10^{-4}T$
31. $NO_2+H=NO+OH$		0.129E+15	0.000	361.600	Ko and Fontijn (1991)
32. $NO_2+OH=HONO_2$	k(*inf*)	0.241E+14	0.000	0.000	Tsang and Herron (1990)
	$k(0,N_2)$	0.642E+33	-5.490	2351.000	$F_c(N_2) = 0.725\text{-}2.5\times10^{-4}T$
33. $NO_2+OH=HO_2+NO$		0.181E+14	0.000	6676.000	Tsang and Herron (1990)
34. $NO_2+NO=N_2O+O_2$		0.100E+13	0.000	60000.000	Thorne and Melius (1989)
35. $2NO_2=NO_3+NO$		0.964E+10	0.730	20920.000	Tsang and Herron (1990)
36. $2NO_2=2NO+O_2$		0.163E+13	0.000	26120.000	Tsang and Herron (1990)
N_2O Reactions					
37. $N_2O=N_2+O$	k(*inf*)	0.130E+12	-0.000	59610.000	Tsang and Herron (1990)
	$k(0,N_2)$	0.723E+18	-0.730	62780.000	$F_c(N_2) = 1.167\text{-}1.25\times10^{-4}T$
38. $N_2O+O=N_2+O_2$		0.102E+15	0.000	28020.000	Tsang and Herron (1990)
39. $N_2O+O=2NO$		0.663E+14	0.000	26630.000	Tsang and Herron (1990)
40. $N_2O+H=N_2+OH$		0.964E+14	0.000	15100.000	Tsang and Herron (1990)
41. $N_2O+OH=HO_2+N_2$		0.200E+13	0.000	10000.000	Miller & Bowman (1989)
42. $N_2O+NO=N_2+NO_2$		0.100E+15	0.000	49675.000	Thorne and Melius (1989)
HNO Reactions					
43. $HNO+O=OH+NO$		0.361E+14	0.000	0.000	Tsang and Herron (1990)
44. $HNO+O=NO_2+H$		0.500E+11	0.500	2000.000	Thorne and Melius (1989)
45. $HNO+H=H_2+NO$		0.181E+14	0.000	993.500	Tsang and Herron (1990)
46. $HNO+OH=H_2O+NO$		0.482E+14	0.000	993.500	Tsang and Herron (1990)
47. $HNO+NO=N_2O+OH$		0.200E+13	0.000	26000.000	Thorne and Melius (1989)
48. $HNO+NO_2=HONO+NO$		0.602E+12	0.000	1987.000	Tsang and Herron (1990)
49. $2HNO=H_2O+N_2O$		0.843E+09	0.000	3102.000	Tsang and Herron (1990)
HONO Reactions					
50. $HONO+O=O+NO_2$		0.120E+14	0.000	5961.000	Tsang and Herron (1990)
51. $HONO+OH=H_2O+NO_2$		0.126E+11	1.000	135.100	Tsang and Herron (1990)
52. $HONO+HNO=H_2O+2NO$		0.100E+13	0.000	40000.000	Miller & Bowman (1989)
NH Reactions					
53. $NH+O_2=HNO+O$		0.100E+14	0.000	12000.000	Miller & Bowman (1989)
54. $NH+O_2=NO+OH$		0.760E+11	0.000	1530.000	Miller & Bowman (1989)
55. $N+HO_2=NH+O_2$		0.100E+14	0.000	2000.000	Miller & Bowman (1989)
56. $NH+O=NO+H$		0.200E+14	0.000	0.000	Miller & Bowman (1989)
57. $NH+H=N+H_2$		0.300E+14	0.000	0.000	Miller & Bowman (1989)
58. $N+OH=NH+O$		0.380E+14	0.000	0.000	Miller & Bowman (1989)
59. $NH+OH=HNO+H$		0.200E+14	0.000	0.000	Miller & Bowman (1989)
60. $NH+OH=N+H_2O$		0.500E+12	0.500	2000.000	Miller & Bowman (1989)
61. $NH+N=N_2+H$		0.100E+15	0.000	0.000	Miller & Bowman (1989)
62. $NH+NO=N_2O+H$		0.240E+16	-0.800	0.000	Miller & Bowman (1989)
63. $N+HNO=NH+NO$		0.100E+14	0.000	2000.000	Miller & Bowman (1989)
64. $NH+NO_2=NO+HNO$		0.100E+12	0.500	4000.000	Miller & Bowman (1989)

N Reactions				
65. $N+NO=N_2+O$	0.327E+13	0.300	0.000	Miller & Bowman (1989)
66. $N+N_2O=N_2+NO$	0.100E+14	0.000	19870.000	Miller & Bowman (1989)
67. $N+NO_2=2NO$	0.400E+13	0.000	0.000	Miller & Bowman (1989)
68. $N+NO_2=N_2O+O$	0.500E+13	0.000	0.000	Miller & Bowman (1989)
69. $N+NO_2=N_2+O_2$	0.100E+13	0.000	0.000	Miller & Bowman (1989)
70. $N+HNO=N_2O+H$	0.500E+11	0.500	3000.000	Miller & Bowman (1989)
71. $N+HO_2=NO+OH$	0.100E+14	0.000	2000.000	Miller & Bowman (1989)

[a]units are cm^3-*mole*-*s*-*cal*, $k = AT^n \exp(-E_a/RT)$

4.0 N_2O DECOMPOSITION AND REACTION WITH H_2

4.1 Introduction

A number of studies exist for the reaction between H_2 and N_2O. However, most of the recent studies are for high temperatures, typically from experiments conducted in flames or shock tubes. Flames studies include the low pressure (40 torr) lean H_2/N_2O flames of Balakhnine *et al.* (1977), the atmospheric pressure stoichiometric H_2/N_2O flame of Cattolica *et al.* (1982) and the flame study of Fine and Evans (1963). Recent shock tube studies of H_2/N_2O mixtures have often been performed to measure the rates of isolated reactions. For example, Hidaka *et al* (1985) studied the rate of N_2O + H and Pamidimukkaln and Skinner (1982) studied the rate of H_2+O. Henrici and Bauer (1964) used a shock tube to study this system at 1700-2600 K and obtained a value for the rate of H+N_2O

In a temperature range slightly below that of this study, Baldwin *et al.* (1975) have studied the H_2/N_2O reaction in a bulb reactor over the temperature range of 810 - 870 K. Their work suggested the importance of NH and HNO in this system. These reactions were considered to lead to termination in the reaction. Further, wall reactions could not be neglected.

The present studies have been conducted over a temperature range too high for bulb experiments and too low for shock tubes (950 - 1073 K) in a flow reactor where wall reactions are minimized. Detailed kinetic modeling and sensitivity analyses are also performed to thoroughly investigate the model.

4.2 Results

TABLE 5 reports the initial experimental conditions of the systems studied for N_2O decomposition and its reaction with H_2. An example of the species profiles for N_2O decomposition is reported in FIGURE 25 for the conditions of EXP 2. Approximately 14% of the N_2O decomposes during an experimental reaction time of 0.75 *s*. During this period, approximately 490 *ppm* of O_2, 50 *ppm* of NO, and 4 *ppm* of NO_2 are formed. For the same reaction time, the results of experiment EXP 1 showed approximately 6% N_2O consumption and formation of 220 *ppm* of O_2, 20 *ppm* of NO and 2 *ppm* of NO_2. Hence, the rate of reaction is nearly proportional to pressure.

TABLE 5. Experimental Conditions of N_2O Experiments

EXP	T/K	P/atm	X_{N2O}	X_{H2}	Φ
1	1075	3.2	0.008	0.0	
2	1096	6.0	0.078	0.0	
3	950	3.0	0.009	0.0097	1.08
4	1014	3.0	0.01	0.0072	0.72
5	1020	3.0	0.0074	0.0052	0.70
6	1073	1.0	0.0074	0.0074	1.0
7	1073	1.0	0.0065	0.0065	1.0
8	1025	3.0	0.0070	0.070	1.0

The results suggest that the rate limiting step, as expected, is the thermal decomposition of N_2O via $N_2O + M \rightarrow N_2 + O + M$ and that the branching ratio of $N_2O + O$ yielding $N_2 + O_2$ vs. $NO + NO$ is 20 to 1. However, according to TABLE 4, the ratio of the rate constants for reaction 38 to that of reaction 39 at 1096 K is 0.81. This mechanism implies NO is being consumed or O_2 is being formed from other reactions than $N_2O + O$, or that the branching ratio given in TABLE 4 is incorrect.

The corresponding modeling calculations are shown in FIGURE 26. The model does not predict the fast reaction for times less than 0.1 s, but generally agrees with the decomposition rate for times greater than 0.1 *s*. The model predicts about 8.5% consumption of N_2O, formation of 230 *ppm* of O_2, 84 *ppm* of NO and 5 *ppm* of NO_2 for a reaction time of 0.75 *s*.

The corresponding sensitivity analysis results for the gradients $\partial Y_{N2O}/\partial lnk_{net}$ are presented in FIGURE 27. The most sensitive reactions in decreasing order of importance are,

$$N_2O + M \leftrightarrow N_2 + O + M \qquad 37$$

$$N_2O + O \leftrightarrow N_2 + O_2 \qquad 38$$

$$NO + O + M \leftrightarrow NO_2 + M \qquad 21$$

$$N_2O + O \leftrightarrow NO + NO \qquad 39$$

$$NO_2 + O \leftrightarrow O_2 + NO \qquad 29$$

The numbers above and in the figures denote the reaction numbers as listed in TABLES 2 and 4. The important parameters of the reactions above are the forward rate constants.

The effect of O_2 and H_2O impurities in the N_2 carrier gas are illustrated in FIGURE 28 for concentrations of 250 *ppm* each added separately to the N_2O system of FIGURE 26. The mechanism used here only included reactions 1 - 52 of TABLES 2 and 3. The model results indicate that O_2 impurities do not have a significant affect on the decomposition rate. In

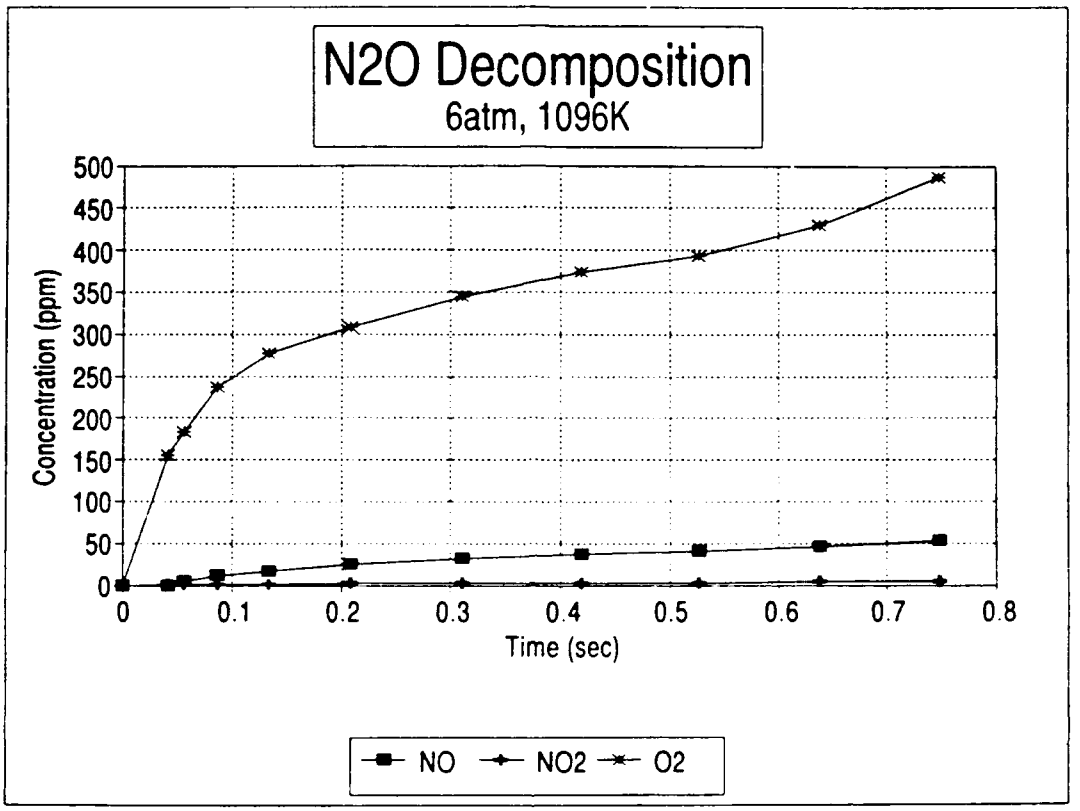

FIGURE 25. Experimental concentration profiles of N_2O decomposition. Initial conditions are reported in TABLE 5 for EXP 2

contrast, water vapor has an appreciable affect on the rate of N_2O decomposition. Sensitivity analysis results indicate that in addition to reactions 33 and 39 above, the reactions

$$HO_2 + NO \leftrightarrow NO_2 + OH \qquad 33$$

$$HO_2 + O \leftrightarrow OH + O_2 \qquad 12$$

$$HO_2 + OH \leftrightarrow H_2O + O_2 \qquad 13$$

$$OH + N_2O \leftrightarrow HO_2 + N_2 \qquad 41$$

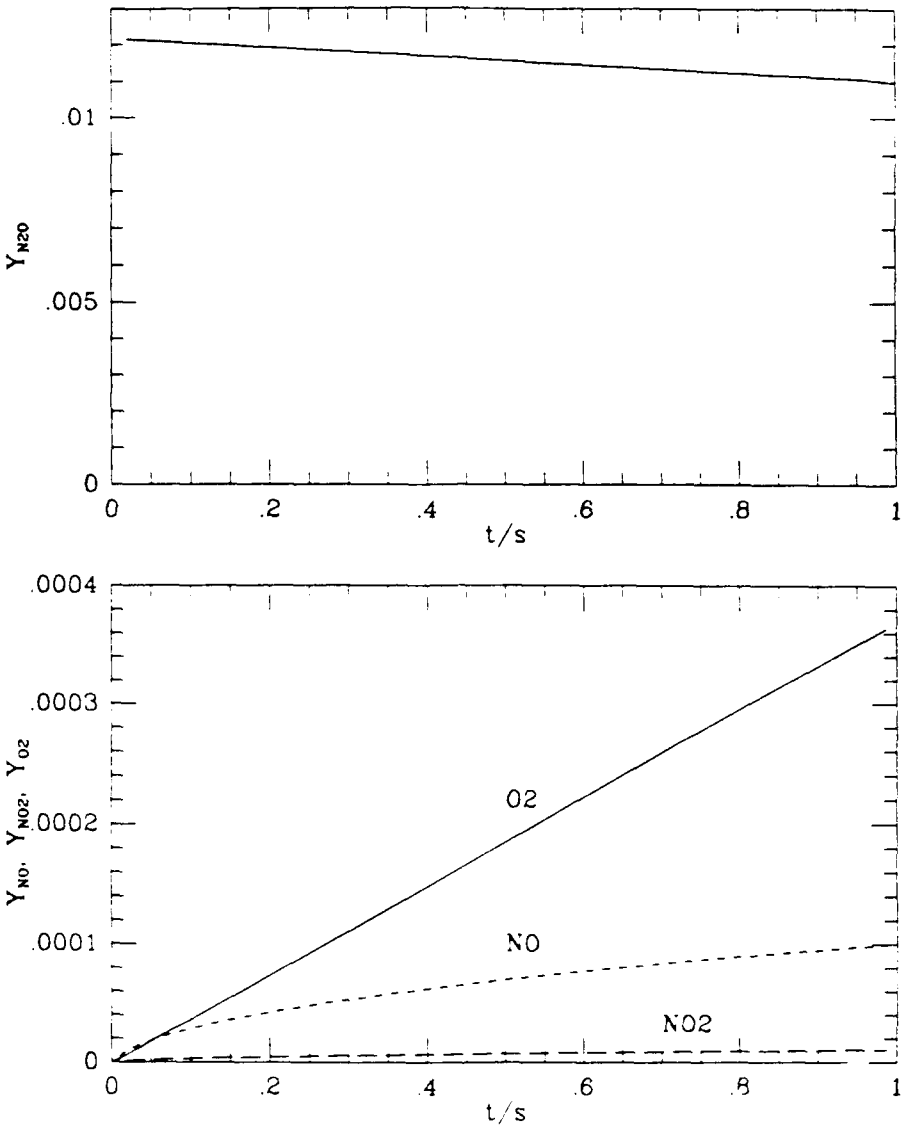

FIGURE 26. Calculated mass fraction profiles of N_2O decomposition. Initial conditions are reported in TABLE 5 for EXP 2

$$H + O_2 \leftrightarrow OH + O \qquad 1$$

$$O + H_2O \leftrightarrow OH + OH \qquad 4$$

are important when H_2O is present. The addition of the NH reactions and N reactions had no affect on the water catalyzed N_2O decomposition reaction because H atoms are not formed in significant quantities in this system.

An example of the kinetics of N_2O reacting with H_2 is given in FIGURE 29 for the conditions of EXP 6. During the reaction period of 0.18 *s*, 50% of the N_2O and H_2 are consumed. No NO was observed in these experiments. The corresponding calculated

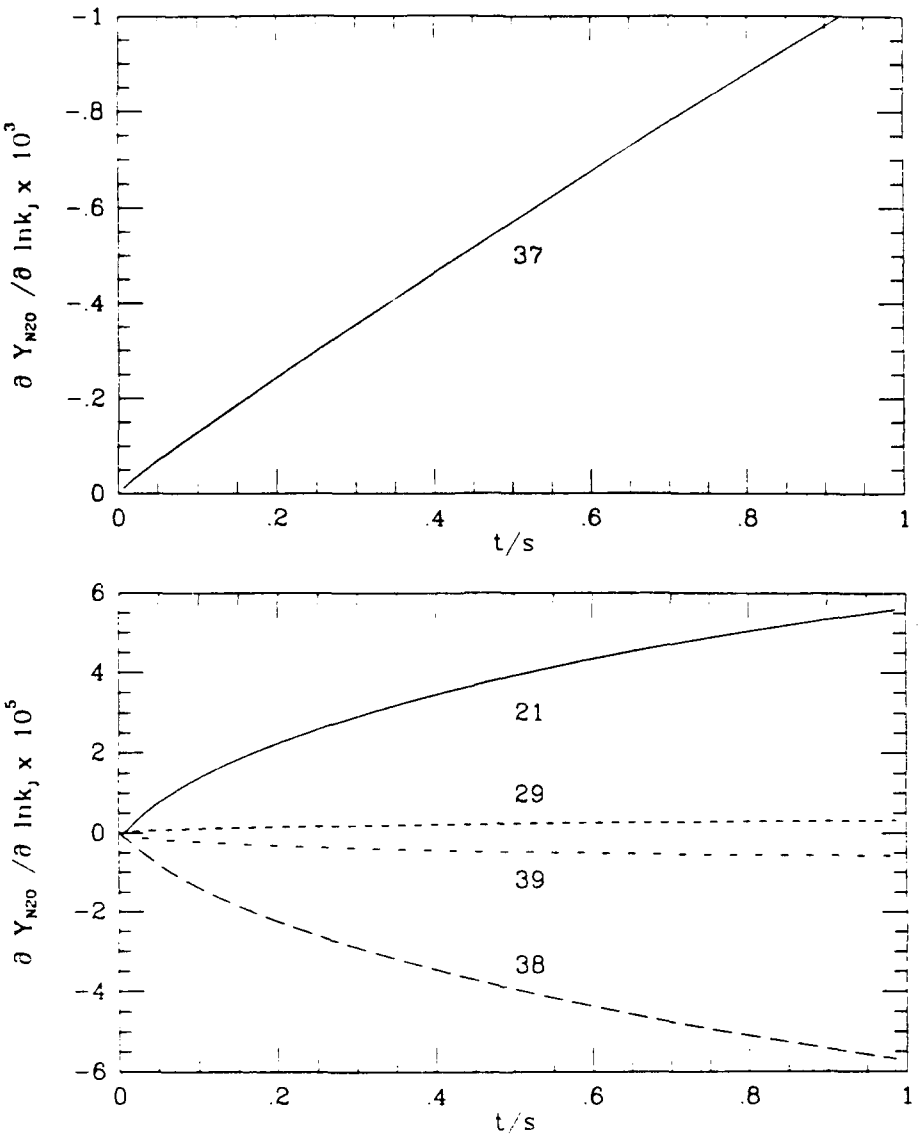

FIGURE 27. Sensitivity gradients $\partial Y_{N2O}/\partial lnk_{net}$ for the response of the N_2O mass fraction to relative variations in the net rate constants. The initial conditions are the same as those of FIGURE 26.

temperature and mass fraction profiles for N_2O, H_2O, H_2, H, O, OH, HO_2, NO, and O_2 for the stoichiometric H_2/N_2O system reacting at 1073 K and 1 atm are presented in FIGURE 30. Note the formation of molecular oxygen and its consumption after approximately 60% of the initial H_2 and N_2O have been consumed. The model predicts 50% consumption of N_2O in about the same period of time as the experiment.

The sensitivity gradients, $\partial Y_{N2O}/\partial lnk_{net}$ and, $\partial Y_{H2O}/\partial lnk_{net}$, for the stoichiometric H_2/N_2O system reacting at 1073 *K* and 1 *atm* are presented in FIGURE 31. The corresponding gradients for both species have opposite signs, but are of similar shape. Both species are sensitive to the same reactions. In decreasing order of importance, these reactions are:

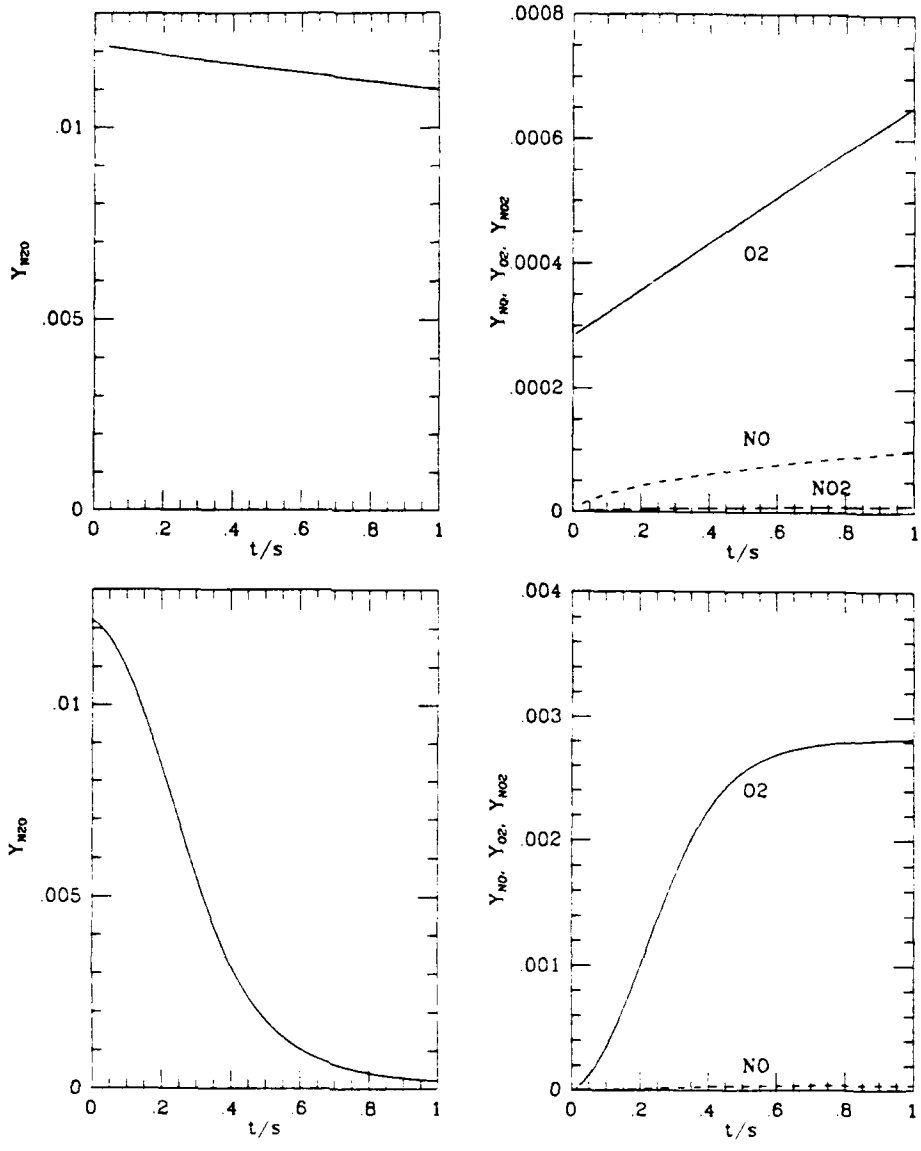

FIGURE 28. (a) and (b): Mass fraction profiles for N_2O decomposition in the present of 250 *ppm* O_2. (c) and (d): Mass fraction profiles for N_2O decomposition in the present of 250 *ppm* H_2O. The initial conditions are the same as those of FIGURE 26, but with the addition of 250 *ppm* O_2 or 250 *ppm* H_2O.

$$N_2O + M \leftrightarrow N_2 + O + M \qquad 37$$

$$H_2 + OH \leftrightarrow H_2O + H \qquad 3$$

$$N_2O + OH \leftrightarrow N_2 + HO_2 \qquad 41$$

$$H + HO_2 \leftrightarrow H_2 + O_2 \qquad 10$$

$$H + HO_2 \leftrightarrow OH + OH \qquad 11$$

$$N_2O + H \leftrightarrow N_2 + OH \qquad 40$$

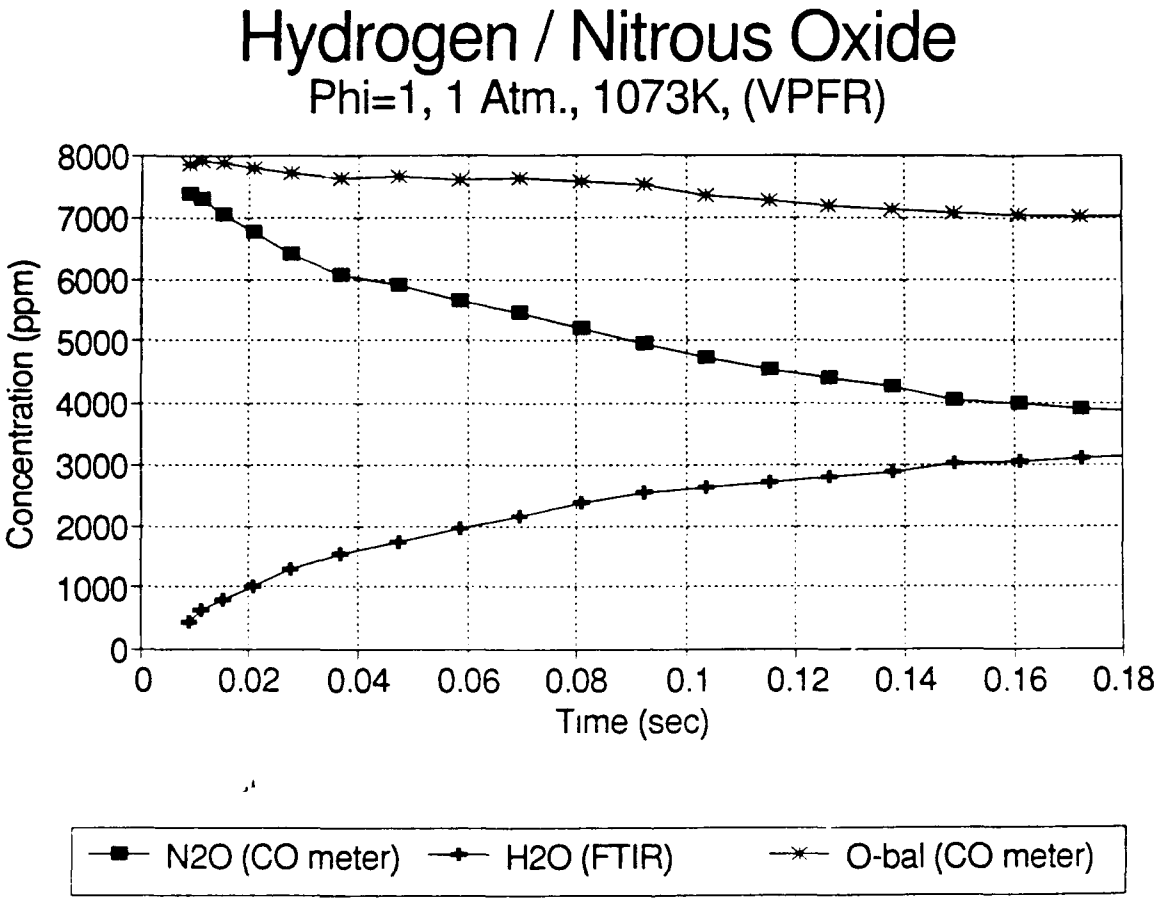

FIGURE 29. Experimental concentration profiles for the reaction of H_2 and N_2O with the conditions of EXP 6 of TABLE 5.

$$H + O_2 \leftrightarrow OH + O \qquad 1$$

Using the upper limit for the reaction between OH and N_2O recommended by Tsang and Hampson and assuming only the product channel to form HO_2 and N_2, the overall reaction is approximately a factor of two slower than the experiment. Note that among the important reactions, this reaction is the one with the largest uncertainty.

In FIGURE 32, the gradients of $\partial Y_{N2O}/\partial lnk_f$ and, $\partial Y_{N2O}/\partial lnk_b$ for the same kinetic system as above are reported. These results illustrate that for all the reactions listed above, the forward rate constant is the important parameter; only for reaction 3 is the backward rate

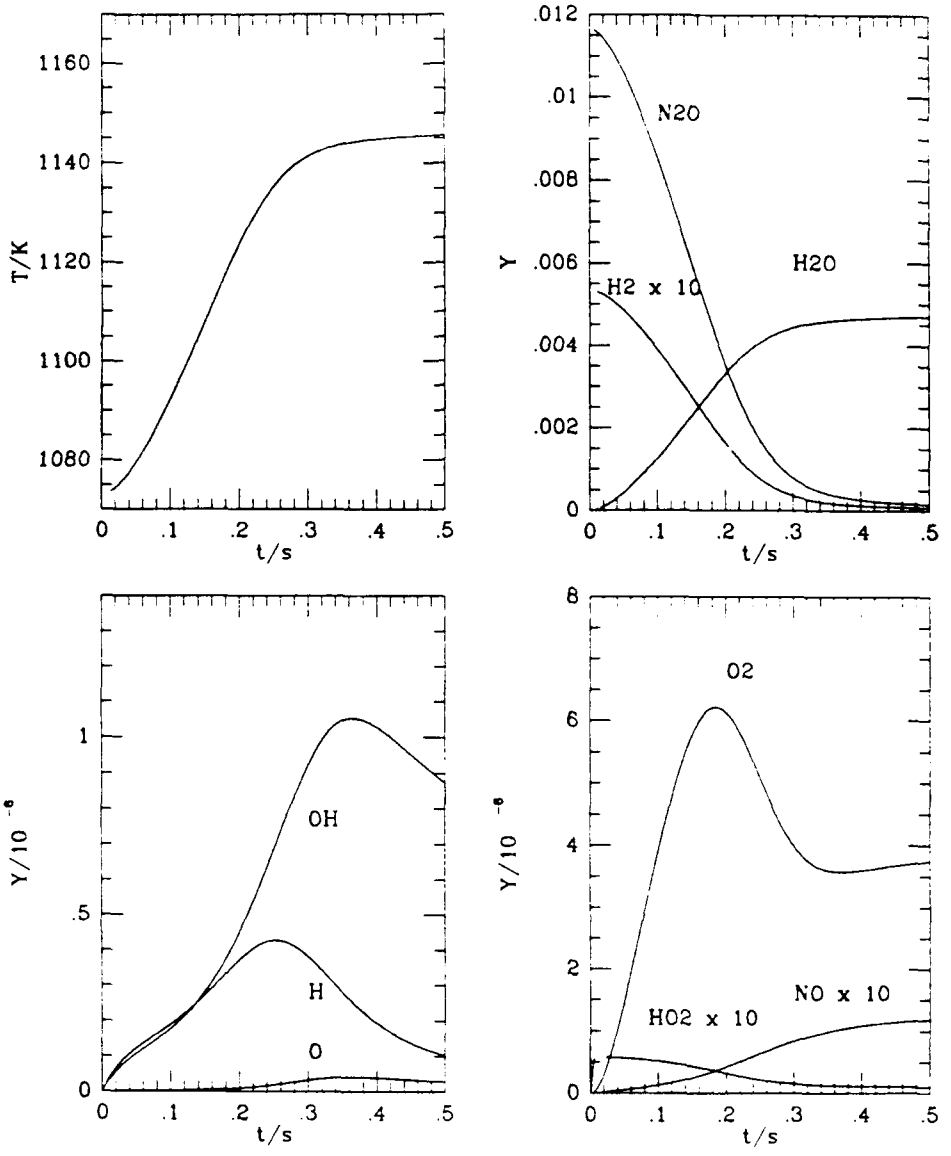

FIGURE 30. Calculated temperature and mass fraction profiles for the reaction of H_2 and N_2O with the conditions of EXP 6 of TABLE 5.

constant somewhat important. For this system, none of the equilibrium constants play a significant role.

The importance of oxygen in this system is illustrated in FIGURE 33. In this figure, the N_2O profiles from stoichiometric mixtures of H_2/N_2O reacting in N_2 at 1073 K and 1 *atm* are presented for the addition of trace amounts of O_2 ranging from 0 *ppm* to 500 *ppm*. After the addition of about 50 *ppm*, the reaction character changes completely to a branched chain system.

The sensitivity gradients $\partial Y_{N2O}/\partial lnk_{net}$ for the system with 250 *ppm* O_2 is reported in FIGURE 34. In decreasing order of importance, the most sensitive reactions are (1), (3),

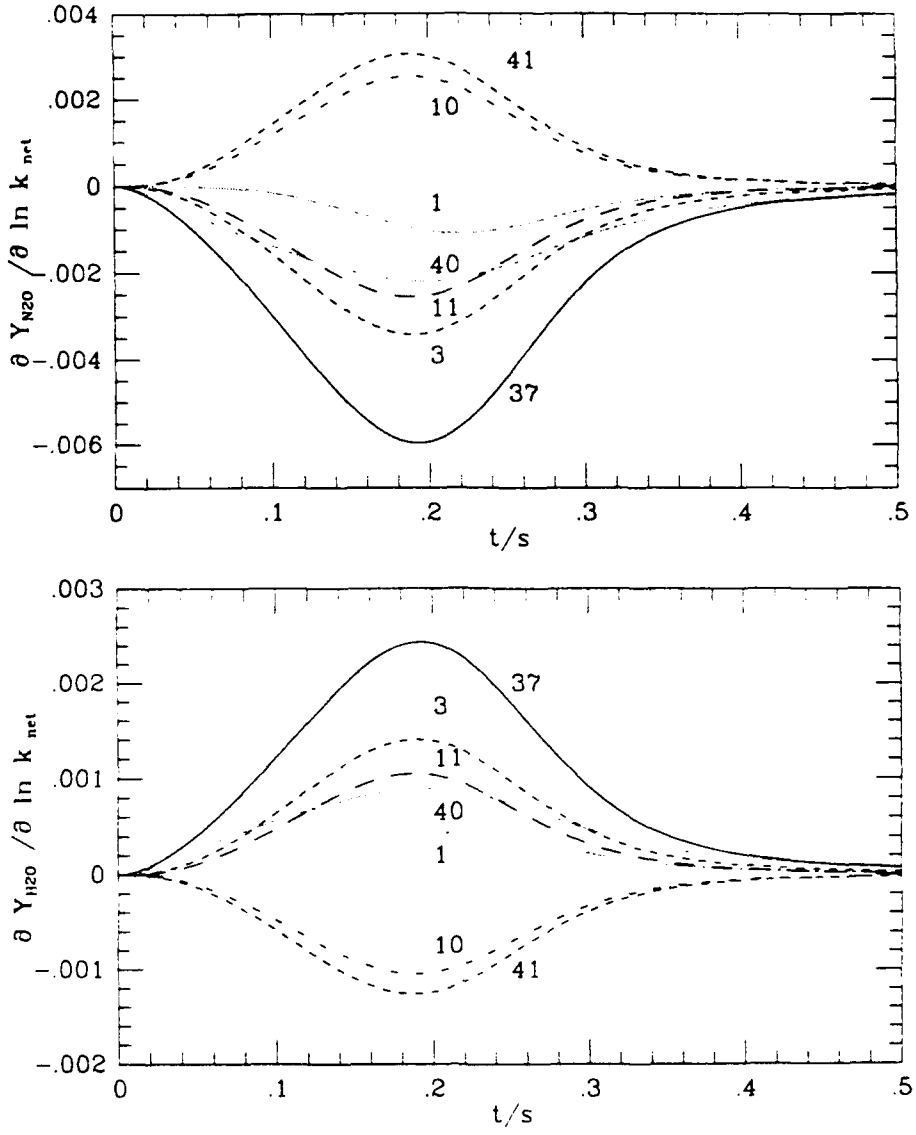

FIGURE 31. Sensitivity gradients $\partial Y_{N2O}/\partial lnk_{net}$ and $\partial Y_{H2O}/\partial lnk_{net}$ for the conditions of FIGURE 31.

(41), (10), (11), (37), (9), and (39). Although the order of most sensitive reactions has changed relative to the system without molecular oxygen, the list contains the same set of reactions.

The importance of NH in this mechanism is illustrated in FIGURE 35. The calculated overall rate of reaction is observed to decrease by approximately 25%. The effect is consistent with that found by Baldwin *et al.* A concentration of approximately 10 *ppm* NO is predicted at the largest extent of reaction studied experimentally (whereas for the calculations without NH, the concentration of NO predicted was less than 0.1 *ppm*). Although 10*ppm* NO is clearly within the detectability limits of the FTIR, NO was not observed in the experiments.

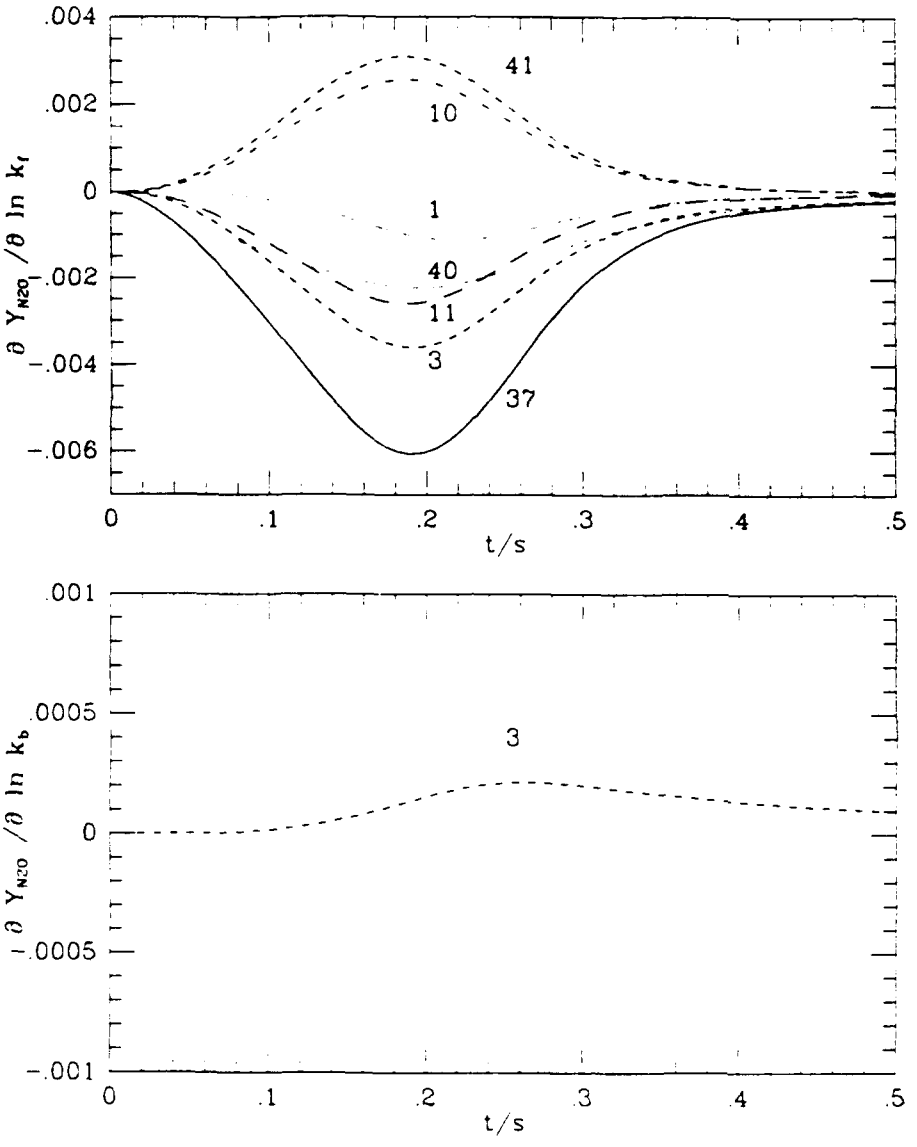

FIGURE 32. Sensitivity gradients $\partial Y_{N2O}/\partial lnk_f$ and $\partial Y_{N2O}/\partial lnk_b$ for the conditions of FIGURE 31.

Sensitivity analysis results reveal that the inclusion of NH to the mechanism add four more reactions to those found important above.

$$N_2O + H \leftrightarrow NH + NO \qquad 62$$

$$H + NO + M \leftrightarrow HNO + M \qquad 23$$

$$NO + H \leftrightarrow N + OH \qquad 24$$

$$N + NO \leftrightarrow N_2 + O \qquad 65$$

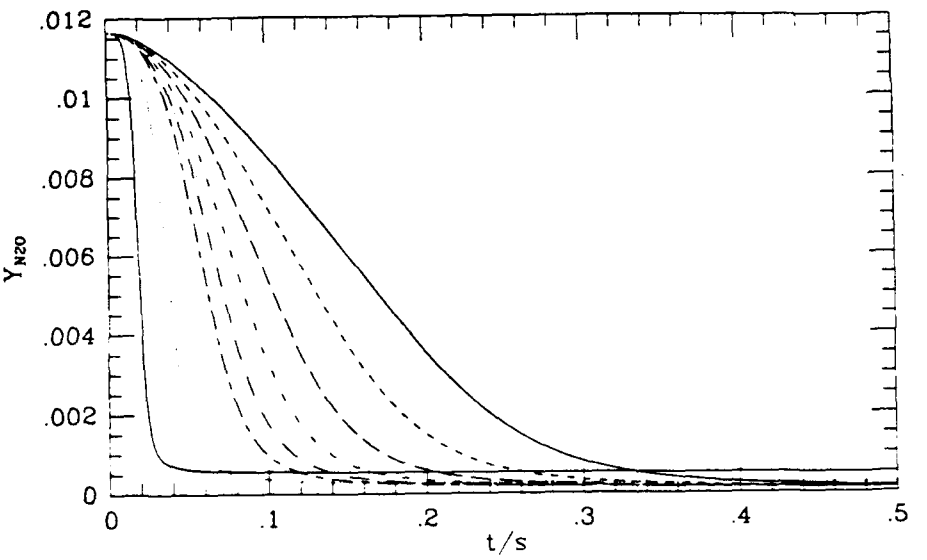

FIGURE 33. Calculated N_2O mass fraction profiles for the initial conditions of EXP 6 of TABLE 5 with various quantities of O_2 added. O_2 concentrations include 0, 10, 20, 30, 40, 50, 100, and 250 *ppm*

Finally, reactions involving NH_2, NH_3, and NNH in the NO_x mechanism of Melius and Bowman were added to this system and found to have no effect.

4.3 Discussion and Conclusions

The results of N_2O decomposition show that the model and experiment are in general agreement. However, further experiments are needed to validate the model. The experiments need to be extended to longer extents of reaction and higher pressures. Trace quan-

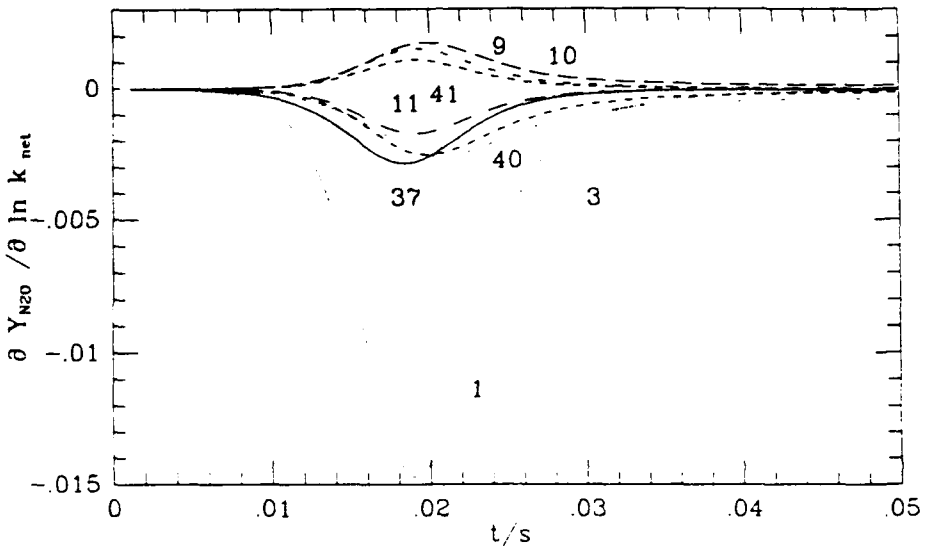

FIGURE 34. Sensitivity gradients $\partial Y_{N2O}/\partial lnk_{net}$ for the conditions of EXP 6 with 250 *ppm* O_2

tities of water vapor have been shown numerically to significantly affect the rate of N_2O decomposition due to the importance of OH radicals reacting with N_2O. The OH radicals are formed from the branching reaction between H_2O and O-atoms, the latter which are formed from the thermal decomposition reaction. The products of the reaction between OH and N_2O are N_2 and HO_2. The HO_2 continues the chain by reacting with the NO formed from the reaction of O-atoms with N_2O. The products of the HO_2 + NO reaction are NO_2 and OH, in which OH is reformed allowing the chain to start over again. Note that H-atoms are not formed in significant quantities in this system and hence the reactions of H+N_2O are not important. Further, without H-atoms, the molecular oxygen which is formed from N_2O and NO_2 reacting with O-atoms does not lead to branching, as it can in systems with H_2 present instead of H_2O. Experiments conducted with various amounts of

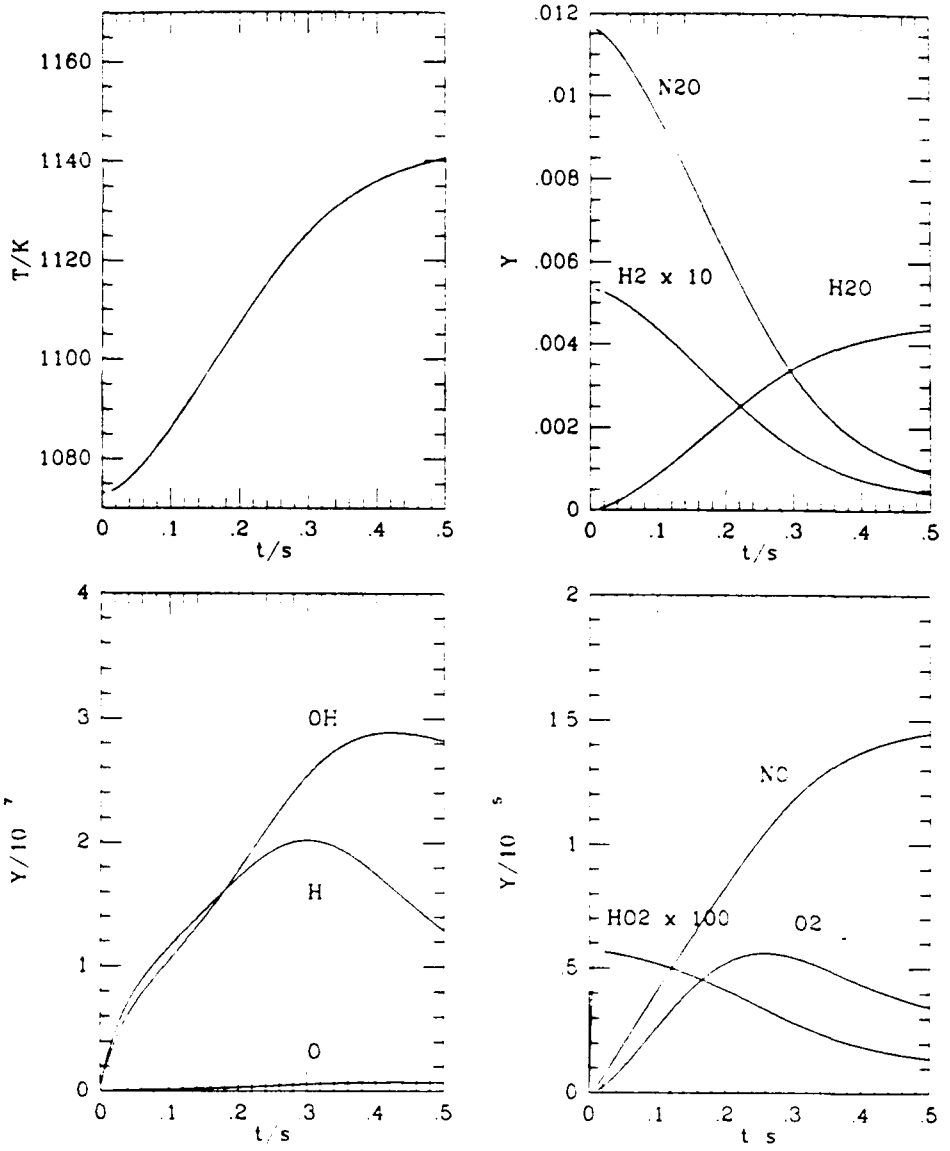

FIGURE 35. Calculated temperature and mass fraction profiles for the reaction of H_2 and N_2O for the conditions of EXP 6 of TABLE 5 with reactions 51-73 of TABLE 4 added to the mechanism.

water vapor are therefore important and will be conducted. Trace amounts of O_2 were found numerically to have little affect the decomposition rate.

The results of the H_2/N_2O reaction again show the model to generally predict the experiments. The results presented here suggest that at the present conditions, the reaction of H + N_2O -> NH + NO may not be important. The rate constants presently available in the literature suggest that the inclusion of NH in the mechanism would slow the overall reaction by approximately 25%. However, the presence of NH in the mechanism predicts higher NO levels than were measured in the experiments. For the H_2/N_2O systems, the reaction between OH and N_2O was again found to be important at our conditions. The importance of this reaction and of HO_2 radicals in the H_2/N_2O system appears to be greater than pre-

viously observed in flame studies or in the lower temperature study of Baldwin *et al.*, (who did not consider it at all). The results also show (which are consistent with other studies, e.g., Balakhnine *et al.*) that the formation of molecular oxygen is important in pure H_2/N_2O systems because it leads to branching through reaction of H-atoms with molecular oxygen. Studies with addition of molecular oxygen are therefore important and can be used to adjust residence times in the experiments for various reaction temperatures.

5.0 NO_2 DECOMPOSITION AND REACTION WITH H_2

5.1 Introduction

At intermediate temperatures, nitrogen dioxide is reduced only partially by hydrogen, according to the stoichiometry,

$$H_2 + NO_2 \rightarrow H_2O + NO$$

At higher temperatures, such as in flames, complete reduction of nitrogen dioxide occurs.

The work of Ashmore and Levitt (1956, 1957, 1958) and of Rosser and Wise (1957) on the thermal reaction between hydrogen and nitrogen dioxide have convincingly shown that the mechanism is straight chain consisting mainly of,

$$NO_2 + H_2 \leftrightarrow HONO + H \qquad 28$$

$$H + NO_2 \leftrightarrow OH + NO \qquad 31$$

$$OH + H_2 \leftrightarrow H_2O + H \qquad 3$$

$$OH + NO_2 + M \leftrightarrow HNO_3 + M \qquad 32$$

$$OH + NO + M \leftrightarrow HONO + M \qquad 25$$

The rate of reaction in the intermediate temperature range was experimentally found to be empirically expressible as

$$-\frac{d[NO_2]}{dt} = \frac{k[NO_2][H_2]^{1.3 to 1.50}}{[NO] + [NO_2]}.$$

According to this relationship, the reaction rate is self-inhibiting because of NO formation, which leads to chain termination. Steady state analysis (Rosser and Wise, 1957) of [H] and [OH] of the above set of elementary reactions yields

$$-\frac{d[NO_2]}{dt} = \frac{k_{28}k_3[NO_2][H_2]^2}{k_{25}[NO] + k_{32}[NO_2]}.$$

The lower $[H_2]$ reaction order observed experimentally was attributed to additional H-atom loss, e.g., via wall termination.

Sawyer and Glassman (1968) studied the H_2/NO_2 reaction in a flow reactor similar to the one used in the present study (where wall termination should be negligible). Yet Sawyer and Glassman found a H_2 dependence similar to that of Rosser and Wise and of Ashmore and Levitt, where wall termination was present. They suggested additional termination through the reaction H + NO + M -> HNO + M and showed that by considering this reaction as the main terminating step that the theoretical H_2 dependence is lowered to unity. Thus any termination reaction removing hydrogen atoms acts to reduce the order with respect to hydrogen.

Anderson et al. (1989) have recently performed a detailed modelling study of the homogeneous ignition kinetics of H_2/NO_2 mixtures. The two stage process of the nitrogen chemistry was shown to occur through conversion of NO_2 to NO by reaction with H atoms in the first stage and conversion of the NO to N_2 by N atoms or via the formation and consumption of HNO, NH, and N_2O in the second stage.

Volponi and Branch (1990) have recently studied the H_2/NO_2 system in laminar premixed flames. Agreement between experiment and numerical model predictions were generally in good agreement. The reaction was found to be most sensitive to the reactions

$$H + NO_2 \leftrightarrow OH + NO \qquad 31$$

$$OH + H_2 \leftrightarrow H_2O + H \qquad 3$$

$$O + H_2 \leftrightarrow OH + H \qquad 2$$

$$H + O_2 \leftrightarrow OH + O \qquad 1$$

$$OH + OH \leftrightarrow O + H_2O \qquad 4$$

$$NO_2 + M \leftrightarrow NO + O + M \qquad 21b$$

$$NO_2 + O \leftrightarrow NO + O_2 \qquad 29$$

In contrast to intermediate and lower temperatures where molecular oxygen and O-atom reactions were found to be unimportant, the flame results show that these reactions are of significant importance. This change in mechanism results from the increased rate of NO_2 decomposition at higher temperatures yielding O-atoms which react with NO_2 to produce O2. Because of the branching introduced into the system via formation of O_2, the reaction of H + NO_2 -> NO + OH acts to inhibit the overall rate.

5.2 Results

TABLE 6 reports the initial experimental conditions of the systems studied for NO_2 decomposition and its reaction with H_2. An example of the experimental results of H_2 reacting with NO_2 is reported in FIGURE 36 for the initial conditions of EXP 4 listed in TABLE 6.

TABLE 6. Experimental Conditions of NO_2 Experiments

EXP	T/K	P/atm	X_{NO2}	X_{H2}	Φ
1	1073	3	0.0002	0.0	
2	953	3	0.0002	0.0	
3	853	3	0.0002	0.004	10
4	873	3	0.0005	0.004	4

The experiments show the consumption of NO_2 and the formation of H_2O. A small temperature rise is also observed. The formation of a currently unidentified species (speculated as HNO_3 or HONO) is observed to occur in appreciable amounts. The FTIR spectra and calibration of these species is currently being investigated. The species shown in the figure is assumed to be HNO_3 and is calibrated by O-atom balance closure. Further studies need to be conducted to verify that this species is a gas phase product and not a result of the sampling process.

Model predictions for this experiment are presented in FIGURE 37. As can be seen from the figure, the experiment is about a factor of 2-3 slower than the model predicts. Further, formation of either HONO or HNO_3 in quantities no greater than 4 ppm are predicted. Of the three radicals, H, O, and OH, only OH is present in appreciable concentrations.

The corresponding sensitivity analysis results for the gradient, $\partial Y_{NO2}/\partial lnk_{net}$ are presented in FIGURE 38. The most sensitive reactions in decreasing order of importance are

$$OH + H_2 \leftrightarrow H_2O + H \qquad 3$$

$$NO_2 + H_2 \leftrightarrow HONO + H \qquad 28$$

$$HONO + OH \leftrightarrow H_2O + NO \qquad 51$$

$$H + NO_2 \leftrightarrow OH + NO \qquad 31$$

$$OH + NO + M \leftrightarrow HONO + M \qquad 25$$

$$NO + H + M \leftrightarrow HNO + M \qquad 23$$

Reactions 3, 28, 31, and 25 are in agreement with previous studies. However, the present model also indicates the importance of reaction 51, which consumes HONO, and of reaction 23, which removes H-atoms from the system. Hence, both of these reactions inhibit the reaction rate.

Of the above reactions with the greatest sensitivity, reactions 28 and 51 have the largest uncertainties. The recommended value for reaction 28 is from Slack and Grillo (1978) who derived the rate from an analysis of the complex kinetics of $H_2/O_2/NO_2$ ignition. An uncertainty of a factor of 5 is assigned by Tsang and Herron. The experiments of Slack and Grillo were conducted with non-dilute mixtures in a shock tube. Significant pressure (factor of 3) and temperature (approx. 200 K) rises are predicted from numerical simulations of their experiments. Hence, their results are highly coupled to the temperature and pres-

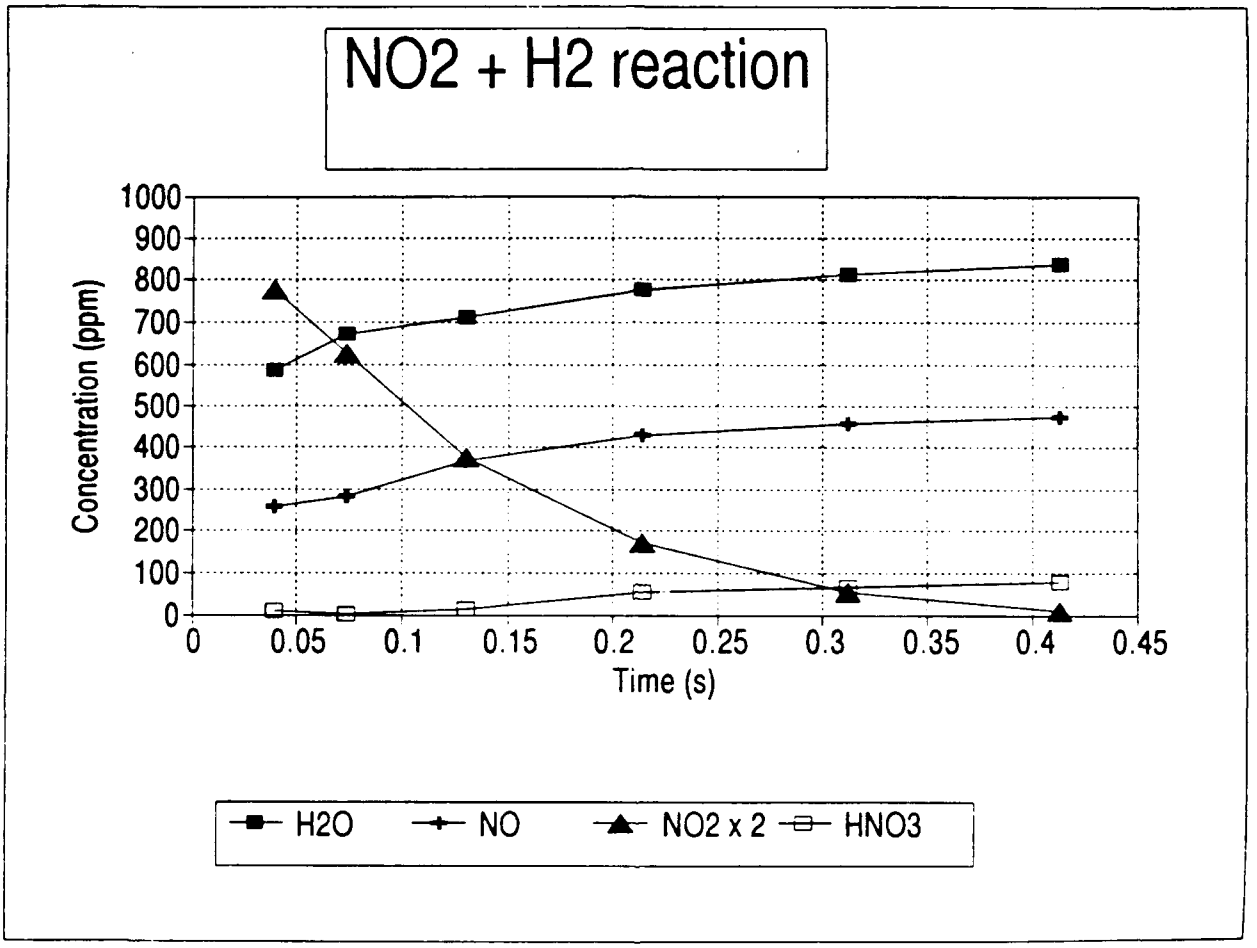

FIGURE 36. Experimental concentration profiles for the reaction of H_2 and NO_2 with the conditions of EXP 4 of TABLE 6.

sure histories of the experiments, which were not monitored. FIGURE 39 reports the numerical results for the experimental condition EXP 4 with a factor of 5 decrease in the rate of reaction 28. The variation is the uncertainty limit and produces good agreement between the experimental and model predicted rates of NO_2 disappearance.

The value for reaction 51 is also that recommended by Tsang and Herron and is derived from low temperature data. The only high temperature data (1000 K) is from Fifer (1976), which is about a factor of 10 lower than the value used here. Tsang and Herron report an uncertainty of a factor of 2 on their low temperature extrapolation. A decrease in reaction 51 would not improve the agreement in the rates of NO_2 disappearance between experi-

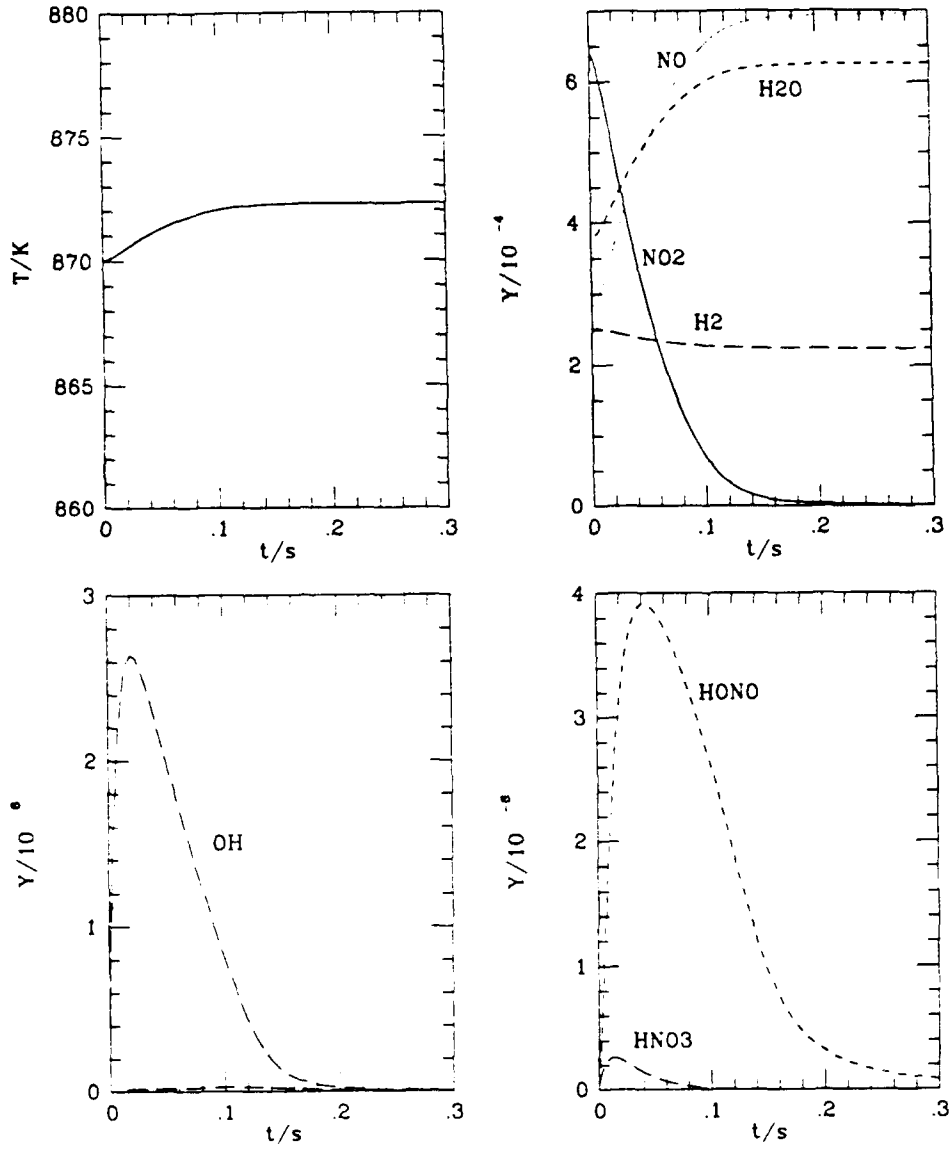

FIGURE 37. Calculated temperature and mass fraction profiles for the reaction of H_2 and NO_2 with the conditions of EXP 4 of TABLE 6

ment and model prediction. However, this change may yield more HONO as a product species.

The value used for reaction 31 is from Ko and Fontijn who note that this reaction has been reported to proceed through a HONO* intermediate.

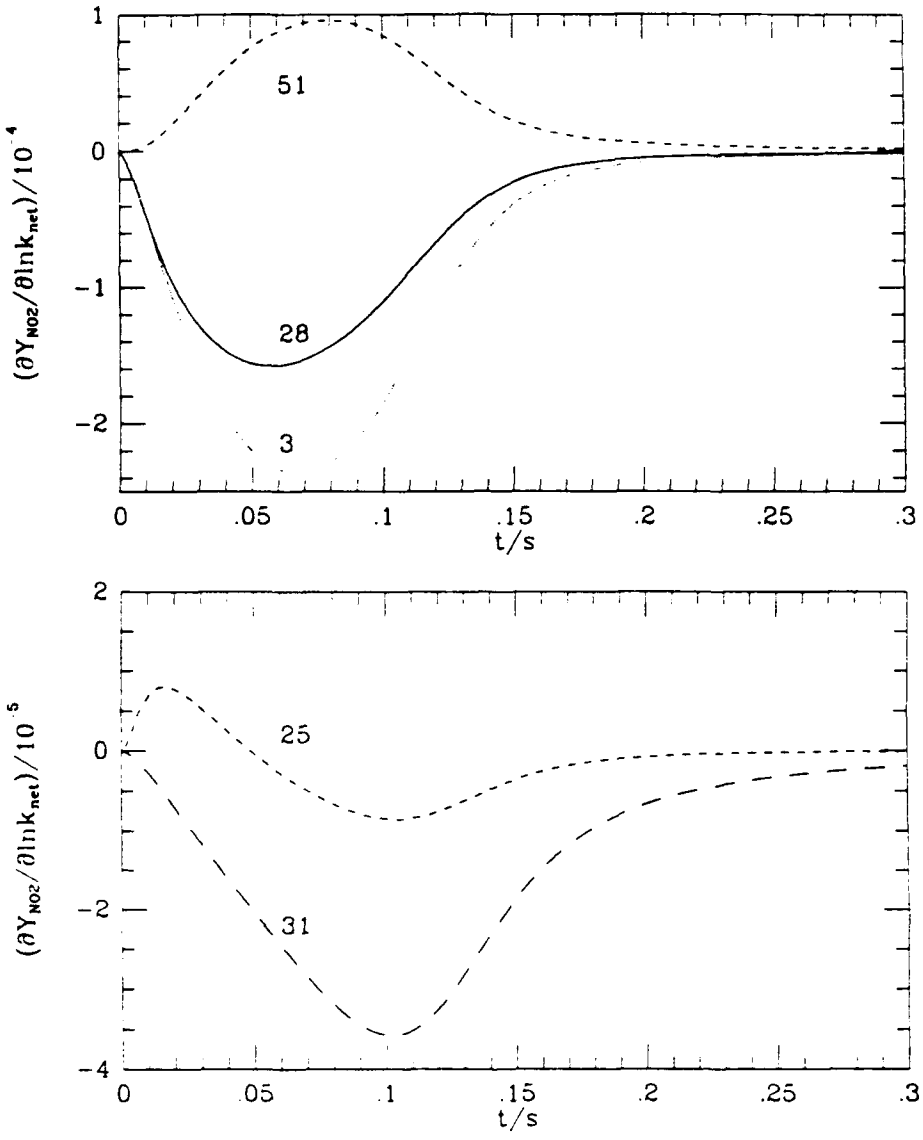

FIGURE 38. Sensitivity gradients $\partial Y_{NO2}/\partial lnk_{net}$ for the conditions of FIGURE 36

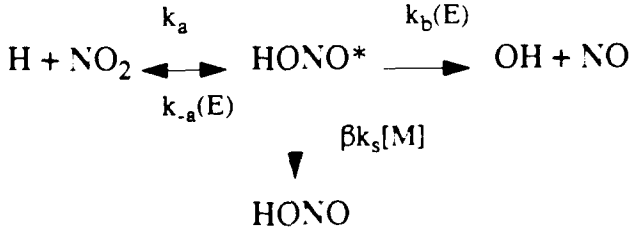

and suggest for propellant combustion that the stabilization channel leading to HONO be included in kinetic mechanisms. They estimate that the stabilization rate is approximately equal to the dissociation rate for [M] approximately 10^{21} cm^{-3}. The stabilization channel would slow the reaction rate in the model predictions here. However, the pressures of the present experiments produce values of [M] two orders of magnitude lower than this estimate.

In the previous section, oxygen addition to the H_2/N_2O system was observed to accelerate the rate of reaction. FIGURE 40 shows the effect of O_2 addition to H_2/NO_2 mixtures. The top figure shows the addition of 10, 20, 30, 40, 50, and 250 ppm O_2 to the initial conditions of EXP 4 of TABLE 6. The results indicate O_2 addition to have an insignificant affect on the rate of NO_2 consumption. The initial temperature of the system is 870 K which at 3 atmospheres is above the extension of the second explosion limit of H_2/O_2 mixtures. As a result, the rate of $H + O_2 + M$ exceeds that of $H + O_2$ and significant branching from the addition of O_2 is prevented. At 3 atmospheres, the transition temperature where branching in the system overtakes stabilization of the hydroperoxyl radical is approximately 970 K. The bottom half of FIGURE 40 shows the kinetics of the same mixtures, except for an initial temperature of 1070 K, which is below the extension of the second limit. Note that in this case, O_2 does not have a significant effect due to the rate of reaction $NO_2 + H$ exceeding that of the reaction $H + O_2$.

Nitric dioxide decomposition was also studied over a limited set of conditions (T > 950 K). Due to complications with the mixer-diffuser design, comparisons of these data with model predictions have not been carried out. The present mixer/diffuser design incorporates some stainless steel surfaces which apparently cause NO2 surface reactions at these conditions. With the new quartz mixer-diffuser section in place, these experiments will be repeated. Modeling studies show the decomposition rate to be controlled by three reactions,

$$NO_2 + O \leftrightarrow NO + O + M$$

$$NO_2 + M \leftrightarrow NO + O + M$$

$$NO_2 + NO_2 \leftrightarrow NO_3 + NO.$$

5.3 Discussion

Although the reactions of H_2/NO_2 system are generally well understand, their rates in the temperature and pressure ranges of the systems studied here appear to need further refinement. The kinetics of the present systems were found to be sensitive to reactions which form and consume HONO. In particular, current values for the initiation reaction may be as much as a factor of 5 to large. Because this system forms the building block on which other mechanisms for the decomposition of nitramines are to be constructed, an accurate description of the kinetics is important.

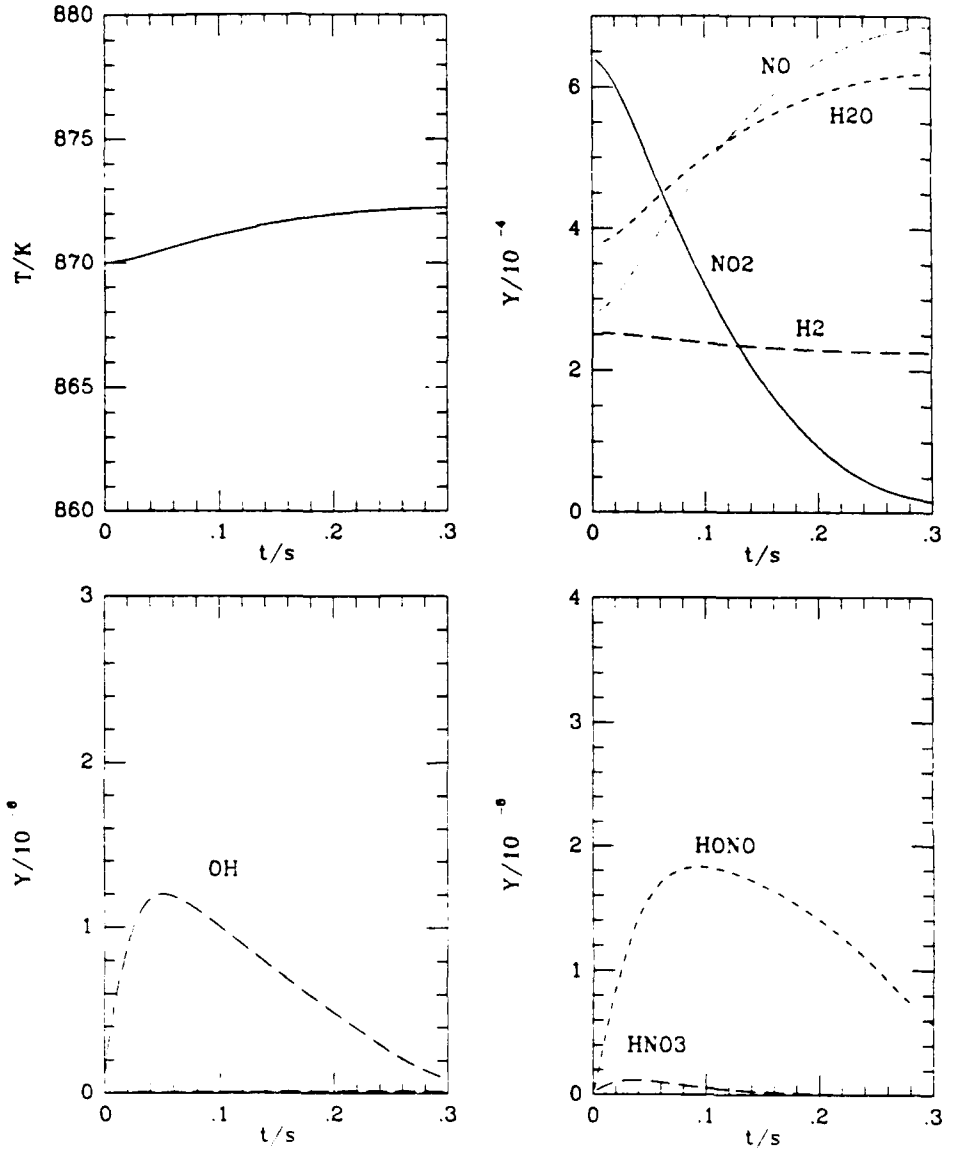

FIGURE 39. Calculated temperature and mass fraction profiles for the reaction of H_2 and NO_2 for the conditions of EXP 4 of TABLE 6 with reaction 28 decreased by a factor of 5

6.0 FUTURE WORK

Research will continue on the H_2/N_2O and H_2/NO_2 systems. Additional fuels which remain to be studied include CO, CH_2O, CH_4, C_2H_4, HCN, and NH_3. We also expect to have in-situ optical diagnostic capability for OH radicals operational in the variable pressure flow reactor during the next year. The kinetic models for $H_2/N_2O/NO_2$ systems will be completed and the experimental and modeling of the kinetics on the additional fuels listed above will be initiated.

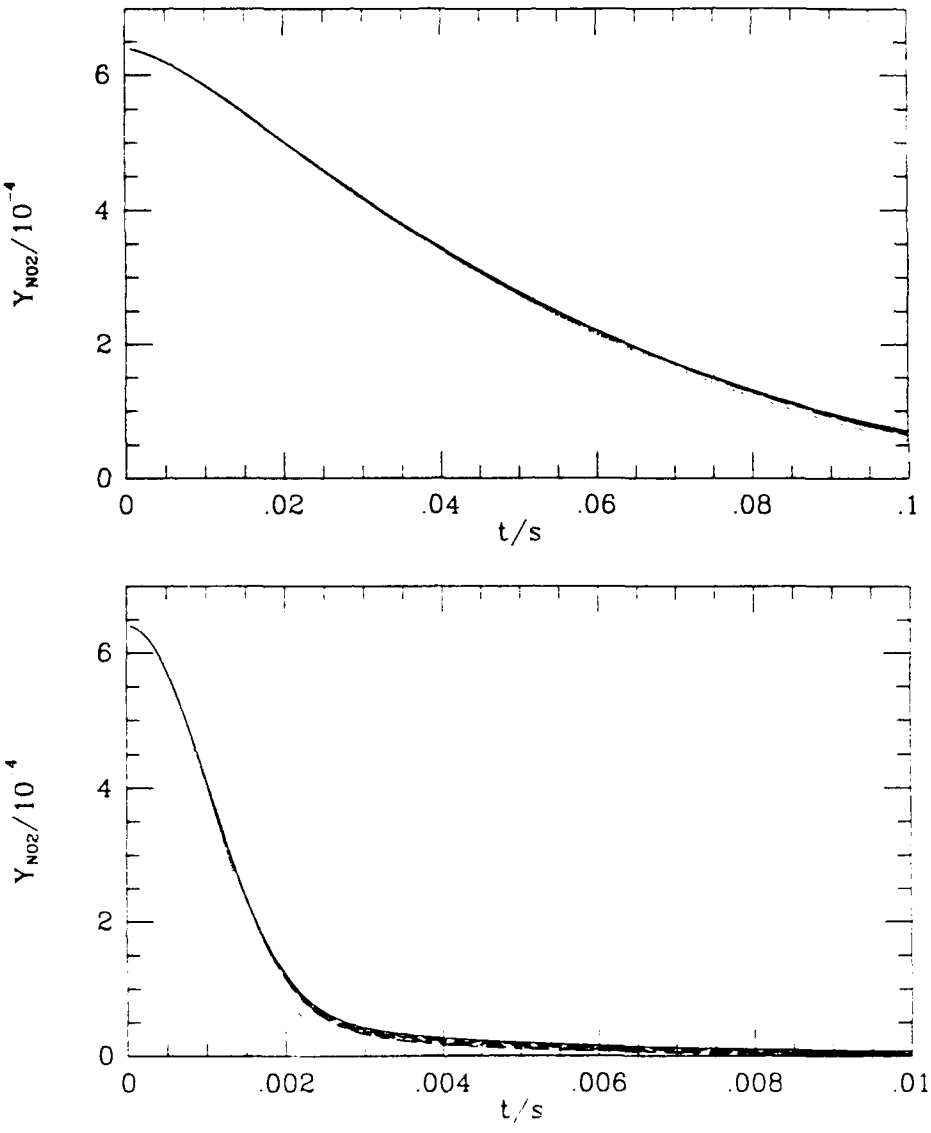

FIGURE 40. Calculated NO_2 mass fraction profiles for the initial conditions of EXP 4 of TABLE 6 with various quantities of O_2 added at 870 K (top) and 1070 K (bottom).

7.0 REFERENCES

Alexander, M.H., Dagdigian, P.J., Jacox, M.E., Kolb, C.E., Melius, C.F., Rabitz, H., Smooke, M.D., and Tsang, W., "Nitramine Propellant Ignition and Combustion Research: New Tools and New Directions", U.S. Army Research Office Technical Report, Army Research Office, Triangle Park, NC, February, 1989.

Anderson, W.R., Kotlar, A.J., and Adams, G.F., "Detailed Kinetic Modeling Relevant to Propellant Combustion", 1989 JANNAF Combustion Meeting, Jet Propulsion Laboratory, Pasadena, CA, 23-27 October 1989.

Ashmore, P.G. and Levitt, B.P., "The Thermal Reaction Between Hydrogen and Nitrogen Dioxide. Part 2 Experimental Work on the Kinetics of the Reaction", Transactions of the Faraday Society, 52, 835 (1956).

Ashmore, P.G. and Levitt, B.P., "The Thermal Reaction Between Hydrogen and Nitrogen Dioxide. Part 3 Further Experimental Work on the Kinetics: Reaction Mechanism", Transactions of the Faraday Society, 53, 945 (1957).

Ashmore, P.G. and Burnett, M.G., "Concurrent Molecular and Free Radical Mechanisms in the Thermal Decomposition of Nitrogen Dioxide" Transactions of the Faraday Society, 58, 253, 1966.

Balakhnine, V.P, Vandooren, J., and Van Tiggelen, P.J., "Reaction mechanism and rate constants in lean hydrogen - nitrous oxide flames", Combust. Flame, 28, 165, (1977).

Baldwin, R.P., Gethin, A., Paistowe, J., and Walker, R.W., "Reaction between hydrogen and nitrous oxide", J. Chem. Soc., Faraday Trans. 1, 71, 1265 (1975).

Borisov, A.A., Zamanskii, V.M., Krestinin, A.V., Skachkov, G.I., "Determination of rate constants for elementary reactions in self-igniting mixtures of nitrous oxide with hydrogen", Khim. Fiz. Protesessov Goreniya i Vzryua. Kinetika Khim. reaktsii. 81-4, 1977. Ref. Zh., Khim 1978.

Bossard, H.R., Singleton, D.L., and Paraskeuopoulos, G., "Kinetic Study of the Recombination Reaction $OD+NO_2+M \rightarrow DNO_3+M$", Int. J. Chem. Kinet. 20, 609, 1988.

Branch, M.C., Alfaragedhi, A.A., Sadeqi, M.A., and Van Tiggelan, P.J., "Measurement of the Structure of Laminar Premixed Flames of $CH_4/NO_2/O_2$ and $CH_2O/NO_2/O_2$ Flames", Combustion and Flame, in press, 1989.

Branch, M.C., Alasfour, F.N., and Habesbullah, M.A., "Structure of Laminar Premixed CH_4/N_2O and CH_2O/N_2O Flames", Proceedings of the Joint Meeting of the British and French Sections of the Combustion Institute, in press, 1989.

Brezinsky, K. (1985), "The High Temperature Oxidation of Aromatic Hydrocarbons", Prog. Energy Combust. Sci., 12, 1.

Brezinsky, K. and Dryer, F.L. (1985), "The High Temperature Pyrolysis of N- Octane and Iso-Octane", Western States Section/The Combustion Institute, Paper 3-5A, April.

Brezinsky, K. and Dryer, F.L. (1986), "A Flow Reactor Study of the Oxidation of Iso-Butylene and an Iso-Butylene/N-Octane Mixture", Combust. Sci. and Tech. 45, 225.

Brill, T., "Chemical Studies Simulating a Burning Surface", Workshop on Propellant Flame Structure, University of Delaware, Delaware, August 30, 1991.

Cattolica, R. Smooke, M., and Dean, A. "A Hydrogen-Nitrous Oxide Flame Study", Presented at the Fall Meeting of the Western States Section of the Combustion Institute, The Combustion Institute, Sandia National Laboratories, Livermore, CA, 1982.

Danby, C.J. and Hinshelwood, J., J. Chem. Soc. 464, 1940.

Dinhi, H., Tai, H.-M., and Branch, M.C., (1991). "Combustion Mechanisms of Carbon Monoxide - Nitrous Oxide Flames".

Dryer, F.L. (1989), "The Phenomenology of Modeling Combustion Chemistry", to appear in Fossil Fuel Combustion - A Sourcebook, W. Bartok and A.F. Sarofim, eds., John Wiley and Sons, Inc., NY, 1989.

Dryer, F.L. and Brezinsky, K. (1986), "A Flow Reactor Study of N-Octane and Iso-Octane", Comb. Sci. and Tech. 45, 199.

Endo, A., Glanzer, K., and Troe, J., "Shock Wave Study of Collisional Energy Transfer in the Dissociation of NO_2, ClNO, O_3, and N_2O", J.Phys. Chem. 83, 2083 (1979).

Fifer, R.A., "Kinetics of the Reaction OH+HNO2->H2O+NO2 at High Temperature Behind Shock Waves", J. Phys. Chem. 80, 2717, 1976.

Fine, B.D. and Evans, A., N.A.S.A. Technical Note D-1736, Washington, 1963.

Hautman, D.J. (1981), "Pyrolysis and Oxidation Mechanisms of Propane", Ph.D. Thesis, Department of Mechanical and Aerospace Engineering, Princeton University, Princeton, NJ, MAE Report No. 1471-T.

Henrici, H. and Bauer, S.H., J. Chem. Phys. 50, 1333, 1969.

Hidaka, Y., Takuma, H. and Suga, M. "Shock-tube study of the rate constant for excited hydroxyl formation in the nitrous oxide- molecular hydrogen reaction", J. Phys. Chem., 89, 4903 (1985).

Hills, A.J.and Howard, C.J., "Rate Coefficient Temperature Dependence and Branching Ratio for the Reaction ClO + OH", J.Chem. Phys. 81, 4458, 1984.

Hiraoka, H. and Hardwick, R., "Emission and Dissociation of NO_2 in Shock Waves", J. Chem. Phys. 39, 2361, (1963).

Holliday, M.G. and Reuben, B.G., "Reaction of hydrogen with nitrous oxide", Bull. Soc. Chim. Fr., 9, 3087 (1969).

Kee, R.J., Ripley, F.M., and Miller, J.A., "The chemkin thermodynmamic data base", Sandia Report SAND87-8231, Livermore, CA 1987.

Ko, T. and Fontijn, A., "High Temperature Kinetics Study of the Reaction H + NO_2 -> OH+NO from 296 to 760 K", J. Phys. Chem., 95, 3984, (1991).

Lin, M.C., International Conference on Chemical Kinetics, NIST, 1989.

Linteris, G., Yetter, R.A., Brezinsky, K., and Dryer, F.L., Hydroxyl Radical Concentration Measurements in Moist Carbon Monoxide Oxidation in a Chemical Kinetic Flow Reactor", Combustion and Flame, 86, 162 (1991).

Lutz, A.E., Kee, R.J. and Miller, J.A., "SENKIN: A fortran program for predicting homogeneous gas phase chemical kinetics with sensitivity analysis", Sandia Report SAND87-8248, Livermore, CA 1987.

Melius, C. (1988), "The Gas-Phase Chemistry of Nitramine Combustion", 25th JANNAF Combustion Meeting, Huntsville, Ala., October.

Miller, J.A. and Bowman, C.T., "Mechanism and Modeling of Nitrogen Chemistry in Combustion", Prog. in Eng. and Comb. Sci., 1989.

Mulcahy, M.F.R. and Smith, R.H., "Reactions of OH Radicals in the H-NO_2 and H-NO_2-CO Systems", J. Chem. Phys. 54, 5215, 1971.

Pamidimukkala, K.M., and Skinner, G.B., "Resonance absorption measurements of atom concentrations in reacting gas mixtures", J. Chem. Phys., 76, 311, (1982).

Parr, T. (1989), "Preliminary Results on Polycyclic Nitramine Flames", ONR Combustion Workshop, Princeton, NJ, October.

Pitz, W.J., Westbrook, C.K., Proscia, W.M., and Dryer, F.L. (1984), "A Comprehensive Chemical Kinetic Reaction Mechanism for the Oxidation of n- Butane", Twentieth International Symposium on Combustion, The Combustion Institute, Pittsburgh, PA, p. 831.

Proscia, W.M. (1983), "High Temperature Flow Reactor Experiments and Multi- Step Overall Kinetics for the Oxidation of High Carbon Number Paraffin Hydrocarbons", M.S.E. Thesis, Department of Mechanical and Aerospace Engineering, Princeton University, Princeton, NJ, MAE Report No. 1625-T.

Rosser, W.A. and Wise, H., "Kinetics of the Reaction between Hydrogen and Nitrogen Dioxide", J. Chem. Phys. 26, 571 (1957).

Sawyer, R. and Glassman, I., The Reactions of Hydrogen with Nitrogen Dioxide, Oxygen, and Mixtures of Oxygen and Nitric Oxide", 12th Symposium (International) on Combustion, The Combustion Institute, Pittsburgh, PA, 1968, p. 469.

Shaaban, A.F., "The Integrated Rate Equation of Nitrogen Dioxide Decomposition Reaction", AFINIDAD XLVI, 422 Julio-Agosto, 1989.

Slack, M.W. and Grillo, A.R., "Rate Constants for H_2+NO_2=HNO_2+H derived from Shock Tube Investigations of H_2-O_2-NO_2 Ignition", Comb. Flame, 31, 275 (1978).

Thorne, L.R., Branch, M.C., Miller, J.A., and Chandler, D., "Interaction Between Nitrogen and Carbon Species in H_2/O_2 Laminar Premixed Flames," Twenty- first Sym-

posium (International) on Combustion, The Combustion Institute, Pittsburgh, 965, 1988.

Thorne, L.R. and Melius, C.F., "The structure of Hydrogen Cynanide-Nitrogen Dioxide Premixed Flames", 27th JANNAF Combustion Meeting, 1989.

Troe, J., J. Chem. Phys., 66, 4725 (1977).

Tsang, W. and Herron, J.T., "Chemical Kinetic Data Base for Propellant Combustion: I Reactions involving NO, NO_2, HNO, HONO, HCN and N_2O", 1990.

Vermeersch, M.L.: Ph.D. Thesis, Department of Mechanical and Aerospace Engineering, Princeton University, 1991.

Volponi, J.V. and Branch, M.C., (1990) "Flame Structure of H_2-NO_2-Argon Laminar Premixed Flames", Western States Section of the Combustion Institute, Oct 14-16.

Wayne, L.G. and Yost, D.M., "Kinetics of the Rapid Gas Phase Reaction between NO, NO_2, and H_2O", J. Chem. Phys. 19, 41, 1951.

Westbrook, C.K. and Dryer, F.L. (1984), Prog. Energ. Sci. and Combust. 10, 1.

Westbrook, C.K., Dryer, F.L., and Schug, K.P. (1983), "A Comprehensive Mechanism for the Pyrolysis and Oxidation of Ethylene", Nineteenth International Symposium on Combustion, The Combustion Institute, Pittsburgh, PA, p. 153.

Westbrook, C.K. and Pitz, W.J. (1984), "A Comprehensive Chemical Kinetic Reaction Mechanism for Oxidation and Pyrolysis of Propane and Propene", Comb. Sci. and Tech., 37, 117.

Yetter, R.A., Dryer, F.L., and Rabitz, H., "A Comprehensive Reaction Mechanism for CO/H_2/O_2 Kinetics", Combust. Sci. Tech. 79, 1-3, 129.

Yetter, R.A. (1985), "An Experimental/Numerical Study of Carbon Monoxide- Hydrogen-Oxygen Kinetics with Applications of Gradient Sensitivity Analysis", Ph.D. Thesis, Department of Mechanical and Aerospace Engineering, Princeton University, Princeton, NJ, MAE Report No. 1703-T.

Yetter, R.A., Cho, S.Y., Rabitz, H., Dryer, F.L., Brown, R.C., and Kolb, C.E.,"Chemical kinetic modeling and sensitivity analyses for boron assisted hydrocarbon combustion", Twenty-second Symposium (International) on Combustion, The Combustion Institute, Pittsburgh, 919, 1988.

Zimet, E. "Thermal Decomposition of N_2O_4 and NO_2 by Shock Waves," J. Chem. Phys., 53, 515 (1970).

8.0 APPENDIX

A.0 The Atmospheric Pressure Flow Reactor Experiment

An atmospheric pressure flow reactor used to obtain the intermediate temperature, atmospheric pressure kinetic data is also available for reaction studies. This reactor is designed to approximate a steady, one-dimensional and adiabatic reacting flow with negligible radial gradients of species and energy. Gaseous samples are withdrawn from the reactor at up to fifteen discrete locations along its longitudinal axis with a variable temperature, convection quenched, isothermal sample acquisition and storage system. The sampling system can operate at temperatures between 25°C and 80°C. Elevated storage temperature prevents the condensation of high boiling point intermediate species and prevents polymerization reactions. The storage system interfaces with a microprocessor controlled gas chromatograph for fully automatic analysis of the stored samples. In addition, a continuous analysis train has been developed for determining CO, CO_2, O_2 and H_2 concentrations in the sample stream from which the discrete samples are obtained. The flow reactor, its sampling system, and the analytical instrumentation are discussed in detail below.

A.1 The Flow Reactor

The atmospheric pressure flow reactor, developed in this laboratory and extensively documented elsewhere [1 - 3] is shown schematically in FIGURE 1. Fundamentally, it consists of a cylindrical quartz duct through which hot inert carrier gas (nitrogen) flows at high velocities. A small fraction of the carrier (5-10%) is diverted through an arc plasma discharge, which heats and partially ionizes it. The hot, partially ionized gas is premixed with the bulk of the nitrogen in a plenum chamber, where recombination results in metastable nitrogen molecules (N_2*). Collisional de-excitation of the metastable N_2 is necessary to prevent its further reaction with O_2:

$$N_2^* + O_2 = 2\,NO$$

and to promote this de-excitation the carrier flow continues through a high surface area, ceramic honeycomb section, and emerges as inert N_2. Because the ceramic section has a large thermal capacity, the temperature of the nitrogen leaving the section is constant, (1 *K*, relative) even though fluctuations in the power output from the plasma torch itself (2%) results in temperature fluctuations in the nitrogen entering the section. Desired reaction temperatures (800-1300 *K*) are achieved by variation of the split ratio of the nitrogen flow and of the power to the plasma torch.

Oxygen is injected into the carrier gas upstream of a converging/diverging inlet section and is well mixed with the carrier gas before it reaches the throat of the section. At that point, gaseous fuel is injected through four radially opposed quartz injector tubes. The technique used to pre-vaporize liquid fuel species is described later.

The high velocity radial injection of gaseous fuel into the flowing carrier provides for rapid mixing of the fuel with the oxygen/carrier gas stream. Through proper control of carrier

gas temperature, mixture ratio, and total gas flow rate, a steady reaction zone extending over approximately a meter in length can be established which represents total chemical reaction times between 10 and 150 *ms*. Mean velocity along the axis of the reactor duct is experimentally determined using static pilot probes [4] in reacting flows and hot wire anemometry in non-reacting flows. The use of small initial concentrations of both fuel and oxidizer and the spreading of the reaction zone over a meter gives rise to longitudinal gradients small enough for diffusion of mass and energy along the length of the duct to be neglected with respect to convection [5]. Furthermore, the dilute nature of the reaction and in particular, the limitations therefore imposed on the turbulent fluctuations of temperature from the mean (1%) limits any turbulent fluctuation coupling [6] with chemical kinetics to be negligible. Measured kinetics have been found to be independent of flow Reynolds number within the limits of experimental accuracy (10%). The relatively large duct diameter (10.16 *cm*) results in a small surface to volume ratio and minimizes wall effects.

Adiabaticity is approximated by heating and insulating the inlet section and main reactor duct, so that the walls are quickly equilibrated to the inlet temperature of the carrier gas. The wall temperature is monitored at four locations along the length of the duct by Pt/Pt 13% Rh thermocouples placed in an air gap between the heaters and the duct.

The flow reactor experiment requires that fuels be in a gaseous state, and thus any liquid material is pre-vaporized using an evaporator. The evaporator is shown schematically in FIGURE 2. Nitrogen pressure on the fuel in the storage tank forces metered amounts of liquid fuel through an orifice onto a heated porous cylinder, which is at a temperature above the boiling point of the fuel. The porous cylinder vaporizes the fuel which is simultaneously mixed with a small amount of heated nitrogen in the evaporator and subsequently directed to a manifold which, in turn, feeds the radial injector tubes. Eventually, a steady state is established in which the liquid fuel flow into the evaporator is equal to the gaseous fuel flow out. In order to prevent condensation in the transfer lines leading into the reactor, the flow lines from the evaporator are heated and insulated.

In summary, the flow reactor provides a well-defined and well-monitored reaction zone which can be accurately represented as:

- constant pressure (small energy release, low Mach number flow system)
- one-dimensional
- quasi-steady
- homogeneous (wall effects negligible)
- adiabatic
- with negligible longitudinal diffusion of mass and energy

These operation characteristics and the reproducibility of the experimental data will be discussed later in this appendix.

A.2 Data Acquisition

A.2.1 Extractive and Immersion Measurements

Mean temperature, and species profiles are measured along the length of the reactor duct. The temperature is measured, with a silica coated Pt 30% Rh/Pt 6% Rh alloy thermocouple with a bead diameter of 38 micrometers and a spatial resolution of about twenty bead diameters. Dryer [2] has discussed this technique at length in his Ph.D. thesis.

The gas sampling techniques, in principle, are also those used in earlier flow reactor studies: combustion gases are withdrawn continuously from the reactor with a hot water cooled, water convection quenched probe. The sample stream can be analyzed continuously and discrete volumes can also be extracted from the sample stream and stored for later analysis by a gas chromatograph.

The gas sample probe itself appears in Section A of FIGURE 1 and is constructed of three concentric type 316 stainless steel tubes. The two outer tubes provide passages for the hot water (60-90°C) used to convection cool the flowing gas sample and maintain the mechanical integrating of the probe. The gas sample quench is accomplished purely by convection heat transfer at a rate greater than 10^7 *K/s* (estimated; see [2]). The sample is transferred from the probe to the sampling assembly through heated (thermostated) teflon lines by a heated stainless steel bellows pump. The flow exiting the pump is at approximately 2 atmospheres pressure supplying sample flow to one or several multiloop sampling valves (described later) and the continuous analysis train.

The continuous analysis system (FIGURE 3) provides two principle advantages in conducting flow reactor research:

- It permits accurate placement of the reaction zone within the reactor and thus optimize the experiment for the ranges of extent of reaction to be studied.
- It relieves several complications imposed when simultaneous gas chromatographic analysis of light permanent gases H_2, CO, CO_2 and higher molecular weight hydrocarbons is required.

Carbon monoxide and carbon dioxide are determined using non-dispersive infrared analysis (Beckman, Inc.). Oxygen is determined using a thermomagnetic technique (Leeds and Northrup). A measurement of hydrogen is obtained by catalytic conversion of the dried sample stream and determination of the resulting water vapor by a Dupont Acoustic water vapor analyzer.

What has recently advanced the analytical technology to deal with the oxidation of higher carbon number paraffins and aromatics is the development of a system which would simultaneously acquire and store up to two discrete, heated samples at each longitudinal position sampled in the flow reactor. This technique permits simultaneous use of a Hewlett Packard HP5840 gas chromatograph (GC) for quantitative analysis of the sample for hydrocarbons and of a HP5895 gas chromatography/mass spectrometer (GC/MS) for the respective specie identifications (both by column retention time and mass fractionation patterns).

Successful discrete chemical sampling involves satisfactory accomplishment of each of the following goals:

- isolation of a flow of reactive media from a specific point in the reaction environment.
- prevention of further chemical or thermodynamic alteration of the contained species.
- introduction of a defined quantity of this sample, intact, to an analytical instrument.

The heated sampling system [3] which is now commonly used has several distinct advantages. It interfaces with all analytical equipment in a manner completely analogous to its GC interface, and allows ready identification of species which are impractical to identify with a GC alone and which would be lost to condensation of room temperature.

A heated storage temperature of 70°C has a second advantage related to the integrity of the stored sample: by preventing polymerization reactions associated with the storage of formaldehyde at room temperature, it should allow accurate formaldehyde analysis. Condensation of other, low vapor pressure species is also prevented by heated storage.

Furthermore, the heated sampling system has the advantages of preventing exposure of stored samples to light and to adsorptive surfaces (e.g. mercury, synthetic rubber), both of which occurred in the older system. All surfaces which contact sample gases in the heated sampling system are stainless steel, so the exposure to light that resulted from storage in glass bottles on an exposed sampling rack is circumvented. Furthermore, gases are pressurized for injection with a stainless steel welded bellows pump and not with the mercury system previously in use.

Operation of the heated sampling storage and chromatographic injection facilities are as follows (FIGURE 4). Combustion gases are withdrawn from the reactor through the probe and a length of heated line by a heated stainless steel welded bellows pump. The bellows pump raises the pressure of the sampled gases to approximately two atmospheres pressure, and the flow proceeds through a heated 7 micro filter and temperature equilibrium coils to two sample storage vales. The temperature equilibration coil and the storage valves are contained in separate, portable, thermostated oven assemblies.

Each storage valve itself is a Valco 32 port, 16 position pneumatically actuated valve fitted with sixteen stainless steel sample storage loops. Each of the valve loops has a pre-determined volume of 12 *cc*. When the valve is actuated, the flow is switched from one loop to the next, a defined quantity of sample is trapped in the sealed loop (P, V and T are all defined), and the next sample loop is purged. Up to fifteen discrete samples can be stored in this manner, with the remaining loop open to the flow path. Once filled, the multiposition valve system is carried (in its oven) to a gas chromatograph, where the loops are flushed, one by one, into a chromatographic gas sample injection system (FIGURE 5) and injected onto the GC columns for analysis.

A heated 1 *cc* single loop sample injection valve is used to determine the sample size for actual analysis. This sample injection valve is connected on the inlet side to the multiposition valve (i.e. to the stored samples) through a length of heated line, and on the outlet side to a manostat/vacuum system. When the multiposition valve is actuated and a new storage loop is exposed to the sample injection system, the gases in the 12 *cc* loop, at 2 atmospheres, flow through the 1 *cc* secondary sample injection loop until the pressure in the system is equilibrated to 0.5 atmospheres (controlled by a cartesian manostat). Sufficient

excess sample is stored in the multiposition valve loops to assure complete displacement of any residual gases in the secondary sample valve and transfer lines. The 0.5 *atm.* sample in the secondary sample valve is then injected onto the gas chromatograph columns for analysis. Actuation of both the multiposition valve and the secondary sample valve is controlled by a microprocessor indigenous to the gas chromatograph, so fully automatic analysis of successive samples is possible. This procedure not only assures a constant systematic error, but minimizes sample storage times and reduces dramatically the manpower which must be devoted to the analysis of samples. Previous (manual) injection techniques required operator attention throughout the 25+ hour analysis time required for a complete flow reactor analysis. With the present system interfaced to the gas chromatograph and the GC microprocessor preprogrammed, no additional operator attention is required for complete analysis.

Because the sample injected onto the GC columns is set in the same loop each time, the effects of loop volume variability are eliminated. Sample storage valve leakage problems are also circumvented: since samples are stored at a positive pressure, gases leak out, not in. Any loss of sample at the small rates resulting from loop to atmosphere and loop to loop diffusion is not reflected in the sample delivered to the sampling injection valve, since a large volume of sample gas is initially stored. Cross leak distortion of the stored sample has been shown to be less than 1%, even for the lightest gas expected in hydrocarbon oxidation studies (CH). Note that since diffusion rates are inversely proportional to the square root of the molecular weight of the diffusing species, errors for most species will be significantly smaller.

In summary, the advantages of this unique sampling storage and chromatographic injection system are:

- control of the sample acquisition and storage temperatures (up to about 80°C).
- sample isolation from adsorptive surfaces.
- sample isolation from light surfaces.
- automation.
- Additional details appear in the recent thesis of Euchner [3].

A.2.2 Reproducibility of Experimental Data

We have recently performed two research studies [4, 7] which adequately demonstrate the nature and quality of the experimental data obtained from the flow reactor.

In a study on the elementary combustion chemistry of the $CO/H_2/O_2$ system [4], we have performed extensive experiments which involve the turbulent flow reactor and the continuous sampling system. In the performance of some of these experiments we investigated the ability to reproduce the same experimental initial conditions and chemical analysis data by attempting to repeat the same experiment on six occasions over a period of 6 months. The experimental conditions and results are shown in FIGURE 6. The precision of these data is clearly evident and indicates both the ability to reproduce experimental variables and also the continuous sampling instrumentation calibration effects.

FIGURE 7 presents the comparison of elementary kinetics calculations performed using accepted literature rate constant and mechanism with experimental measurements on the $CO/H_2/O_2$ system [4] (See TABLES 5 and 6). In the four flow reactor experiments (point data), only the initial reaction temperature was changed. The three calculations (line data) performed show very good agreement with the experimental data, even for reaction times approaching 0.6 seconds! It should be emphasized that there was no performance of "empirical fitting" of the model to the data, and no effects of diffusive and turbulent transport or coupling with chemistry were considered in the model. These comparisons therefore support the "pure chemistry" interpretation of flow reactor data. Finally it should be emphasized that the experimental and calculated results are for condition crossing the explosion limit regime for $CO/H_2/O_2$ chemistry at one atmosphere.

A second set of data which demonstrate the precision of the discrete chemical sampling and gas chromatographic analytical results are presented in FIGURE 8. These data were performed as part of a recent thesis [7] and were obtained from the analysis of samples (16 samples by each valve, one sample in each valve at each sampling position) taken by two sample storage valves in parallel in the flow reactor sampling systems. The 16 loops of each sample valve were then analyzed sequentially, with the analysis of the second valve samples following the first. The chemical analysis thus spanned a period of some 72 hours after the flow reactor experiment had been concluded. The reproducibility of this data is again excellent.

A.2.3 Optical Measurements

The flow reactor has optical access at three axial positions for line of site absorption measurements. Linteris [8], has shown that OH can be quantitatively measured in the $CO/H_2O/O_2$ reactor system at flow reactor temperatures using resonance absorption, and that the results compare favorably with those predicted [4]. In order to obtain measurements at other locations in the reactor, a unique optical probe was developed [8], based on 180° laser induced fluorescence (LIF). The technique has been shown to be feasible and to produce OH profiles which could be successfully calibrated by simultaneous resonance absorption measurements. Examples of the results are reported in FIGURE 9.

A.3 REFERENCES

41. Crocco, L., Glassman, I. and Smith, I.E., Jet Propulsion, 1266 (1957).

42. Dryer, F.L., Ph.D. Thesis, Department of Aerospace and Mechanical Sciences, Princeton University, Princeton, NJ (1972).

43. Euchner, J.A., M.S.E. Thesis, Mechanical and Aerospace Engineering Department, Princeton University, Princeton, NJ (1980).

44. Yetter, R.A., Ph.D. Thesis, Mechanical and Aerospace Engineering Department, Princeton University, Princeton, NJ (1985).

45. Westbrook, C.K., Creighton, J., Lund, C. and Dryer, F.L., J. Phys. Chem., 81, 2542 (1977).

46. Gouldin, F.C., Comb. Sci. Tech., 9, 17 (1974).

47. Proscia, W.M., M.S.E. Thesis, Mechanical and Aerospace Engineering Department, Princeton University, Princeton, NJ (1983).

48. Linteris, G.T., Ph.D. Thesis, Department of Mechanical and Aerospace Engineering Department, Princeton University, Princeton, NJ (1990).

A.4 TABLES

TABLE 7. $CO/H_2/O_2$ Thermochemical Parameters[a]

SPECIES	$\Delta H_{f,298}$	S_{298}	$C_{p,300}$	$C_{p,400}$	$C_{p,500}$	$C_{p,600}$	$C_{p,800}$	$C_{p,1000}$	$C_{p,1500}$
H	52.10	27.39	4.97	4.97	4.97	4.97	4.97	4.97	4.97
O	59.56	38.47	5.23	5.14	5.08	5.05	5.02	5.00	4.98
OH	9.32	43.88	7.15	7.10	7.07	7.06	7.13	7.33	7.8
H_2	0.00	31.21	6.90	6.96	7.00	7.02	7.07	7.21	7.73
O_2	0.00	49.01	7.01	7.22	7.44	7.65	8.07	8.35	8.72
H_2O	-57.80	45.10	8.00	8.23	8.44	8.67	9.22	9.87	11.26
HO_2	3.00	54.43	8.36	8.95	9.48	9.96	10.75	11.37	12.34
H_2O_2	-32.53	55.66	10.41	11.44	12.34	13.11	14.29	15.21	16.85
CO	-26.42	47.21	6.95	7.03	7.14	7.27	7.61	7.95	8.41
CO_2	-94.06	51.08	8.91	9.86	10.65	11.31	12.32	12.99	13.93
HCO	10.40	53.66	8.24	8.78	9.28	9.77	10.74	11.52	12.56
N_2	0.00	45.77	6.95	7.01	7.08	7.19	7.50	7.83	8.32

[a] units are *kcal/mol* for $\Delta H_{f,298}$ and *cal/mol-K* for S and C_p

TABLE 8. $CO/H_2/O_2$ Reaction Mechanism

	ΔH_{298}	$\log(A_f)$	n_f	$E_{a,f}$	UF	T_{RANGE}
H_2-O_2 Chain Reactions						
1. $H+O_2 = O+OH$	16.77	14.28	0.00	16.44	2	962-2577
2. $O+H_2 = H+OH$	1.86	4.71	2.67	6.29	1.5	297-2495
3. $OH+H_2 = H+H_2O$	-15.02	8.33	1.51	3.43	1.5	250-2581
4. $OH+OH = O+H_2O$	16.87	$k=5.46\times10^{11}\exp(0.00149\times T)$[c]			2.5	250-2000
H_2-O_2 Dissociation/Recombination Reactions						
5. $H_2+M = H+H+M$	104.1	19.66	-1.40	104.38	3.0	600-2000
6. $O+O+M = O_2+M$	-119.1	15.79	-0.50	0.00	1.3	2000-10000
7. $O+H+M = OH+M$	-102.3	18.67	-1.00	0.00	10.0	-----
8. $H+OH+M = H_2O+M$	-119.2	22.35	-2.00	0.00	2.	1000-3000
Formation and Consumption of HO_2						
9. $H+O_2+M = HO_2+M$	-49.07	19.83	-1.42	0.00	3.	200-2000

10. $HO_2+H = H_2+O_2$	-55.07	13.82	0.00	2.13	2.	298-773
11. $HO_2+H = OH+OH$	-36.44	14.23	0.00	0.87	2.	298-773
12. $HO_2+O = OH+O_2$	-53.22	13.24	0.00	-0.40	1.2	200-400
13. $HO_2+OH = H_2O+O_2$	-70.09	16.16	-1.00	0.00	2.	298-1400
Formation and Consumption of H_2O_2						
14. $HO_2+HO_2 = H_2O_2+O_2$	-38.51	12.48	0.00	1.39	3.	650-800
15. $H_2O_2+M = OH+OH+M$	51.14	17.08	0.00	45.50	2.	700-1500
16. $H_2O_2+H = H_2O+OH$	-68.02	13.00	0.00	3.59	3.	283-800
17. $H_2O_2+H = H_2+HO_2$	-17.56	13.68	0.00	7.95	5.	250-800
19. $H_2O_2+OH = H_2O+HO_2$	-32.57	12.85	0.00	1.43	2.	98-800
Oxidation of CO						
20. $CO+O+M = CO_2+M$	-127.01	13.40	0.00	-4.54	4.	1000-3000
21. $CO+O_2 = CO_2+O$	-8.08	12.40	0.00	47.69	2.	500-3000
22. $CO+OH = CO_2+H$	-24.85	$k=6.75x10^{10}exp[0.000907xT]^c$			1.5	250-2500
23. $CO+HO_2 = CO_2+OH$	-60.79	13.78	0.00	22.95	3.	700-1000
Formation and Consumption of HCO						
24. $HCO+M = H+CO+M$	15.27	17.27	-1.0	17.00	5.	637-832
25. $HCO+O_2 = CO+HO_2$	-34.30	12.62	0.00	0.00	5.	295-713
26. $HCO+H = CO+H_2$	-88.87	13.86	0.00	0.00	2.	296-418
27. $HCO+O = CO+OH$	-87.02	13.48	0.00	0.00	3.	---
28. $HCO+OH = CO+H_2O$	-103.09	13.48	0.00	0.00	3.	---

[a]units are cm^3-*mole-s-kcal*, $k = AT^n \exp(-E_a/RT)$

[b] $[M] = [N_2]+[H]+[O]+[OH]+2.5[H_2]+[O_2]+12[H_2O]+[HO_2]+[H_2O_2]+1.9[CO]+3.8[CO_2]+[HCO]$

A.5 FIGURES

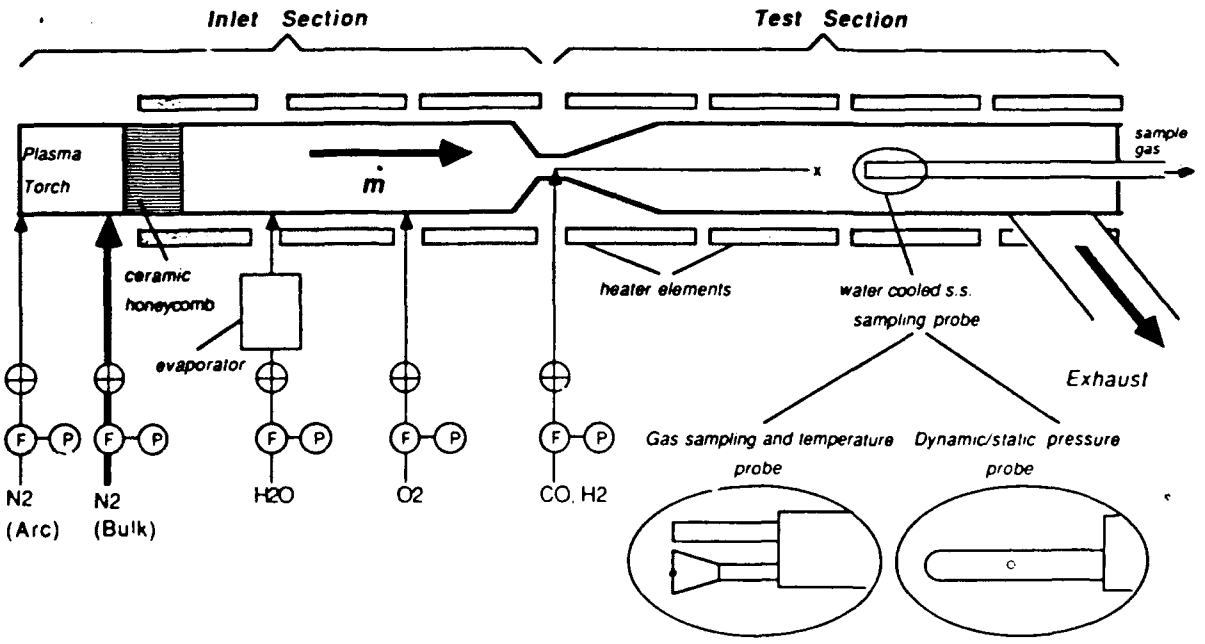

FIGURE 1. Schematic diagram of flow reactor and flow measurements, respectively. T, P and F indicate temperature, pressure

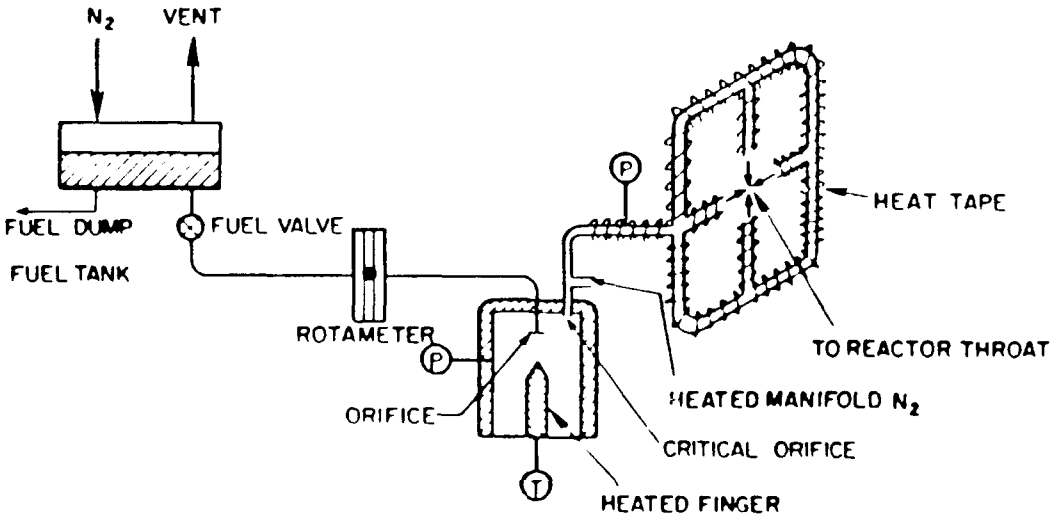

EVAPORATOR SCHEMATIC

FIGURE 2. Evaporator schematic

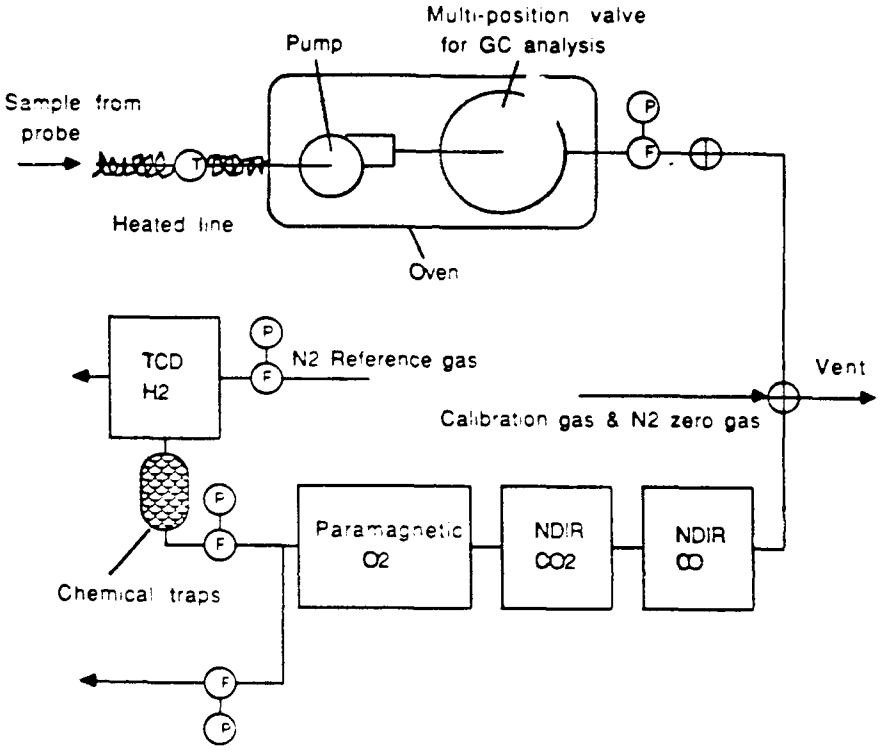

FIGURE 3. The continuous analysis system

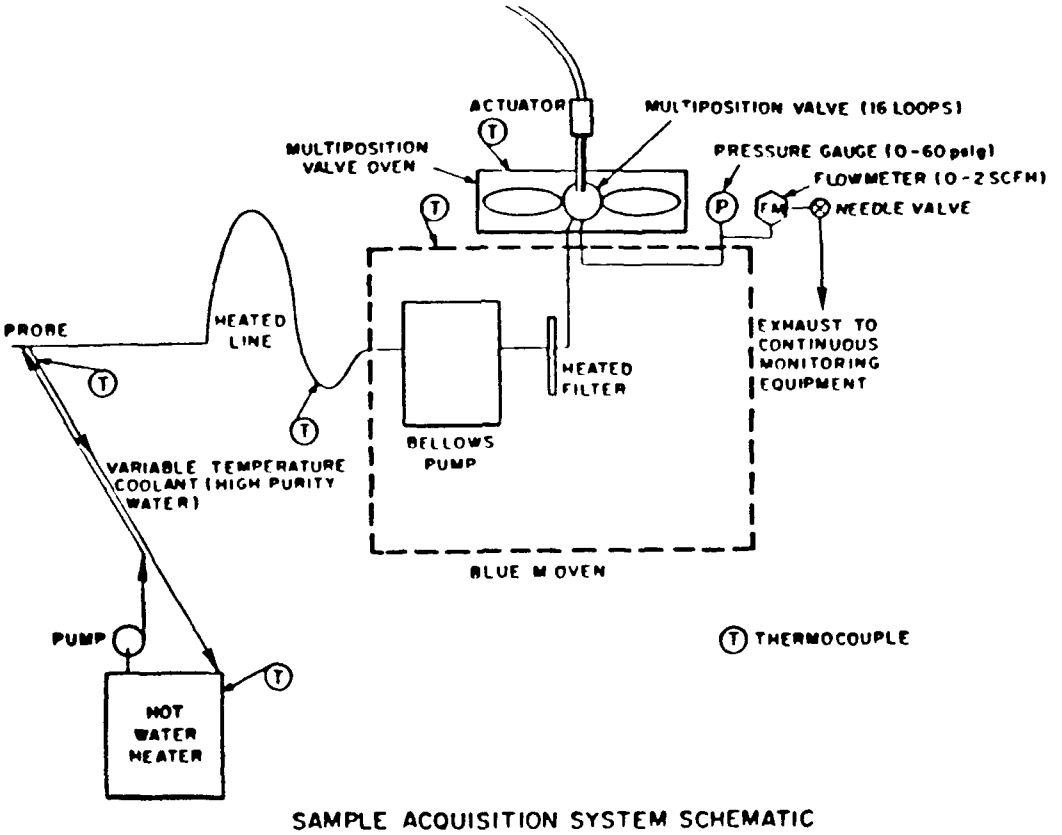

SAMPLE ACQUISITION SYSTEM SCHEMATIC

FIGURE 4. Sample acquisition system schematic

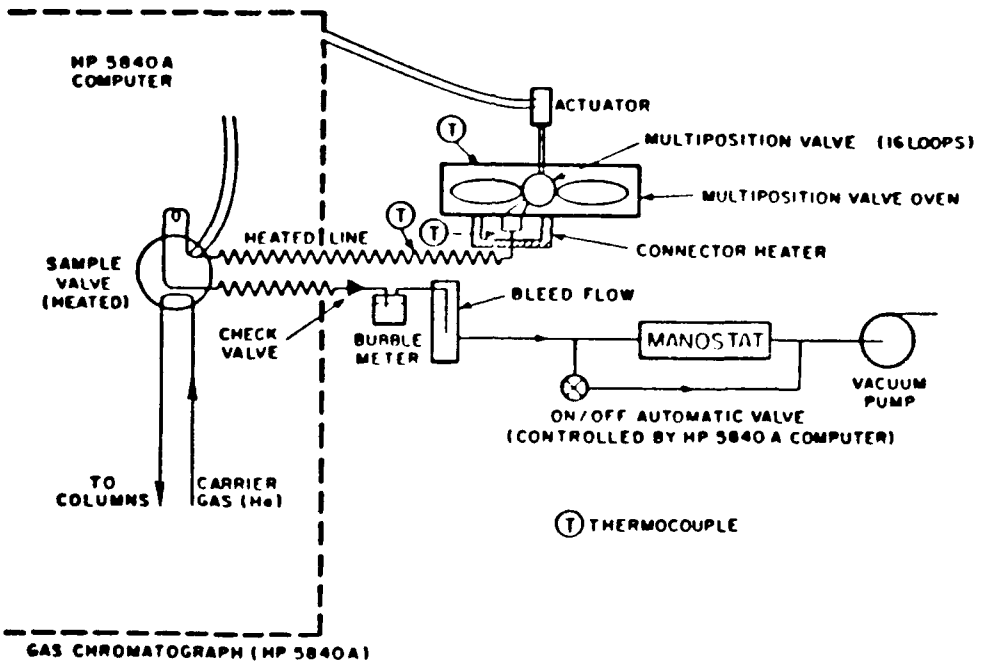

SAMPLE ANALYSIS SYSTEM SCHEMATIC

FIGURE 5. Sample analysis system schematic

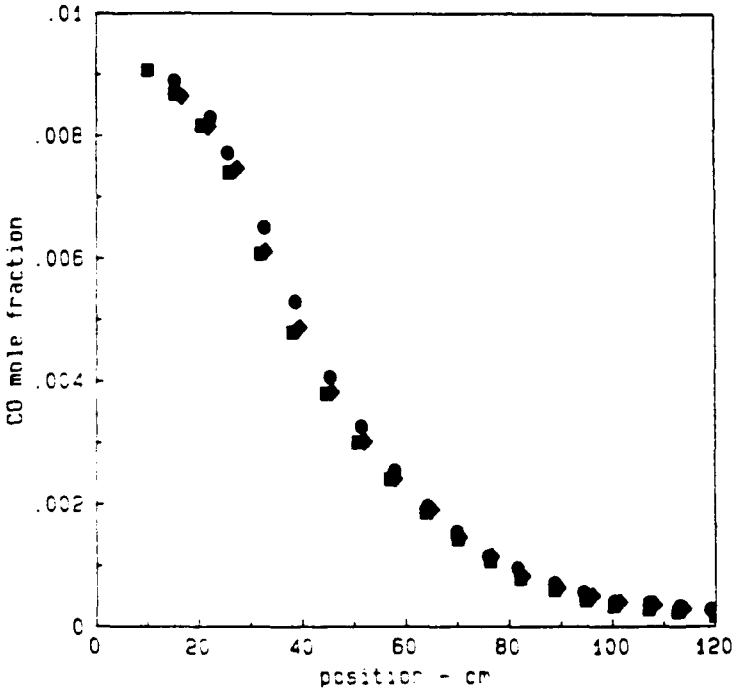

FIGURE 6. Experimental profiles of carbon monoxide disappearance for three different flow reactor experiments performed on a one-year period. Initial conditions: T = 1038K, p = 1 atm, m = 32.06 gm/s, XCO = 0.0096, XH_2O = 0.0056, XO_2 = 0.010$_2$, XN_2 = 0.9746.

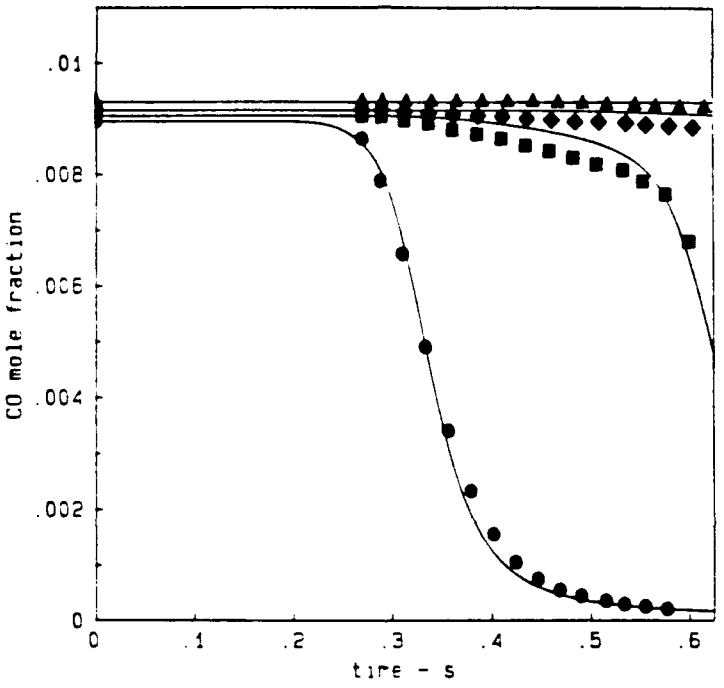

FIGURE 7. Mean CO concentration profiles for $CO/H_2O/O_2$ mixtures with the initial temperature ranging from 917 to 952K. Initial conditions: circles; $X(CO) = 0.00895$, $X(O_2) = 0.00438$, $X(H_2O) = 0.01235$, $X(N_2) = 0.97432$, T = 952K, p = 1 atm, m = 6.39 gm/s, squares; $X(CO) = 0.00905$, $X(O_2) = 0.00442$, $X(H_2H_2O) = 0.01324$, $X(N_2) = 0.97329$, T = 943K, p = 1 atm, m = 6.26 gm/s, diamonds; $X(CO) = 0.00915$, $X(O_2) = 0.00448$, $X(H_2O) = 0.0133$, $X(N_2) = 0.97307$, T = 932K, p = 1 atm, m = 6.28 gm/s, triangles; $X(CO) = 0.0093$, $X(O_2) = 0.00455$, $X(H_2O) = 0.0147$, $X(N_2) = 0.97145$, T = 917K, p = 1 atm, m = 6.17 gm/s.

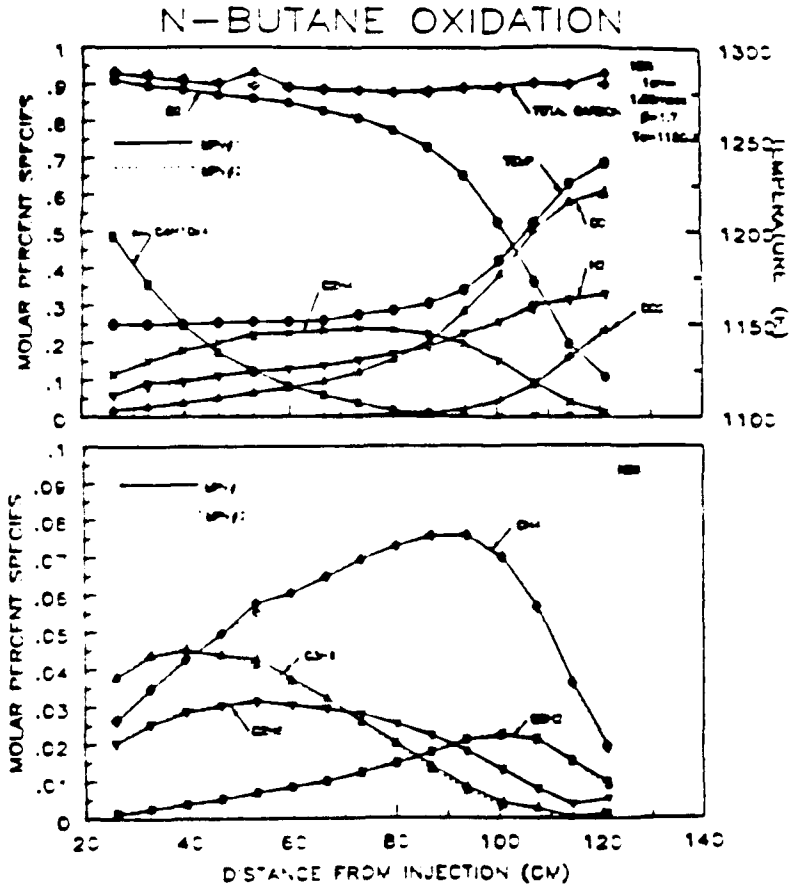

FIGURE 8. Mole fraction profiles the oxidation of N-Butane at 1150 K. The results show the comparison of two gas-chromatograph analysis.

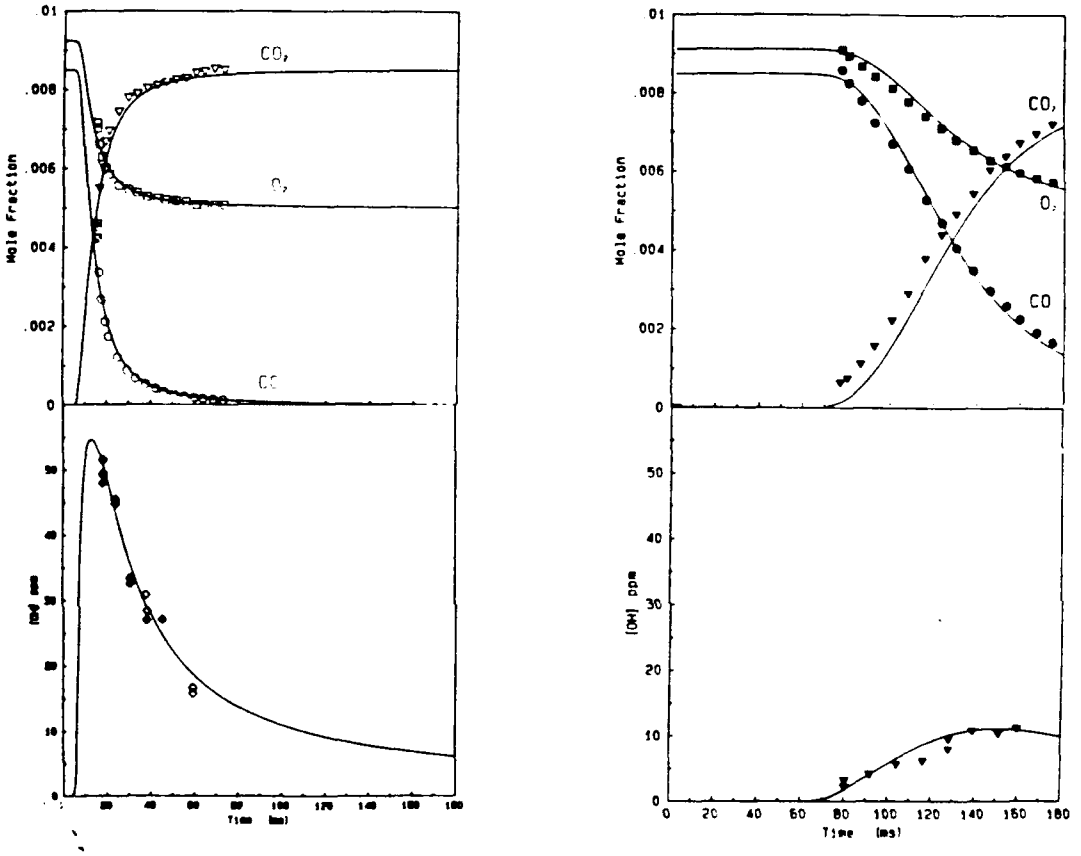

FIGURE 9. Hydroxyl measurements in the flow reactor for moist carbon monoxide oxidation at two temperatures, 1116 K and 980 K, respectively. The solid symbols are fluorescence measurements and the open symbols are absorption measurements.